STRATEGIES TO INCREASE THE SERVICE LIFE OF CONCRETE BRIDGE DECKS

Final Report

SPR 780

Oregon Department of Transportation

STRATEGIES TO INCREASE THE SERVICE LIFE OF CONCRETE BRIDGE DECKS

Final Report

SPR 780

by
O. Burkan Isgor, Ph.D., P.E. (ON)
Jason H. Ideker, Ph.D.
David Trejo, Ph.D., P.E. (CA)
Vahid Jafari-Azad, Ph.D.
David A. Rodriguez, M.S.C.E.
Silas Shields, M.S.C.E. Candidate
Parnian Husseini, PhD.

Oregon State University

for

Oregon Department of Transportation
Research Section
555 13th Street NE, Suite 1
Salem OR 97301

and

Federal Highway Administration
1200 New Jersey Avenue SE
Washington, DC 20590

March 2017

Technical Report Documentation Page

1. Report No. FHWA-OR-RD-17-10	2. Government Accession No.	3. Recipient's Catalog No.
4. Title and Subtitle Strategies to Increase the Service Life of Concrete Bridge Decks		5. Report Date March 2017 6. Performing Organization Code
7. Author(s) O. Burkan Isgor, Jason H. Ideker, David Trejo, Vahid Jafari-Azad, David A. Rodriguez, Silas Shields, and Parnian Husseini		8. Performing Organization Report No.
9. Performing Organization Name and Address Oregon State University School f of Civil and Construction Engineering 101 Kearney Hall, Corvallis, OR 97333		10. Work Unit No. (TRAIS) 11. Contract or Grant No. SPR 780
12. Sponsoring Agency Name and Address Oregon Dept. of Transportation Research Section and Federal Highway Admin. 555 13th Street NE, Suite 1 1200 New Jersey Avenue SE Salem, OR 97301 Washington, DC 20590		13. Type of Report and Period Covered Final Report 14. Sponsoring Agency Code
15. Supplementary Notes		

16. Abstract: Corrosion of the steel in reinforced concrete bridge decks is a critical issue for structures that are exposed to chloride-containing de-icing chemicals or marine salts. Oregon Department of Transportation (ODOT) has a large number of bridges that are vulnerable to this form of deterioration. An obvious indicator of a corrosion problem is visible damage; unfortunately, if corrosion damage is visible, the window for preventive action is likely closed. Pre-emptive actions and early detection of potential problems are more cost effective than repair or replacement of bridge decks that have already experienced corrosion. In recent years, electrical-based methods have emerged as durability-related performance indicators for reinforced concrete structures. Several investigations have shown the existence of relationships between electrical resistivity (or formation factor) of concrete and other durability-related parameters such as corrosion rate of steel reinforcement and transport properties of concrete. The main motivation of this research is to provide ODOT with a protocol to select bridges for its ongoing bridge deck treatment operations using quantitative tools that are practical and quick. Although rapid surface resistivity measurements are highly correlated with water and chloride transport properties of concrete, they do not directly provide the actual chloride depth profiling. However, transport properties that are revealed by surface resistivity measurements can be used in chloride ingress models that can be used to predict chloride profiles in concrete. The accuracy of the predictions improves with additional easily accessible quantitative information such as concrete mixture design properties (e.g. water-to-cement ratio), environmental data (e.g. temperature and relative humidity), and salt exposure histories. Most of these additional quantitative data are readily available for most locations in Oregon. These predictions, coupled with surface resistivity data, will also indicate if additional chloride profiling is necessary, and if so, at which locations on the deck it should be conducted. To achieve the project goals, the following tasks have been performed: (1) An experimental investigation was conducted to establish the relationship between electrical properties of concrete (e.g. SR or formation factor), environmental data (e.g. temperature and relative humidity), and chloride ingress in reduced-size reinforced concrete slabs simulating bridge decks commonly used in Oregon. (2) The effect of freeze-and-thaw action on the observed relationship was investigated. (3) A comprehensive modeling framework that relates the electrical properties of concrete, environmental data and chloride ingress was developed, verified, and validated. (4) A virtual test bed using the validated modeling framework was developed to conduct statistically significant number of virtual experiments to obtain closed-form relationships between electrical properties of concrete, environmental data and chloride ingress for bridge decks in different geographical areas in Oregon. (5) A demonstration case study was performed to show the development of a closed-form equation and how it can be used in a bridge-deck evaluation-protocol that can be used by ODOT in practice.

17. Key Words	18. Distribution Statement Copies available from NTIS, and online at http://www.oregon.gov/ODOT/TD/TP_RES/		
19. Security Classification (of this report Unclassified	20. Security Classification (of this page) Unclassified	21. No. of Pages 131	22. Price

SI* (MODERN METRIC) CONVERSION FACTORS

APPROXIMATE CONVERSIONS TO SI UNITS

Symbol	When You Know	Multiply By	To Find	Symbol
		LENGTH		
in	inches	25.4	millimeters	mm
ft	feet	0.305	meters	m
yd	yards	0.914	meters	m
mi	miles	1.61	kilometers	km
		AREA		
in^2	square inches	645.2	millimeters squared	mm^2
ft^2	square feet	0.093	meters squared	m^2
yd^2	square yards	0.836	meters squared	m^2
ac	acres	0.405	hectares	ha
mi^2	square miles	2.59	kilometers squared	km^2
		VOLUME		
fl oz	fluid ounces	29.57	milliliters	ml
gal	gallons	3.785	liters	L
ft^3	cubic feet	0.028	meters cubed	m^3
yd^3	cubic yards	0.765	meters cubed	m^3
NOTE: Volumes greater than 1000 L shall be shown in m^3.				
		MASS		
oz	ounces	28.35	grams	g
lb	pounds	0.454	kilograms	kg
T	short tons (2000 lb)	0.907	megagrams	Mg
		TEMPERATURE (exact)		
°F	Fahrenheit	(F-32)/1.8	Celsius	°C

APPROXIMATE CONVERSIONS FROM SI UNITS

Symbol	When You Know	Multiply By	To Find	Symbol
		LENGTH		
mm	millimeters	0.039	inches	in
m	meters	3.28	feet	ft
m	meters	1.09	yards	yd
km	kilometers	0.621	miles	mi
		AREA		
mm^2	millimeters squared	0.0016	square inches	in^2
m^2	meters squared	10.764	square feet	ft^2
m^2	meters squared	1.196	square yards	yd^2
ha	hectares	2.47	acres	ac
km^2	kilometers squared	0.386	square miles	mi^2
		VOLUME		
ml	milliliters	0.034	fluid ounces	fl oz
L	liters	0.264	gallons	gal
m^3	meters cubed	35.315	cubic feet	ft^3
m^3	meters cubed	1.308	cubic yards	yd^3
		MASS		
g	grams	0.035	ounces	oz
kg	kilograms	2.205	pounds	lb
Mg	megagrams	1.102	short tons (2000 lb)	T
		TEMPERATURE (exact)		
°C	Celsius	1.8C+32	Fahrenheit	°F

*SI is the symbol for the International System of Measurement

ACKNOWLEDGEMENTS

The authors of this report would like to express their sincere appreciation to the ODOT project coordinators Steven Soltesz and Matthew Mabey, as well as Technical Advisory Committee Members Ray Bottenberg (ODOT Bridge Section), Craig Shike (ODOT Bridge Section), Bill Bennett (ODOT Construction Section), and Tim Rogers (FHWA). We also would like to thank Linda Perkins (ODOT Research Section) for her assistance during the progress report updates.

We would like to acknowledge the contributions of Monica Morales on the literature review section of this report. We also would like to note that this research would not be possible without the dedicated work of the undergraduate research assistants Suellen Nerone, Brianne Velasquez, Walter Lee Webster, Kristin Jones, Raven Merritt-Shorb, and Christine Baker. We sincerely appreciate the help of the staff at the OSU Hinsdale Wave Laboratory.

DISCLAIMER

TABLE OF CONTENTS

LIST OF TABLES

LIST OF FIGURES

1.0 INTRODUCTION

1.1 POJECT BACKGROUND

Corrosion of the steel in reinforced concrete bridge decks is an important issue for structures that are exposed to chloride-containing de-icing chemicals or marine salts. Once the amount of chloride at the steel reinforcement reaches a critical level, corrosion is likely to initiate. Oregon Department of Transportation (ODOT) has a large number of bridges that are vulnerable to this form of deterioration. An obvious indicator of a corrosion problem is visible damage; unfortunately, if corrosion damage is visible, the window for preventive action is likely closed. Pre-emptive actions that prevent corrosion initiation and early detection of possible deterioration are more cost effective than repair or replacement of bridge decks that have already experienced corrosion.

ODOT uses chloride depth profiling on occasion to provide quantitative insight into the corrosion risk of bridge elements, but the method is time consuming and relatively expensive. It is also not practical for routine monitoring of bridge decks with current limited ODOT resources. Other measurement technologies are at various stages of maturity and are likely to be useful either by themselves or when used in combination. Whatever measures are used, the values need to be turned into predictions regarding time to corrosion damage and when pre-emptive actions should be applied. Much valuable research is already available on detection technologies and models to predict corrosion.

Every year, ODOT treats the riding surface of select bridge decks with sealers, coatings, and thin overlays to protect the decks from deicing chemicals. Currently, the mitigation actions are selected based on the judgment of field personnel, occasionally with additional data from chloride profiles. There is no routine methodology in place to select decks based on quantitative measurements coupled with time-to-damage predictions.

In recent years, electrical-based methods of concrete, such as electrical resistivity measurements, have emerged as durability-related quantitative performance indicators. For example, several investigations have shown the existence of relationships between electrical resistivity and other durability-related parameters such as corrosion rate of steel reinforcement and transport properties of concrete. Alonso et al. *(Alonso et al. 1988)*, Lopez and Gonzalez *(Lopez and Gonzalez 1993)* and Gowers and Millard *(Gowers and Millard 1999)* reported that concrete resistivity and corrosion rate are inversely proportional over a wide range of concrete resistivity values. The literature also shows that concrete resistivity is strongly affected by the concrete characteristics, the degree of concrete pore saturation, and the chloride concentration *(Hussain et al. 1995, Song and Saraswathy 2007)*. Low resistivity values are associated with high water-to-cement ratio (w/c or w/cm) and/or high moisture contents *(Neville 1996; Morris et al. 2004)*.

Lately, surface resistivity (SR) measurements of concrete cores have been replacing the widely used Rapid Chloride Permeability Test (RCPT) because both tests provide a measure of resistance of concrete to ionic movement under an applied electrical potential difference. In most cases, RCPT and SR measurements have nearly perfect correlation *(Hooton et al. 2012)*;

while RCPT takes many hours to complete, SR measurements can be taken in seconds. Several researchers have also shown in studies on cores extracted from concrete structures and laboratory-produced cylinders that SR measurements are also strongly correlated well with water permeability *(Kessler et al. 2005)* and bulk chloride diffusion coefficient *(Hamilton et al. 2007, Sengul and Gjorv 2008)* of concrete.

All these developments have led to increased efforts to standardize SR measurement procedures *(AASHTO TP 095-11UL 2011, CAN/CSA A23.2 2009, ASTM WK37880 2014).* A number of jurisdictions even started requiring resistivity measurements as part of ongoing construction and maintenance procedures *(FDOT FM 5-578 2004; MTO LS-444 2013).* Consequently, a number of companies producing SR measurement devices have been increasing, while the cost of units for SR measurements has been declining. The current cost of a typical SR probe ranges from $3,000 to $5,000.

Resistivity of concrete can be measured in a number of ways; however, the four-point Wenner probe technique is the most commonly used approach for field application because of its speed, simplicity, and practicality. It can be used to measure resistivity of concrete cores extracted from concrete structures, but it can also be used directly on concrete surfaces without the need of coring or without the need for access (i.e., connect) to the steel reinforcement (as in the case of half-cell potential measurements). In all cases, measurements are made in seconds. There are, however, a number of gaps in the literature and practical challenges before SR data can provide quantitative insight into the corrosion risk of bridge decks.

The main motivation of this research is to provide ODOT with a protocol to select bridges for its ongoing bridge deck treatment operations using quantitative tools that are practical and quick. Although SR measurements are highly correlated with water and chloride transport properties of concrete, they do not directly provide the actual chloride depth profiling. However, transport properties that are revealed by SR measurements can be used in chloride ingress models that can be used to predict chloride profiles in concrete. The accuracy of the predictions improves with additional easily accessible quantitative information such as concrete mixture design properties (e.g. water-to-cement ratio), environmental data (e.g. temperature and relative humidity), and salt exposure histories. Most of these additional quantitative data are readily available for most locations in Oregon. These predictions, coupled with SR data, will also indicate if additional chloride profiling is necessary, and if so, at which locations on the deck it should be conducted.

1.2 PROJECT OBJECTIVES

The main objectives of the project are summarized as follows:

i. Conduct an experimental investigation to establish the relationship between electrical properties of concrete (e.g. SR or formation factor), environmental data (e.g. temperature and relative humidity), and chloride ingress in reduced-size reinforced concrete slabs simulating bridge decks commonly used in Oregon.

ii. Investigate the effect of freeze-and-thaw (F-T) cycles on the observed relationship between electrical properties of concrete (e.g. SR or formation factor), environmental

data (e.g. temperature and relative humidity) and chloride ingress in reduced-size reinforced concrete slabs simulating bridge decks commonly used in Oregon.

iii. Develop and experimentally validate a comprehensive modeling framework that relates the electrical properties of concrete (e.g. SR or formation factor), environmental data (e.g. temperature and relative humidity), and chloride ingress in reduced-size reinforced concrete slabs simulating bridge decks commonly used in Oregon.

iv. Develop a virtual test bed using the validated modeling framework to conduct statistically significant number of virtual experiments to obtain closed-form relationships between electrical properties of concrete (e.g. SR or formation factor), environmental data (e.g. temperature and relative humidity), and chloride ingress for bridge decks in different geographical areas in Oregon.

v. Conduct a demonstration case study to show the development of a closed-form equation that relates electrical properties of concrete (e.g. SR or formation factor), environmental data (e.g. temperature and relative humidity), and chloride ingress for bridge decks in a particular geographical location in Oregon.

vi. Demonstrate how the developed closed-form equation can be used in a bridge-deck evaluation-protocol that can be used by ODOT in practice.

1.3 ORGANIZATION OF THE REPORT

The organization of this report is outlined in Figure 1.1. Chapter 2 presents the literature review that was conducted as part of this research. Chapter 3 presents the details of the experimental study program. Chapter 5 presents the results of the experimental study to relate salt ingress and electrical properties of concrete, as well as the effect of freeze-thaw action on the observed relationship. The theoretical background is also presented in Chapter 5 along with the validation of the developed FEM modeling framework that is later used as a virtual experiment test bed. Chapter 6 presents a demonstration case study to show the development of a closed-form equation that relates electrical properties of concrete (e.g. SR), environmental data (e.g. temperature and relative humidity), and chloride ingress for bridge decks in a particular geographical location in Oregon. Conclusions and recommendations for ODOT are presented in Chapter7, followed by references and appendices.

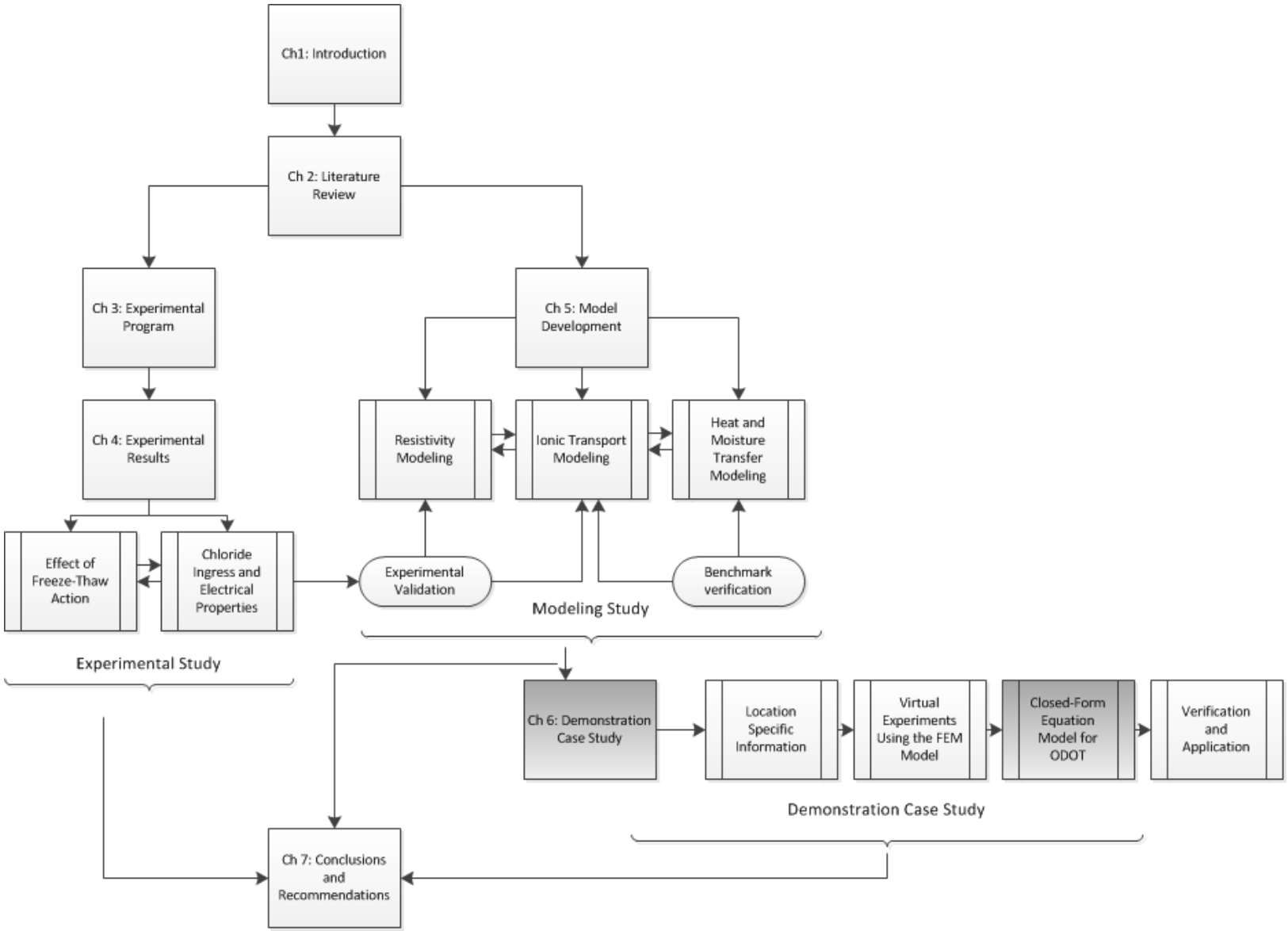

Figure 1.1: Project plan and organization of the report.

2.0 LITERATURE REVIEW

2.1 BACKGROUND

There are over 350,000 reinforced concrete bridges in the United States alone, and the average age of these bridges is between 40 and 50 years *(Mahmoodian and Alani 2015)*. In order to manage the issue of ageing infrastructure, State and Federal regulations mandate that these structures are regularly inspected to ensure their safe operation — bridges, for instance, must be inspected one every two years in most jurisdictions, including Oregon. Unfortunately, the large number of reinforced concrete structures and the limited number of qualified inspectors restrict the duration and quality of individual inspections, especially when inspections warrant unwanted traffic disruptions *(Gucunski et al. 2013)*. Therefore, most routine inspections are in the form of rapid visual surveys, which do not generally provide accurate assessments of the durability condition of concrete *(Zhu et al. 2010, Moore 2011, Isgor 2016)*.

The most significant type of deterioration in reinforced concrete bridge decks that are exposed to de-icing chemicals or marine salts is the corrosion of the reinforcing steel *(Koch et al. 2002)*. Detecting reinforcement corrosion in bridge decks, however, can be time consuming and expensive. The early stages of corrosion cannot be captured in most routine inspections. As stated in ODOT Bridge Inspection Program Manual *(ODOT Bridge Inspection Program Manual 2013)*, "…Such an evaluation is frequently based on the personal judgment, intuition, and perhaps experience of each inspector. As a result, different inspectors may assess a given bridge differently…" Once the corrosion can be detected during visual surveys, the extent of deterioration and damage is typically already beyond the point of efficient mitigation options, hence the time required and the resources needed to mitigate it increase exponentially. Unfortunately, detailed inspections that provide mapping, sampling, and testing are not generally practical or feasible for most jurisdictions.

Laboratory testing of extracted cores from the structure might provide accurate condition assessments, but the number of samples to be extracted to represent the entire structure and the time involved in testing restrict their applications to more detailed condition surveys that are only performed on selected structures. For example, the Rapid Chloride Penetration Test (RCPT), ASTM C1202, which is a test to measure concrete's transport properties, can be performed on cores extracted from concrete structures, but each test takes about 24 hours (approximately 18 hours for sample preparation and six hours for the actual test) *(Rupnow and Icenogle 2011)*. ASTM C1152 and ASTM C1218 are used to determine the acid- and water- soluble chloride profiles in concrete, respectively; however, these tests require grinding the cores into powder and chemically analyzing the chloride contents, which can be rather time consuming and resource intensive. Another example is the ASTM C856 test method for petrographic analysis of concrete core samples. This test not only involves several hours to complete the sample preparation and analysis, but also requires a certified petrographer, which in total can be very costly.

The current non-destructive testing (NDT) methods used to determine the durability or service life of a structure are also expensive and time consuming. In addition, the traditional NDTs, in most cases, do not assess the durability properties of concrete accurately *(Khalim et al. 2011)*. Some of the more common, NDT methods, which can help evaluate the performance of the structure, include Schmidt rebound hammer test *(ASTM C805 2013)*, which determines the compressive strength of the concrete, chain drag *(ASTM D4580 2003)* provides the location of delaminated areas, ultrasonic pulse velocity test *(ASTM C597 2010)*, which provides insight on the quality of the concrete although the reinforcing steel of the concrete structure can affect the results, ground penetrating radar *(ASTM D6432 2011)* which supplies information of the subsurface, and impact echo test *(ASTM C1383 2015)*, which uses impact waves to help identify internal cracks or flaws. Half-cell potential mapping *(ASTM C876 2012)* can be very useful in identifying potential corrosion in the reinforcing steel, and SR measurements can be used as an indicator of concrete deterioration.

Unfortunately, there is not a single technology that can accurately provide information on deterioration *(Gucunski et al. 2013)*. Combining technologies provide the most precise information on deterioration of bridge decks. A study performed at the University of Genova *(Brencich et al. 2013)* concluded that the Schmidt hammer test results were greatly affected by the properties of the materials and the limited area in which the test is performed which suggests that this test may only provide a rough estimation of the strength of concrete. A separate study at the University of Malaya *(Shariati et al. 2011)*, also determined that the use of rebound hammer testing alone was not enough to determine compressive strengths. The study reiterated that combining the rebound hammer test with ultrasonic pulse velocity would provide a much higher degree of accuracy. A study focused on detecting bridge deck deterioration by Maser et al. *(Maser et al. 2012)* analyzed the accuracy of hammer sounding, ultrasonic impact echo, half-cell potential and ground penetrating radar, and concluded that the combination of ground penetrating radar with half-cell potential was the most useful technique for detecting deterioration of bridge decks early on in its service life. The findings in these studies show that combining test methods, for either destructive or non-destructive methods, provides more accurate results; this is well established and is supported by various researchers *(Jianhong et al. 2008, Khalim et al. 2011, Gucunski et al. 2013, Sadowski 2013).*

There is also a lack of documented information about a particular bridge deck that can be vital when it is being assessed. As part of a study led by ODOT, Shi et al. *(Shi et al. 2013)* and Huang et al. *(Huang et al. 2014)* concluded that issues with data availability and quality were key. It was recommended that the following information be collected about bridge decks to aid in assessment: deicer type and application rate, traffic volume, weather condition information, and bridge mix-design data. This additional information will provide inspectors and researchers a better understanding of problems that may arise throughout the service life of these structures.

In summary, there is currently no established practical protocol for evaluating the remaining service-life of bridge decks that is based on a system that combines computable measurements with time-to-damage predictions. An established system that can predict the deterioration rate of these decks would be beneficial, as it would allow DOTs, in particular ODOT, to take action during the early stages of deterioration of the concrete, thereby saving the DOT resources. Whatever measures are used, data obtained during inspection needs to be turned into predictions about time to corrosion damage in order to provide a proactive approach to repair that would

optimize financial and material resources required to repair bridge decks before significant damage occurs.

2.2 ELECTRICAL-BASED MONITORING OF CONCRETE DETERIORATION

2.2.1 Electrical Resistivity of Concrete

In recent years, electrical resistivity of concrete has emerged as a durability-related quantitative performance indicator *(Andrade et al. 2013)*. Many DOTs are actively investigating the use of resistivity measurements as a possible quality control tool or specification *(TRB 2015, 2016)* LaDOT has developed a specification while INDOT has used this in shadow specifications. The Florida DOT hosted a sample exchange, as has the National Concrete Consortium, to provide DOTs with familiarity in the use of this test method. TRB has hosted a workshop as well as a webinar on the use of resistivity-based measurements.

Several investigations have shown relationships between electrical resistivity and other durability-related parameters, such as corrosion rate of steel reinforcement and transport properties of concrete. Lopez and Gonzalez *(Lopez and Gonzalez 1993)*, and Gowers and Millard *(Gowers and Millard 1999)* reported that concrete resistivity and corrosion rate are inversely proportional over a wide range of concrete resistivity values. The literature also shows that concrete resistivity is strongly affected by the concrete characteristics, the degree of concrete pore saturation, and the chloride concentration *(Hussain et al. 1995, Morris et al. 2004, Song et al. 2007)*. Low resistivity values are associated with high water-to-cement ratios, high moisture contents, and presence of chlorides *(Neville 1996, Morris et al. 2004)*. All these developments have led to increased efforts to standardize surface resistivity (SR) measurement procedures *(AASHTO TP 095-11UL 2011; CAN/CSA A23.2 2009; ASTM WK37880 2014)*. A number of jurisdictions even started requiring resistivity measurements as part of ongoing construction and maintenance procedures *(FM 5-578 2004; MTO LS-444 2013)*.

Electrical resistivity of concrete can be measured in a number of ways; however, the four-point Wenner probe technique is the most commonly used approach for field application because of its speed, simplicity, and practicality. It can be used to measure resistivity of concrete cores extracted from concrete structures, but it can also be used directly on concrete surfaces without the need of coring or without the need for access to the steel reinforcement (as in the case of half-cell potential measurements). In all cases, measurements are made in seconds. A Wenner probe and a functional schematic are provided in Figure 1.1. After the probe's four linearly spaced electrodes are placed on the concrete surface, an AC current, I, is induced from the outer two electrodes and a change in voltage, or potential difference (ΔV), is measured *(Gucunski 2013, Angst and Elsener 2014, Garzon et al. 2014)*. The electrical SR of concrete can be calculated via *(Morris et al. 1996, Simon and Vass 2012, Gucunski et al. 2013, Angst and Elsener 20143, Garzon et al. 2014)*:

$$r = \frac{2\pi aV}{I} \tag{2.1}$$

where s is the probe spacing. Since SR measurements are influenced greatly by temperature, all measurements can be normalized to a reference temperature using the Hinrichsen-Rasch law *(Hope 1987)* which is given by:

$$r_2 = r_1 * exp\left[2900\left(\frac{1}{T_1} - \frac{1}{T_2}\right)\right] \quad \textbf{(2.2)}$$

where r_1 is the measured resistivity, r_2 is the normalized resistivity, T_1 (K) is the temperature of the concrete during the measurement, and T_2, is the normalized temperature.

Equation (2.1) assumes homogeneity and isotropy of the medium, semi-infinity of the conductive volume, and point contact between the electrodes and the medium (Angst and Elsener 2013). For clarification, resistivity is a property of a material such as concrete, whereas resistance is a property of a dimensional material such as a concrete cylinder. Typical electrical resistivity values for concrete vary from 1 to 1000 kΩ-cm depending on its composition and moisture content *(Polder and Peelen 2002, du Plooy et al. 2013, Sadowski 2013)*. To reduce noise and time spent when measuring electrical resistivity of concrete, commercial Wenner probes use frequencies greater than 10 hertz (Hz). However, at these higher frequencies, embedded reinforcement provides alternate impressed current paths, because it is more conductive than concrete. This path alteration can then impose error to the measured electrical resistivity of concrete *(Millard 1991, Gowers and Millard 1999, Angst and Elsener 2014*

).

One numerical study *(Salehi et al. 2014)*, in particular, investigated the effect of the presence of rebar mesh on Wenner probe electrical resistivity measurements. Different cover thicknesses, slab thicknesses, rebar mesh densities, and probe orientations with respect to the rebar mesh were also considered when examining effects to measurements. From the numerical results, it was observed that significantly less error could be achieved by performing electrical resistivity measurements simply by using a different probe orientation than suggested by current guidelines.

A parallel numerical study *(Salehi et al. 2014)* investigated the effect of cracks, conductive and insulative, and at different depths and widths, on electrical resistivity measurements using a Wenner probe. Probe orientation with respect to a crack was also considered in the investigation. In conjunction with observing the effect that cracks in unreinforced concrete have on electrical resistivity measurements, the effect of cracks in reinforced concrete was also considered for different rebar mesh variables. The numerical results had shown that errors could derive from the presence of certain cracks where the observed resistivity was as much as two-times or half that of true resistivity. The effect of the presence of rebar and cracks were observed to act independently of one another, where rebar reduced measured electrical resistivity values.

(a)

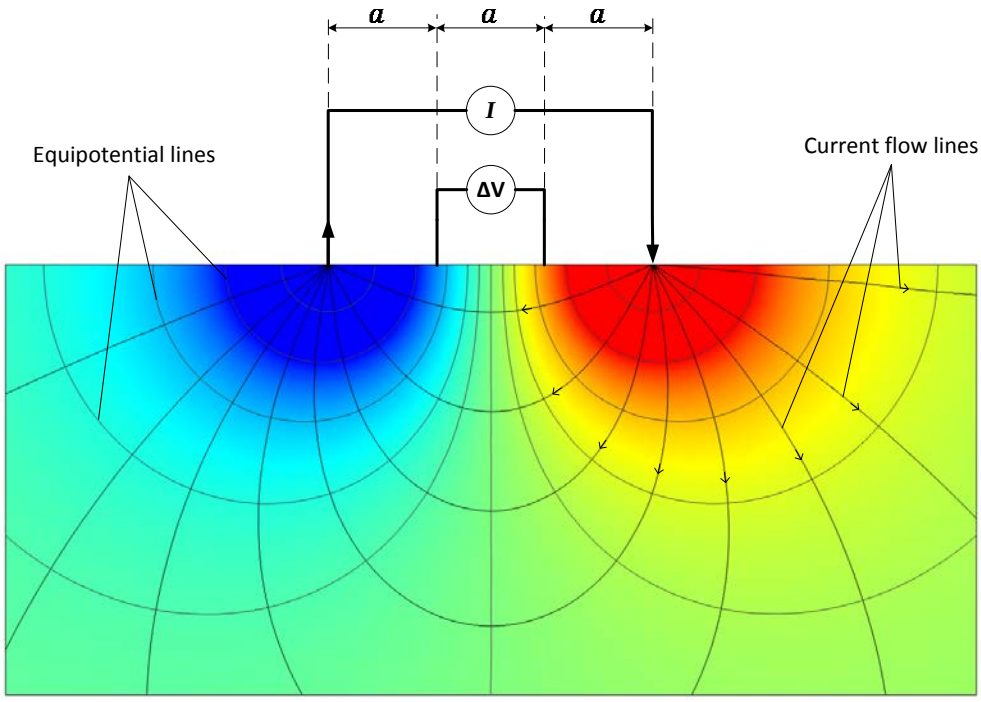

(b)

Figure 2.1: (a) A commercial Wenner probe *(Proceq 2011)*; (b) functional schematic of the probe *(Salehi 2013)*.

Morales *(Morales 2015)* conducted an extensive experimental investigation to supplement these numerical studies. In these studies, the effects of steel reinforcement and chloride-induced corrosion initiation on the electrical resistivity measurements using the Wenner probe technique were studied experimentally on custom-designed reinforced concrete slabs. Investigation parameters included (1) probe configurations with respect to rebar mesh, (2) rebar density, (3) epoxy coating on the rebar, (4) concrete cover thickness over embedded reinforcement, (5) chloride ingress, (6) corrosion of rebar, and (7) the moisture content of concrete. It was determined that concrete moisture condition and concrete cover thickness played a role in the effect of rebar mesh and corrosion, and it was hypothesized that bound chlorides increased electrical resistivity measurements. Although uncoated rebar affected resistivity measurements, particularly for saturated and semi-saturated concrete, it was shown that epoxy coated rebar did not have any effect on electrical resistivity measurements from the similar results received for different probe configurations with respect to epoxy coated rebar mesh. Recommendations were made to minimize the measurement errors on reinforced concrete slab surfaces.

In addition, Morales *(Morales 2015)* performed an experimental study on a custom-designed reinforced concrete slab to investigate the effects of delamination and cracking of concrete cover on electrical resistivity measurements using the Wenner probe technique. Investigation parameters included (1) crack and delamination properties, (2) crack locations and orientations with respect to the probe position, (3) density and location of embedded reinforcement, (4) orientation of the probe with respect to reinforcement, and (6) moisture content of concrete. It was determined that insulative cracks either provide for over-measurements or under-measurements of electrical resistivity and conductive cracks provided for under-measurements of electrical resistivity. Surficial microcracking, in the form of crazing, did not affect electrical resistivity measurements. Electrical resistivity detected delamination for small concrete cover thicknesses. For small concrete cover thicknesses (e.g. < 25 mm), it was observed that insulative cracks between topmost rebar tended to create for more error than insulative cracks that were along bottommost rebar, especially for a saturated concrete moisture condition. Also for small concrete cover thicknesses, deep conductive cracks increased the error to electrical resistivity measurements and errors increased as the concrete moisture condition increased. Recommendations to minimize the measurement errors on reinforced concrete slab surfaces containing cracks were suggested.

2.2.2 Electrical Resistivity vs. Formation Factor of Concrete

It has been shown in past research that formation factor of concrete is a unique parameter that can be used to characterize durability performance of concrete structures *(Presuel-Moreno et al. 2010, Spragg et al. 2011, Weiss 2014, Jenkins 2015)*. The formation factor is directly related to critical performance indicators, such as w/cm or porosity of concrete. It provides critical information about both durability and mechanical performance of structures during their service life *(Whittington et al. 1981, Mancio et al. 2010, Wei and Xiao 2011, Bentz et al. 2014, Salehi 2013)*. The concept of formation factor was originally postulated by Archie *(Archie 1942)* to be a useful way to characterize the pore structure of porous materials (originally used to characterize rocks). In concrete, the formation factor (F) is defined as the ratio of the resistivity of a bulk concrete (r) and the resistivity of the pore solution (r_o) via *(Archie 1942):*

$$\boldsymbol{F = \frac{r}{r_o}} \tag{2.3}$$

Since electrical resistivity of the solid phase (i.e., aggregates, hydrated or un-hydrated solids) and vapor phase in concrete is orders of magnitude larger than the electrical resistivity of the pore solution (i.e., the fluid in concrete), the formation factor is mainly dependent on the pore volume (ϕ) and pore connectivity (β) such that

$$\boldsymbol{F \cong \frac{1}{\phi}\frac{1}{\beta}} \tag{2.4}$$

An alternative way that the formation factor can be expressed is by using Archie's Law, which establishes generic relationship for most porous materials via *(Archie 1942):*

$$F = A\phi^{-m} \tag{2.5}$$

where *A* is a factor that is related to the connectivity of pore structure and *m* is a coefficient that is related to the type of the porous medium.

The moisture content of concrete affects electrical resistivity measurements; therefore, for the same concrete with the same amount of chloride ingress, different values of resistivity will be measured depending on the degree of saturation of concrete *(Neville 1996, Hussain 2011, Ryu et al. 2011, Wang et al. 2014).* Since electrical conductivity is greater through a liquid phase compared to a solid phase, the higher the moisture content in the concrete matrix, the lower the electrical resistivity will be. To obtain consistent and comparable resistivity measurements, the moisture content of concrete needs to be relatively similar between distinct specimens. This can be achieved in extracted cores by consistently measuring resistivity after saturating the specimens; however, saturating bridge decks before collecting resistivity measurements will seldom be practical. Therefore, a new method for correcting for the effect of moisture content of concrete will need to be developed to ascertain that the resistivity values measured at different times are comparable, even though moisture contents of the deck might differ in each measurement. The concept of formation factor also resolves this issue since the effect of degree of saturation can be incorporated into the calculation of formation factor.

The use of the formation factor as a performance index for hardened concrete has been increasing in recent years *(Whittington et al. 1981, Mancio, Moore et al. 2010, Wei and Xiao 2011, Bentz et al. 2014).* One advantage of the formation factor is that it can be determined rapidly and related to other more time consuming and expensive tests. For example, it has been shown that the rapid chloride penetration test can be replaced using electrical resistivity *(Presuel-Moreno et al. 2010, Spragg et al. 2011, Weiss 2014, Jenkins 2015).* While several empirical studies have been performed the charge passed (Q) in the RCP test can be computed directly to be inversely related to the resistivity of the concrete based on first principles as shown in equation 4 and Figure 2.2a:

$$Q = V\,\frac{A}{L}\,t\,\frac{1}{\rho} = V\,\frac{A}{L}\,t\,\frac{1}{\rho_0}\frac{1}{F} = \frac{206,830\,V}{\rho_o}\,\frac{1}{F} \tag{2.6}$$

where V is the voltage of the sample (60 V), R is the resistance of the sample (Ω), A is the cross sectional area of the sample ($\pi \cdot 50^2$ mm^2), L is the length of the sample (50 mm), and t is testing time (6 h = 21600 s).

Similarly, the formation factor can be used to replace the time consuming diffusion test, which is used to predict the time to corrosion initiation. To do this the diffusion coefficient D can be related to the formation factor, and therefore to the electrical resistivity using:

$$D = \frac{D_o}{F} = \frac{D_o \rho_o}{\rho_c} \tag{2.7}$$

where D_o is the diffusion coefficient for a chloride ion in water ($2.03x10^{-9}$ m^2/sec at 25°C) ρ_o is the resistivity of the pore fluid, and ρ_c is the resistivity of the concrete. The formation factor can be directly related to the time of corrosion (t) using Fick's second law (equation 6 and Figure 2.2b) for a given environmental exposure to chloride (C_s), background chloride (C_o), known chloride content to initiate corrosion (C_x) and cover thickness (x).

$$F = \frac{4tD_0}{x^2}\left[erf^{-1}\left[\frac{C_s - C_x}{C_s - C_o}\right]\right]^2 \quad \textbf{(2.8)}$$

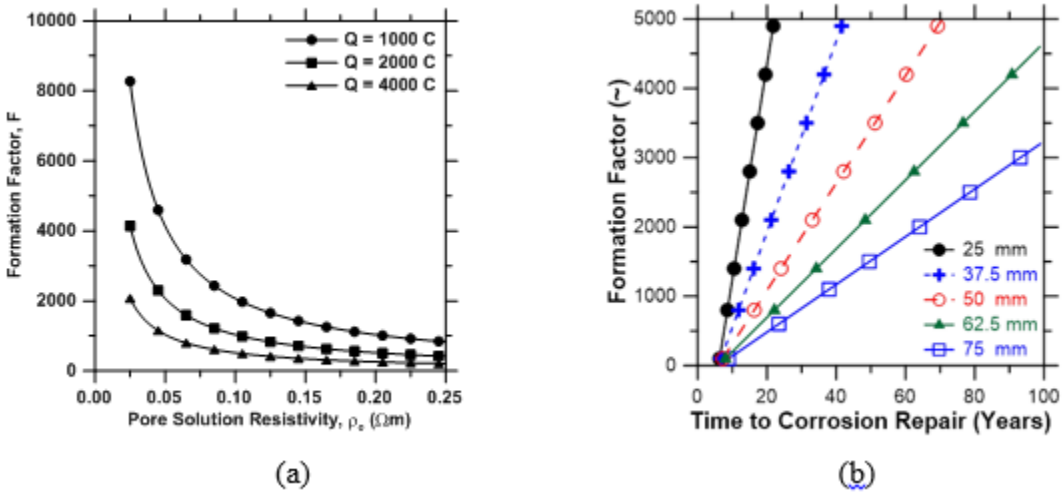

Figure 2.2: The relationship between (a) the RCP test and the formation factor for various pore solution resistivities, and (b) the predicted time to corrosion as a function of cover thickness *(Weiss et al. 2016).*

Although the benefits of using the formation factor for hardened concrete as a performance index are clear, historically, the use of the formation factor has been limited in practice due to challenges in determining the resistivity of the pore solution. This limitation can be overcome using a series of approximations applied to concrete at an age greater than ~ 36 or 48 hours beyond which the chemical composition of the pore solution become rather stable. However, during chloride ingress, the composition of the pore solution changes, affecting its electrical resistivity, and consequently the formation factor. This challenge also yields an opportunity. By using electrical resistivity measurements of concrete (e.g. through SR measurements using Wenner probe) and mechanistic modeling approaches for simulating formation factor, the chloride profiles can be obtained indirectly.

2.2.3 Relationship between Electrical Properties and Chloride Transport in Concrete

The most common standard for estimating the resistance of concrete to chloride ingress is ASTM C1202 Standard Test Method for Electrical Indication of Concrete's Ability to Resist Chloride Ion Penetration, also known as RCPT. This test can provide insight on the concrete's resistance to chloride ion penetration and it does so by applying a constant voltage through a two-inch by

four-inch diameter sample that on one side is submerged with sodium chloride and the other side with sodium hydroxide. The test takes 18 hours to prepare and six hours to run. The total amount of charge that passes through the concrete sample during the six hours is then compared to a table on the standard that indicates the penetrability of the sample. Table 2.1 shows the chloride ion penetrability potential from ASTM C1202.

Table 2.1: Chloride Ion Penetrability vs RCPT *(ASTM C1202 2012)*

Charge Passed (coulombs)	Chloride Ion Penetrability
>4,000	High
2,000–4,000	Moderate
1,000–2,000	Low
100–1,000	Very Low
<100	Negligible

The RCPT determines the electrical conductance of the concrete sample, which inversely provides its resistance to chloride ion penetration. RCPT however, has its limitations. Since the test takes six hours, the conductivity and temperature of the sample may change due to the movement of chloride ions and the porosity of the sample. Nevertheless, the use of electrical resistivity as it has been used in RCPT and SR methods seem to prove to be a good indicator for determining chloride penetrability. Surface resistivity devices have emerged in the last few years. These devices have proven to be more practical and reliable methods for measuring the electrical resistivity of concrete. This is because, while both tests provide a measure of resistance of concrete to ionic movement under an applied electrical potential difference, they differ in terms of both precision and the time required to complete the test. In most cases, RCPT and SR measurements have nearly perfect correlation *(Rupnow 2011, Jackson 2013)*, but while RCPT takes 24 hours to complete and is prone to testing errors, SR measurements can be taken accurately in seconds.

Electrical resistivity is deemed a reliable indicator of corrosive environments, including concrete suffering from chloride ingress. Researchers have studied the detection of chlorides in concrete using electrical resistivity, how electrical resistivity correlates to chloride transport, as well as how electrical resistivity can serve as an aid in calculating and predicting diffusion coefficients of concrete. Gowers and Millard *(Gowers and Millard 1999)* concluded that the presence of chloride decreases the electrical resistivity of mortar. Electrode spacing was varied for measurements on a mortar specimen subjected to chloride ingress. It was found that numerical results agreed with the experimental results in that measured resistivity was less than true resistivity for larger electrode spacing when compared to the surface layer thickness. The experimental data and theoretical model results are depicted in Figure 2.3. Although mortar with chlorides in its surface layer was studied, no other comments were made as to the effect of chloride ingress at different levels within the surface layer. The specimens were of mortar and not concrete, which may affect electrical resistivity measurement results and analysis.

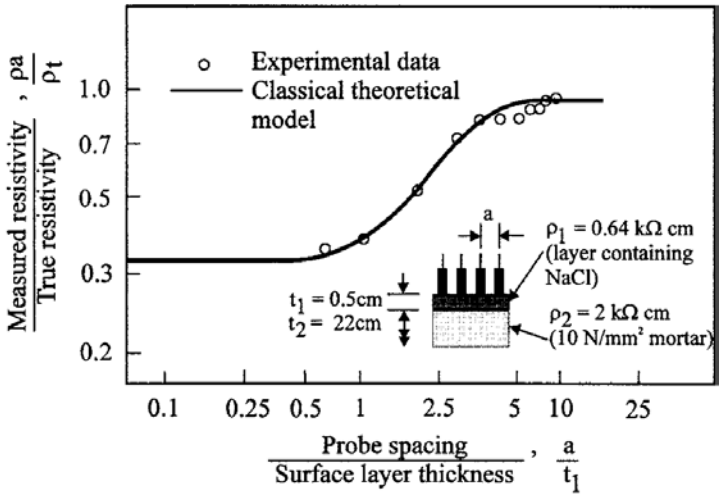

Figure 2.3: Normalized resistivity values over the ratio of probe spacing to surface layer thickness containing chlorides *(Gowers and Millard 1999).*

Polder *(Polder 2001)* suggested recommendations and guidelines for on-site electrical resistivity measurements according to the RILEM TC 154-EMC technical recommendation (2000) as well as how to interpret those measurements. It was stated that resistivity is inversely related to chloride penetration, where low resistivity equates to areas where chloride ingress will be the quickest in concrete. However, Polder stated that the effect of the penetration of chloride ions on electrical resistivity was relatively small. Polder reviewed the literature and emphasized the inverse relationship between chloride diffusion rate and concrete resistivity. Although the relationship between electrical resistivity of concrete and chloride ingress was addressed, the effect of chloride ingress on measured resistivity considering different concrete cover thicknesses was not addressed.

Polder and Peelen *(Polder and Peelen 2002)* readdressed the inverse relationship between chloride ingress and concrete resistivity determined by previous theoretical and experimental studies. They stated that the chloride diffusion coefficient is also inversely related to concrete resistivity. Therefore, low resistivity values will distinguish areas where concrete is more permeable and chloride penetration is higher. It was mentioned again that there is a relatively small effect on electrical resistivity measurements due to the increased chloride content. It was not discussed in detail as to the mechanics behind the effect of chloride ingress at different levels within the concrete cover and no original investigations were conducted to further corroborate the statements on the relationship between electrical resistivity measurements and chloride ingress.

Morris et al. *(Morris et al. 2004)* proposed a relationship to be used to predict chloride threshold values from electrical resistivity measurements taken on the concrete surface. The experimental investigation involved sixteen, 15 cm in diameter by 22 cm in height, cylindrical concrete specimens. These specimens contained four rebar segments positioned so that each rebar was protected by a 1.5 cm concrete cover. The reinforced concrete specimen and chloride profile methodology is displayed in Figure 2.4.

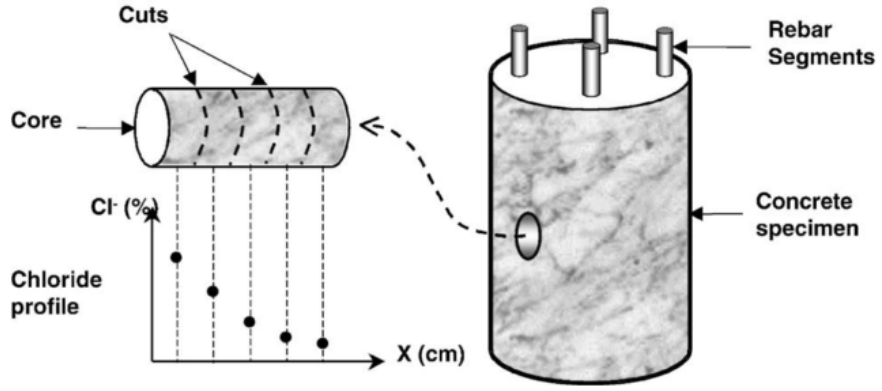

Figure 2.4: Reinforced concrete specimen geometry and chloride profile sample selection *(Morris et al. 2004).*

Each cylindrical reinforced concrete specimen was exposed to 1000 days in a marine environment, where half of the specimens were on the seashore and the other half were immersed in seawater. Periodic electrical resistivity measurements were taken over the exposure period. These electrical resistivity measurements were taken on the side of and in between the rebar segments of each cylindrical concrete specimen. Geometrical effects were accounted for when compiling electrical resistivity measurements. It was observed that the rebar was at a passive behavior for resistivity values greater than 30 kΩ-cm, and at a state of corrosion for resistivity values lower than 10 kΩ-cm. The best line of fit for the relationship between chloride content (which was assumed to be the chloride threshold value, Cl_{TH}), in terms of percent chlorides relative to the weight of cement, and resistivity, r, in terms of kΩ-cm, was expressed by *(Morris et al. 2004)*:

$$\boldsymbol{Cl_{TH}}\ (\%) = \mathbf{0.019}\boldsymbol{r} + \mathbf{0.4} \qquad \textbf{(2.9)}$$

From the data collected, Morris et al. *(Morris et al. 2004)* concluded that resistivity measurements were a good indicator of concrete quality, and that the inverse relationship between chloride ingress and concrete resistivity stands. Because the study involved cylindrical specimens rather than reinforced concrete slabs where rebar mesh is present, chloride ingress for bridge decks is not closely simulated, and achieving more than one probe configuration with respect to rebar is not possible. Therefore, results from this study may differ for reinforced concrete bridge decks where chloride ingress is sourced from deicing salts and is gravity fed.

Torres-Luque et al. *(Torres-Luque et al. 2014)* reviewed the literature for the ability, advantages, and disadvantages of destructive and nondestructive test methods, including electrical resistivity, to measure chloride ingress in concrete in the laboratory and on-site. The researchers summarized that electrical resistivity is sensitive to chloride presence. It was reviewed that the presence of chloride can increase electrical current and reduces concrete resistivity, and that electrical resistivity measurements could be used to determine chloride diffusion coefficients by estimating chloride profiles. Electrical resistivity using the Wenner probe method was found to

be a durable test device in that the embedded parts are manufactured with durable materials such as stainless steel and do not have to be embedded into the structure for testing. Challenges for the development of nondestructive devices were summarized to be the independence of environmental actions such as temperature and moisture condition, the independence of geometry, such as embedded rebar and edges, multi-measurement ability to account for different environmental conditions, and chemical stability, durability and maintainability, as well as cost. Although the literature was reviewed, it was not described in detail how sensitive electrical resistivity is to the presence of chloride ions, or how the transport of chlorides affects measurements. Further, electrical resistivity was not stated to be useful in calculation of the free chloride concentration.

Andrade et al. *(Andrade et al. 2014)* introduced a factor to be applied to electrical resistivity measurements conducted with a four-point Wenner probe to account for the retardation of chloride penetration due to the chloride reaction or binding with hydrated phases. This chloride-penetration retardation-factor was presented in order to predict a more accurate diffusion coefficient of concrete. An experimental investigation followed by numerical modelling was conducted. The experimental investigation consisted of: 1) cylindrical concrete specimens cured for 28 days, 2) electrical resistivity measurements of the concrete specimens, and 3) subjecting the specimens to chloride ingress to determine diffusion coefficients and if any retardation had occurred. Although the effect on the estimation of the diffusion coefficient was investigated systematically, it was not researched as to how chloride ingress affected electrical resistivity measurements themselves.

2.2.4 Relationship between Electrical Properties and Corrosion in Concrete

The four main types of general deterioration for reinforced concrete are reinforcement corrosion, delamination, vertical cracking, and concrete degradation *(Gucunski et al. 2013)*. Because corrosion is such a common issue in structures undergoing life span assessments, research about identifying corrosion using nondestructive techniques is necessary.

Although electrical resistivity is an efficient indicator of concrete durability, the only standardized test method for corrosion monitoring is the ASTM C876 half-cell potential mapping technique. Even though ASTM C876 provides the probability of corrosion for a certain point on the reinforced concrete structure, it does not provide for the corrosion rate of the reinforcement, which is an important piece of information when gaging the remaining service life span of a structure. If the probability of corrosion is high, but the corrosion rate is very slow, the half-cell potential mapping is concluding a false sense of urgency for repair, when in fact the remaining service life span of the reinforced concrete structure is not being cut short. In the opposite sense, if the corrosion rate is accelerating quickly, but the corrosion probability is read to be low, the half-cell potential testing provides a false indication of the remaining service life span of the structure. Therefore, the appropriate maintenance actions are not taken in order to resolve the first signs of detrimental corrosion to insure the safety of the public, and provide potential cost savings due to repairs made before corrosion is destructive.

Studies have corroborated the inverse relationship between corrosive environments in reinforced concrete and electrical resistivity measurements of concrete. As the severity of reinforcement corrosion increases, the electrical resistivity of concrete decreases. However, the effects of the

presence of corrosion on electrical resistivity measurements have not been thoroughly investigated. Many researchers have stated the relationship of corrosion and electrical resistivity, such as Morris et al. *(Morris et al. 1996)* who had mentioned how electrical resistivity of concrete correlates with the possibility of corrosion macrocell currents of the embedded reinforcement.

Carino *(Carino 1999)* reviewed the literature and provided an overview of nondestructive techniques, including concrete resistivity, in identifying the status of corrosion in reinforced concrete structures. Concrete resistivity was considered one of the controlling factors for corrosion rate. Thereby, the use of half-cell potential measurements and electrical resistivity measurements in conjunction makes it possible to examine both corrosion probability and corrosion rate. The relationship between concrete corrosion rate and concrete resistivity is shown in Figure 2.5.

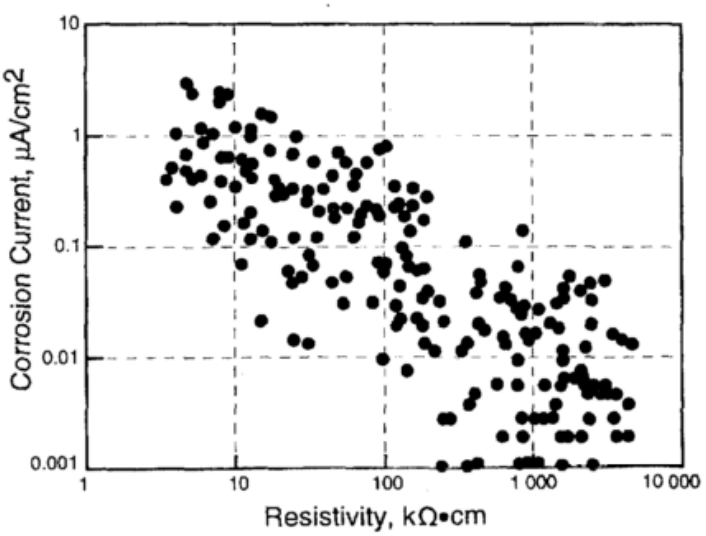

Figure 2.5: Inverse relationship between corrosion current and concrete resistivity from field measurements *(Carino 1999).*

It was reviewed that for a high resistivity value, even if the steel is actively corroding as determined by half-cell potential measurements, the corrosion rate may be low; therefore, when steel depassivates, concrete resistivity correlates better with corrosion rate than half-cell potential. Although Carino *(Carino 1999)* provided a review of the correlation between resistivity and corrosion, no research was stated to examine the effect of corrosion initiation on electrical resistivity measurements.

Polder *(Polder 2001)* also reviewed the literature and provided recommendations for on-site measurements of electrical resistivity on concrete. Contradictory to Carino's review, Polder stated that mapping resistivity measurements did not indicate whether the embedded reinforcement in concrete was actively corroding, and that this information was to be obtained by using other methods. It was stated that resistivity mapping can show where corrosion was most severe. Polder restated the inverse relationship between corrosion rate of reinforcement after depassivation and concrete resistivity, but this relationship could be different for different concrete compositions. Polder was skeptical of the clear relationship between corrosion rate and

concrete resistivity, but provided a general guideline when interpreting electrical resistivity measurements in terms of corrosion risk when applied to ordinary Portland cement concrete at 20 degrees Celsius, as seen in Table2.2.

Table 2.2: Concrete resistivity and risk of corrosion of steel reinforcement *(Polder 2001)*

Concrete Resistivity (kΩ-cm)	Risk of Corrosion
<10	High
10-50	Moderate
50-100	Low
>100	Negligible

For values less than 10 kΩ-cm, risk of corrosion was stated to be high, rather than corrosion rate. Although a general rule of thumb was provided for interpreting electrical resistivity values for concrete when assessing corrosion risk, it was not reviewed as to how corrosion initiation itself affects electrical resistivity and the relationship between corrosion rate and electrical resistivity is deemed questionable *(Polder 2001)*.

Morris et al. *(Morris et al. 2002)* evaluated the risk of corrosion of reinforcing steel using electrical resistivity measurement by immersing reinforced concrete specimens in a saline solution. Corrosion possibilities were identified by half-cell potential measurements. It was suggested that the steel reinforcement is likely to reach a corrosion state when resistivity measurements are lower than 10 kΩ-cm, and reach a passive state when resistivity measurements are higher than 30 kΩ-cm. The corrosion state resistivity confirmed Polder's review *(Polder 2001)*, but Morris et al. *(Morris et al. 2002)* recorded a lower passivation resistivity value than Polder. Morris et al. confirms that the corrosion rate depended primarily on the concrete quality and initial chloride concentration, and that electrical resistivity is a good indicator of corrosion risk rather than of corrosion rate. Again, the effect of corrosion initiation on electrical resistivity measurements was not studied and error corrections were not suggested.

Polder and Peelen *(Polder and Peelen 2002)* confirmed the inverse proportionality between corrosion rate and concrete resistivity, and cautions that this relationship is dependent on concrete composition. It was stated that low resistivity values are associated with relatively high corrosion rates after embedded rebar depassivate. Polder and Peelen found that resistivity measurements of concrete reflect its properties in conditions such as chloride ingress, corrosion initiation and corrosion propagation. Corrosion initiation was referred to as the probability of corrosion and corrosion propagation was referred to as corrosion rate. This contradicted Polder's *(Polder 2001)* previous study that resistivity is an indicator of corrosion risk and not corrosion rate. Corrosion initiation with respect to electrical resistivity was indicated, but no relationship or effect was developed or elaborated upon.

Gulikers *(Gulikers 2005)* stated how it is very likely that concrete resistivity (specifically of the layer directly near the steel reinforcement rather than the entire concrete cover) plays a decisive role in controlling corrosion rates of embedded reinforcement due to microcell geometric arrangements of anodic and cathodic sites. Gulikers also suggested that concrete resistivity does not inherently control the overall corrosion cell resistance, but rather cathodic activation controls in most cases, whereas in other situations, oxygen diffusion controls where concrete is

continuously exposed to wet conditions. Because alternating areas of passively and actively corroding reinforcement will be present in reinforced concrete, the active and passive macrocells will complicate interpretations of half-cell potential and corrosion rate measurements. Gulikers suggested that electrical resistivity may not be the only indication of corrosion rate, but did not review how corrosion initiation may influence electrical resistivity readings and interpretations.

Song and Saraswath *(Song and Saraswath 2007)* reviewed the literature and stated the inverse relationship between concrete resistivity and embedded reinforcement corrosion rate. However, it was found that the evaluation of the degree of rebar corrosion was different amongst researchers. They stated how electrical resistivity was an effective identifier of corrosion risk of reinforcement, especially when corrosion is chloride induced. A table was provided to relate resistivity to corrosion risk in order to assess resistivity measurements as depicted in Table 2.3.

Table 2.3: Concrete resistivity and risk of corrosion of steel reinforcement *(Song and Saraswathy 2007)*

Concrete Resistivity (kΩ-cm)	Corrosion Risk
<5	Very High
5-10	High
10-20	Low
>20	Negligible

The relationship between corrosion risk and resistivity Song and Saraswath *(Song and Saraswath 2007)* provided was different from what Polder *(Polder 2001)* provided where resistivity values were considerably lower for all corrosion risk levels, and a moderate corrosion risk was not provided. Song and Saraswath *(Song and Saraswath 2007)* suggested that for resistivity values less than 5 kΩ-cm, the corrosion risk is very high, and that for resistivity values greater than 20 kΩ-cm, the corrosion risk is negligible. Corrosion rate and corrosion risk were both referred to within this review, but no clear indication of which resistivity values have a better correlation with was not given. Although relationships between corrosion and resistivity were suggested, how corrosion initiation affects resistivity measurements was not indicated.

Dunn et al. *(Dunn et al. 2010)* evaluated multiple nondestructive techniques in assessing concrete bridge decks including electrical resistivity. Dunn et al. confirmed that electrical resistivity provides information for the potential for a corrosive environment within areas of reinforced concrete, but did not indicate the relationship between resistivity and corrosion rate of embedded reinforcement or the effect that corrosion initiation may have on electrical resistivity measurements.

A commercial Wenner probe instrument manual *(Proceq 2011)* provided two different ways in which electrical resistivity measurements can be evaluated within its instruction manual for its four-point Wenner probe devices. One was for the estimation of the likelihood of corrosion and the other is the indication of corrosion rate shown in Table 2.4.

Table 2.4: Concrete resistivity and likelihood of corrosion of steel reinforcement (a) and indication of corrosion rate (b) *(Proceq 2011)*

Estimation of the Likelihood of Corrosion (a)	
Concrete Resistivity (kΩ-cm)	**Corrosion Risk**
≤ 10	High
10-50	Moderate
50-100	Low
≥ 100	Negligible
Indication of Corrosion Rate (b)	
Concrete Resistivity (kΩ-cm)	**Corrosion Rate**
<5	Very High
5-10	High
10-20	Low
>20	Negligible

In contrast to Song and Saraswath *(Song and Saraswath 2007)*, the commercial probe instrument manual *(Proceq 2011)* indicated that the lower resistivity values do not relate to corrosion risk, but rather corrosion rate, where Polder's values relate to corrosion risk *(Polder 2001)*. The discrepancy between the relationship between concrete resistivity and corrosion risk or corrosion rate is further convoluted. No suggestions as to how to correct electrical resistivity measurements for errors when corrosion is present, as well as other factors, was given within the instruction manual.

Du Plooy et al. *(Du Plooy et al. 2013)* reiterated, after reviewing the literature, how solely using electrical resistivity will not conclude the determination of the initiation of corrosion for a reinforced concrete slab due to the number of variables influencing its response. It was suggested that more than one nondestructive test be used in order to garner a more accurate assessment of the structure under evaluation.

Gucunski et al. *(Gucunski et al. 2013)* reviewed the literature on electrical resistivity and other nondestructive techniques for their applications and limitations. The primary application of electrical resistivity was found to characterize corrosive environments within reinforced concrete structures and areas susceptible to chloride ingress, as well as an effective indicator of corrosion activity when paired with half-cell potential measurements. Its limitations were listed that the interpretation of electrical resistivity measurements is challenging in that there are many variables that can affect measurements, such as moisture condition, salt content, etc. How each specific variable affects the overall measurement was difficult to assess. Pre-wetting of the concrete surface was also found to be a limitation in that added preparation was needed in order to conduct electrical resistivity measurements; therefore, more time was needed to conduct the measurements.

Along with a review of the literature, Gucunski et al. *(Gucunski et al. 2013)* conducted an experimental investigation to assess rebar corrosion within a concrete bridge deck using three technologies, one of which is electrical resistivity. The evaluation was based on how well the devices were able to differentiate the area constructed with new rebar and the area constructed with corroded rebar. The detection of the degree of rebar corrosion was not assessed but rather

corrosion activity, corrosion rate and the determination of a corrosive environment. A limitation was found in evaluating corrosion activity and corrosion rate of epoxy-coated rebar. Measurements were collected, but interpretations of measurements with regard to epoxy-coated rebar were not available. It was stated that electrical resistivity is not affected by epoxy coating within the deck, but no further evidence is provided. It was suggested that electrical resistivity or half-cell potential measurements should be used when evaluating deterioration caused by corrosion due to their low cost, relative speed and simplicity. They report that the advantage that electrical resistivity has over half-cell potential is the lack of the need to obtain an electrical connection to embedded reinforcement, although the information obtained from half-cell potential may be of greater importance to certain agencies. Although corrosion was detected, Gucunski et al. *(Gucunski et al. 2013)* lacks the investigation on the degree of corrosion, which, as they stated, is of interest when assessing corrosion in structures.

Sadowski *(Sadowski 2013)* reviewed the literature and found that there were few papers that determined the probability of corrosion by coupling electrical resistivity and half-cell potential techniques to gain perspective on the degree of reinforcement corrosion in concrete. Sadowski also noted that it was difficult to find a systematic methodology when assessing corrosion probability. It was suggested that using electrical resistivity conducted with a four-point Wenner probe and half-cell potential techniques, the following methodology should be used when interpreting measurements as seen in Figure 2.6. Although a systematic analysis of results was suggested by Sadowski, no correction factors were suggested for electrical resistivity measurements for corrosion conditions. Only identifying the probability of corrosion was suggested when conducting a corrosion assessment *(Sadowski 2013)*.

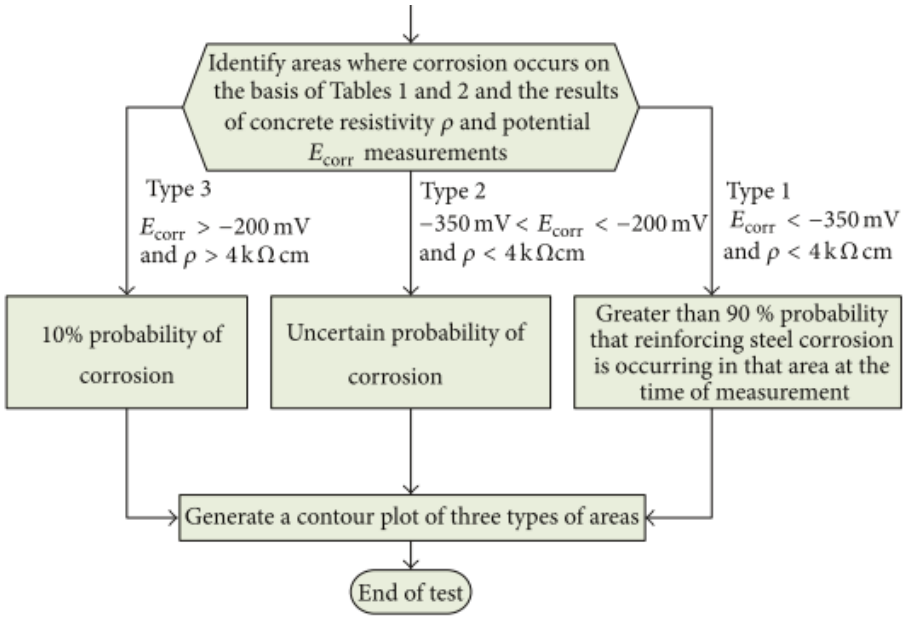

Figure 2.6: Suggested methodology when assessing four-point Wenner probe electrical resistivity and half-cell potential measurements *(Sadowski 2013)*.

Hornbostel et al. *(Hornbostel et al. 2013)* reviewed the literature for the relationship between corrosion rate of embedded reinforcement and concrete resistivity. They confirm the inverse

relationship between concrete resistivity and corrosion rate, not risk. The discrepancies within the literature was summarized and included: (1) the large range and scatter for correlations between corrosion rate and concrete resistivity for resistivity measurements assessments, (2) corrections to corrosion rate measurements may not have been applied, (3) graphical data was not consistent between investigations to show relationships, (4) large scatter of data and few investigations on the effect of moisture state and temperature on the corrosion and resistivity relationship, (4) the lack of investigation of the effect of the cause of corrosion on the corrosion and resistivity relationship, and (5) the lack of knowledge on which mechanism dominates the corrosion process and how this influences resistivity measurements. It was suggested that more field data should be collected and analyzed to assess the corrosion and resistivity relationship, and that; overall, the relationship between corrosion rate and resistivity should be investigated further.

2.3 OTHER CONSIDERATIONS

2.3.1 Bound and Free Chlorides

When chloride ions travel through the concrete matrix, some ions may become bound physically and chemically to the hydration products of the binder in the concrete. If enough chlorides are present, the free chlorides can eventually reach the surface of the reinforcing steel, and once they reach a certain concentration on the surface, corrosion can initiate. The ability to measure free and bound chloride concentrations, therefore, is crucial in understanding the corrosion risks of a certain structure. Research has been done on quantifying the chloride binding process in ordinary Portland cement (OPC) mixtures because this would enhance the ability to predict the duration or service-life of concrete structures exposed to marine environments or de-icing chemicals, as well as find ways to decrease the amount of chlorides reaching the steel surface. According to Neville *(Neville 1996)*, from "Properties of Concrete", the main form of chemical binding of chloride ions is through the reaction of the cement compound tricalcium aluminate, C_3A, and the formation of Friedel salt. A similar reaction with the cement compound tetracalcium aluminoferrite, C_4AF, results in calcium chloroferrite. From the stoichiometry of these reactions, it can be calculated that one gram of C_3A will consume 0.263 grams of chloride, while one gram of C_4AF will consume 0.146 grams of chlorides. The testing procedures for determining free chlorides are very time-consuming and intricate. ASTM C1218 is the most commonly used testing procedure for finding concentrations of water-soluble chlorides, which can represent the amount of free chlorides. ASTM C1152 standard provides the acid soluble chloride concentration, which is also known to provide the "acid soluble chloride" concentration, which is an indicator of total chlorides. The values are typically shown in chloride percentage by weight of cement. In a study done by Sirivivatnanon et al. *(Sirivivatnanon 2012)*, chlorides were tested using both, acid soluble and water-soluble methods following ASTM C 1202 and ASTM C1218 respectively. This study concluded that the extractive techniques and level of aggressiveness determine the type and amount of chlorides. It was found that the aggressive solvents and surface area of the materials tested controlled the amount and type of chlorides extracted. The use of boiling water on materials passing an 850-micron sieve offered the most accurate amount of free chloride content. This is important to establish since quantifying chloride content, for either total or free chlorides, is a very delicate procedure. Once the accurate chloride content is determined, the appropriate corrosion mitigation techniques can be made.

2.3.2 De-icing Solutions

In environments where F-T action is common, DOTs can remove ice off the surface of the concrete by plowing, using deicers, and anti-icers (2004). The DOTs either use anti-icing agents, which lower the freezing point so that when precipitation falls, it does not freeze, or use de-icing chemicals on the roads to decrease the freezing point, melting any ice formed on them, allowing vehicles to drive safely. This practice of applying salts to roads during freezing weather was first implemented in the 1930s *(Lord 1988)*, and since then, numerous types of de-icing chemicals have been developed to provide safe travel conditions. Some of the more common de-icing chemicals used today, based on the FHWA manual of practice for an effective anti-icing program include sodium chloride (NaCl), calcium chloride ($CaCl_2$), and magnesium chloride ($MgCl_2$).

While the use of de-icing chemicals has proven to be effective, these chemicals are harmful to the environment and to the reinforcing steel in concrete structures. Environmental concerns regarding the use of de-icing chemicals, according to Lord, *(Lord 1988)*, include drinking water contamination and degradation of habitats surrounding areas where salt accumulates from runoff. These chemicals also have a detrimental effect on structures. The corrosion of structures, specifically bridge decks, has been of high concern for the last few decades. Corrosion occurs when chlorides from de-icing chemicals infiltrate the concrete and reach the steel reinforcement. A study by Conciatori *(Conciatori 2008)*, determined that chloride ingress was controlled mainly by the concentration of the de-icing chemicals the composition of the concrete, due to the density and permeability of the materials used *(Jaegermann 1990, Hong 1999)*, and by the weather conditions. Weather conditions are vital when analyzing the chloride ingress since cyclic wetting and drying environments promote a faster rate of chloride ingress *(Hong 1999, Ji 2009)*. Hot weather also influences the rate of ingress. A study performed by Yuan *(Yuan 2008)*, evaluated the temperature effect on migration of chlorides. The results showed that the greater the temperature of the concrete, the greater the diffusion coefficients. They also concluded that the chloride penetration, while influenced by temperature, did not change the chloride profile trends. Once the chlorides build to a critical level, corrosion of the reinforcing steel can initiate. Various studies have concluded that concrete, that is saturated with deicer solutions, undergoing F-T cycles shows considerable deterioration including mass change, expansion, decrease in dynamic modulus of elasticity, and increase in permeability *(Sutter et al. 2008; Cody et al.1994; Cody et al. 1996; Mussato 2004; Kozikowski et al. 2007)*. These studies concluded that the magnesium chloride ($MgCl_2$) deicer solution physically and chemically reacted with hardened cement paste at a fast rate and performed poorly in various durability tests when compared to the other de-icing solutions. Interestingly, samples that were saturated with MgCl2 solution did not show significant salt scaling, which was contrary to expectation. These samples showed similar scaling to the specimens saturated with other de-icing solutions.

2.3.3 Freeze-Thaw (F-T) Action

Concrete exposed to F-T action can deteriorate at a rapid rate due to water expansion in the concrete pores. According to the Portland Cement Association (PCA) *(Kosmatka et al. 2011)*, water expands around 9% when frozen. When the water in the concrete matrix freezes, the expansion provides internal tensile forces that cause cracks. These cracks continue to escalate with continuous freezing and thawing action. F-T cycles also cause scaling and spalling on the

surface of the concrete. The bond between the aggregate and the paste weakens and causes the aggregates to separate causing “pop-outs”. The most effective way to protect concrete from F-T deterioration is to develop a proper air entrainment system. Air-entraining admixtures provide evenly distributed air voids throughout the concrete matrix to alleviate internal or localized tensile forces that create cracks in the concrete during F-T cycling. In order to determine if a concrete sample has adequate protection from F-T action, the standard test method ASTM C666 can be used to test the resistance of concrete to rapid freezing and thawing. This test method can be utilized when the concrete samples undergo rapid freezing and thawing in water, or freezing in air and thawing in water. Regardless of the type of environment in which the samples are placed, they undergo 300 F-T cycles or the number of cycles until the original relative dynamic modulus is reduced below 60%. This test method states that the specimens’ mass needs to be recorded and tested for fundamental transverse frequency every 36 cycles.

There is a gap in literature for relating SR to F-T action. One group was able to use electrical resistivity to assess frost damage *(Wang et al. 2014, 2015).* Wang showed that as temperature decreased, electrical resistivity increased, and as F-T cycles continued, the resistivity continued to increase. This increase was attributed to frost damage that was progressively resulting in more micro fracturing of the concrete and thus a loss of connectivity within the specimen. Frost damage was also confirmed by the loss of strength and visible cracks on their specimens. No literature specifically regarding SR values with chloride ingress and F-T action was found, which is of great concern since de-icing chemicals are used only in environments in which F-T occurs.

3.0 EXPERIMENTAL PROGRAM

3.1 BACKGROUND

This chapter presents the details of the experimental program conducted as part of this project. It starts with the description of the materials and reinforces concrete slabs used in the investigation. The exposure conditions and F-T testing regime are presented. The chapter is concluded with the test methods used to monitor the changes and environmental conditions of the exposed slabs.

3.2 MATERIALS

The experimental study involved continuous monitoring of SR measurements, temperature, relative humidity, and chloride ingress of reinforced concrete slabs that were cast at the Oregon State University Outdoor Exposure Site. The slabs were designed to represent bridge decks commonly used by Oregon Department of Transportation (ODOT) in Oregon from 1960s to present. Based on concrete mixture properties from three different periods, twenty slabs were cast and investigated. Slab Type 1 (ST1), composed of twelve air-entrained slabs designed per 1960s specifications, Slab Type 2 (ST2) consisted of three non-air-entrained slabs designed per 1960s specifications, Slab Type 3 (ST3) were two air-entrained slabs designed per 1990s specifications and slab Type 4 (ST4) consisted of three air-entrained slabs designed per current specifications.

3.2.1 Concrete

The concrete mixtures were ordered from a local ready-mix concrete plant. The six concrete mixtures were used to construct six different slab types. These are representative of Oregon bridge decks that have been built in the past six decades. The mixture proportions for each concrete type are included in Table 3.1. Slab Type 1 (ST1) contained a Type I/II ordinary Portland cement (OPC) concrete mixture with no supplementary cementitious materials (SCMs) as per 1960s specifications. It should be noted that 1960s specifications did not specify w/cm but define the mixture using specified workability requirements. A range of w/cm values (ST1-A, ST1-B, ST1-C) were investigated for concrete of this era and are depicted in Table 2.1. Slab Type 2 (ST2) was also cast with the same OPC as the ST1 specimens but without air entrainment; these slabs represent non-air-entrained bridge decks from the 1960s. Slab Type 3 (ST3) represents bridges from the 1990s; this concrete mixture is an air-entrained concrete with 20% Class F fly ash replacement. Slab Type 4 (ST4) represent modern air-entrained high performance mixture (HPC) which contained 30% Class F fly ash and 4% silica fume. The chemical compositions of OPC, fly ash and silica fume used in this study are provided in the appendix. The coarse aggregate used was rounded river rock with a gradation that ranged from 3/4-inch (1.91 cm) to 0.187 inches (.475 cm). The fine aggregate used was natural sand with a fineness modulus of 3.02 and a gradation that ranged from 0.187 inches (.475 cm) to 0.0059 inches (0.0149 cm). Detailed information on the gradation of the coarse and fine aggregates is found in the Appendix.

Table 3.1: Fresh properties and six concrete mixture designs used in this study.

	ST1-A	ST1-B	ST1-C	ST2	ST3	ST4
w/cm	0.60	0.40	0.47	0.53	0.35	0.43
Measured slump, in (cm)	9.5 (24.1)	1.25 (3.2)	6.25 (15.9)	5.5 (14.0)	3.25 (8.3)	3.5 (8.9)
Measured air (%)	9	3.25	5	1	3	2.5
Measured unit weight,	132.1	145.9	142.16	148	147.52	145.88
lb/ft^3 (kg/m^3)	(2116.0)	(2337.1)	(2277.2)	(2370.7)	(2363.0)	(2336.8)
Cement, lb (kg)	525	528	512	515	510	461
	(238.1)	(239.5)	(232.2)	(233.6)	(231.3)	(209.1)
Fly ash, lb (kg)	0	0	0	0	129 (58.5)	204 (92.5)
Silica Fume, lb (kg)	0	0	0	0	0	25 (11.3)
Water, lb (kg)	317	209	240	275	222	300
	(143.8)	(94.8)	(108.9)	(124.7)	(100.7)	(136.1)
3/4" - No.4, lb	1693	1688	1690	1693	1753	1714
(19.1 mm – 4.76 mm (kg)	(767.9)	(765.7)	(766.6)	(767.9)	(795.1)	(777.5)
Sand, lb (kg)	1133	1456	1196	1401	1306	617
	(513.9)	(660.4)	(542.5)	(635.5)	(592.4)	(279.9)
Total, lb (kg)	3668	3881	3638	3884	3920	3321
	(1663.8)	(1760.4)	(1750.2)	(1761.8)	(1778.1)	(1506.4)

Fifteen 4-inch by 8-inch (10.16 cm by 20.32 cm) cylinders were cast from each one of the different mixture types. These cylinders were used for additional mechanical property and performance testing. The slabs and the cylinders were each cured under wet burlap for 28 days after casting. Compressive strength testing \ was performed at 28 and 90 days.

3.2.2 Reinforcement

All slabs were reinforced with #5 (5/8 in, 16 mm) ASTM A615 carbon steel rebar. Historical data on bridge decks show that most decks in Oregon are reinforced with #5 (5/8 in., 16 mm) rebar. Although #4 rebar is also common, previous studies showed that resistivity measurements are not affected by the difference between these two bar sizes *(Salehi 2013)*; therefore, for consistency #5 (5/8 in., 16mm) bars were used. In this research, as shown in Figure2.1, an unreinforced zone was left in each slab for the extraction of cores to be used in bulk resistivity measurements, mechanical testing, and moisture content determination.

Most slabs were reinforced with orthogonal rebar with 8-inch (20.3 cm) center-to-center spacing. Two slabs with 4-inch (10.16 cm) rebar center-to-center spacing were used to verify the results of a parallel investigation. The slabs in this study had either 1-inch (2.54 cm) or 2.5-inch (6.35 cm) concrete cover thickness. Historical data shows that a large number of bridge decks in Oregon have 1-inch (2.54 cm) to 2.5-inch (6.35 cm) concrete covers, and some of these bridge decks are exposed to de-icing chemicals. Therefore, slabs with both a 1-inch (2.54 cm) and 2.5-inch (6.35 cm) cover thickness were investigated. Figure 3.1 shows typical slab dimensions and positioning of the reinforcement.

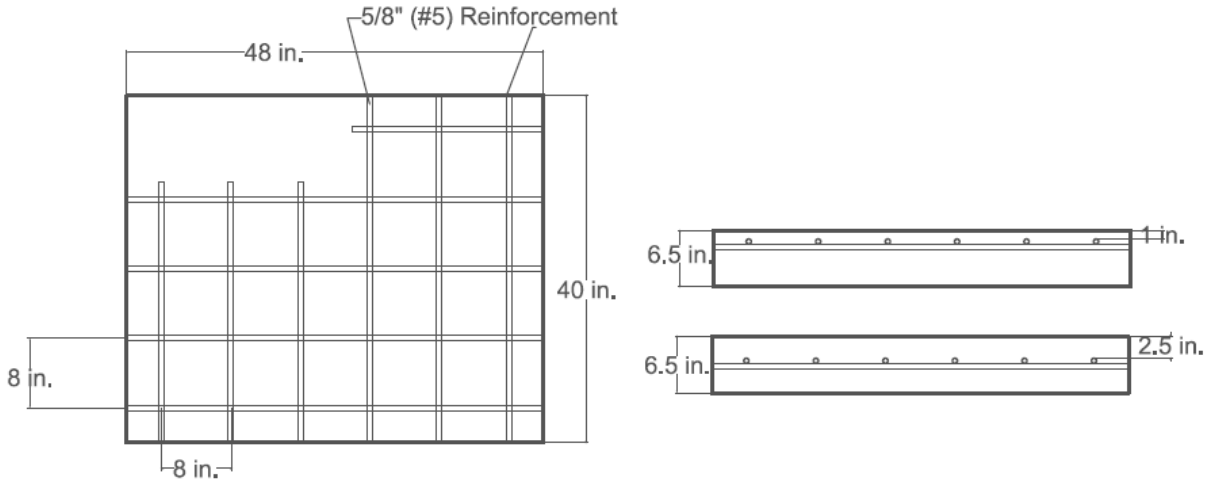

(a)

(b)

(c)

(d)

Figure 3.1: (a) Geometrical details of the concrete slabs; (b) a sample slab with placed reinforcement before casting of concrete; (c) a completed slab ready for ponding; (d) a sample concrete slab during ponding with the deicing solution. The section that is unreinforced was used to take measurements and to extract cores for additional testing.

3.3 EXPOSURE REGIME

3.3.1 Ponding Cycles

After 28 days of wet curing, the slabs were exposed to commercially available 30% magnesium chloride ($MgCl_2$) deicing solution that contained a corrosion inhibitor in alternating wet/dry cycles to increase chloride ingress rates. This is the same deicing solution used by ODOT. The composition and type of the corrosion inhibitor are not disclosed by the supplier; therefore, the inhibitor type is not reported here. In each cycle, the slabs were ponded with the deicing solution for 96 hours. After 96 hours, the deicing solution was removed by vacuum, and then the slabs were exposed to ambient conditions for a 10-day period. The duration of each cycle was decided based on the needs of the project in addition to previous studies that showed this cycling approach increased chloride ion ingress but still remained reasonable compared to field exposure *(Hong 1999)*. After 7 cycles it was determined that chloride ingress was occurring at a higher rate than expected. Control slabs, one for each type of concrete, also had the same ponding regime. However, these slabs were ponded with tap water instead of the de-icing solution. The cycles were postponed for ten weeks after the seven cycles. During this time, the slabs were exposed to the ambient conditions without ponding. After this period, the slabs were exposed to the deicing solution once again continuing the ponding regime.

3.3.2 Internal and Atmospheric Conditions

In-situ Wagner Rapid RH® probes were installed at various depths inside the slabs. These probes measure temperature and relative humidity inside the concrete and data were provided at the time that SR measurements were taken. All control slabs and one slab for each type of concrete had probes thus resulting in 12 slabs having probes. The probes were installed at 1 inch (2.54 cm) and 2.5-inches (6.35 cm) from the surface of the slabs. The depths of the probes were chosen based on practicality. At 1 inch (2.54 cm), it decreased the chance of cracks near the surface. At 2.5-inches (6.35 cm), it provided information regarding the change in temperature and relative humidity with depth compared to the 1-inch probe. Surface temperature was measured with an infrared temperature gun. In addition to these measurements, a weather station continuously collected weather data onsite. This included relative humidity, wind speed, wind direction, precipitation, barometric pressure, etc. This data was used to calibrate measurements and provide additional information for the companion modeling study.

3.3.3 Freeze-Thaw (F-T) Exposure

Three slabs (ST1-C, ST2, and ST4) were exposed to F-T cycling. Slab type A (ST1-C), and slab type B (ST2) were slabs designed from 1960's specifications, which used ordinary Portland cement (OPC) concrete with no supplementary cementitious materials. ST2 was not air-entrained. Slab type C (ST4) was a modern air-entrained HPC mixture with class F fly ash with a CaO content of 13.94% and silica fume at a 30% and 4% replacement of Portland cement, respectively. Mixtures ST1-C and ST4 did not meet the target air-content that was specified, which was 6 percent. Mixture ST4 was dosed with increasing amounts of air entraining admixture with minimal increase in air content. Achieving an adequate air-content in a previous mixture also proved difficult. In that previous case, the air content dramatically increased to 9% after the final dosage. In an effort to avoid that happening, mixture ST4 was used despite not

meeting the target air percentage. Fifteen 4-inch by 8-inch (10.16 cm by 20.32 cm) cylinders were cast from each one of the different mixture types. These cylinders were used for additional mechanical property and performance testing.

These slabs went through eight de-icing solution ponding cycles before they were exposed to F-T. The concrete slabs were exposed to 300 F-T cycles commensurate with ASTM C666 Procedure B. The cycles were divided into five segments of 60 cycles per each segment. Each F-T cycle involved 1 hour of freezing at 3.2°F (-16°C) and 1 hour of thawing at 60.8°F (+16°C) with a 30-minute temperature increase or decrease in between. The goal of this regime was to achieve an approximate cycling range of 14°F/+50°F (-10°C/+10°C) at 1.5-inch (3.81cm) depth. Each F-T exposure period started at the end of a de-icing ponding cycle and lasted eight days before the slabs were placed back into ambient conditions where they underwent three additional ponding cycles in between each F-T exposure. Concrete cylinders, made from the same concrete as the slabs, were subjected to F-T cycles following ASTM C666 in a Scientempt F-T chamber for 300 cycles and were compared to additional cylinders that were placed in the F-T environmental chamber with the slabs. ASTM C666 standard provides two procedures for testing. Procedure A requires that the specimens undergo freezing and thawing submerged in water. Procedure B requires specimens to undergo freezing in air and thawing in water. To keep the environment consistent between the slabs and the cylinders, the cylinders followed the ASTM C666 went through a wet thawing and dry freezing exposure (Procedure B). The cylinders were conditioned by saturating them in a fog room until their saturated surface dry mass stopped increasing.

3.4 TESTING METHODS

The concrete slabs, cylinders, and cores that were extracted from the unreinforced zone of the slabs went through various tests throughout the duration of the project. The tests that were performed on concrete slabs, cylinders, and cores are described in the following sections.

3.4.1 Mechanical Testing

Compressive strength of cylindrical concrete specimens was measured after 28 days and 90 days following ASTM C39.

3.4.2 Moisture Content

Moisture content of concrete cores were determined from select slabs at select times by taking cores with a handheld core drill and oven drying the cores to determine the free water content inside the concrete matrix. In addition, a side study was performed on wet coring to determine if dry coring to affects the water content when using a coring drill. Six cores 3-inches (7.62 cm) in diameter were taken from a concrete slab; three cores were dry cored and three were wet cored. The samples were then cut into 2- inch (5.08cm) sections to establish moisture-content in relation to depth. The wet samples were surface dried and the mass was recorded for all the samples taken. The samples were then placed in an oven at 230° Fahrenheit (110 °C) for 24 hours and the mass was recorded once again. The evaporable moisture content of the concrete samples was then determined. Once the study was completed, cores were taken from each type of concrete in two different occasions to determine the evaporable moisture content of the

concrete slabs. Cylinders that were cast with the slabs were also tested for moisture content. Three cylinders from each type of concrete were placed in a fog room the mass did not increase. Once the cylinders were fully saturated, they were placed in an oven at 230° Fahrenheit (110 °C) for 24 hours and the mass was recorded once again. The evaporable moisture content of the concrete samples was then determined.

3.4.3 Chloride Profiling

Chloride profiling was performed on each slab at various ages using a field profile grinder. There were nine possible chloride-profiling sites on each slab due to the location of rebar and the unreinforced zone. Collected powders were analyzed for acid soluble and water soluble chloride content following ASTM C1152 and ASTM C1218 respectively and profiles were generated for determination of chloride transport properties per ASTM C1556. After each chloride profile was taken, the area where the grinding occurred was sealed with a commercial self-consolidating, shrinkage compensating, concrete repair material that is also used by ODOT.

3.4.4 Surface Resistivity Measurements

SR measurements were taken using a four-point Wenner probe at two locations on the slab surface. Five readings were taken on the unreinforced section of the slabs and five readings were taken on the reinforced section. The median value was taken for each set of measurements as suggested by the RILEM TC-154 *(Andrade et al. 2004)*. When taking SR measurements in sections where rebar was present, the probe was oriented perpendicular to the topmost rebar and parallel to the bottommost rebar. The orientation of the probe and procedure was decided following the study performed on probe orientation *(Morales 2015)*. Because these measurements were rapid, they were performed weekly or bi-weekly, depending on the ponding cycles, they were taken when chloride profiles were performed and they were taken half way through the dry period of the ponding cycle for consistency.

3.4.5 Bulk Electrical Conductivity/Resistivity

Bulk resistivity was measured after every 36 cycles on the cylinders undergoing F-T cycles following ASTM C1760. The values obtained from bulk resistivity measurements were used to validate and compare the SR measurements of the cylinders. Bulk resistivity was done using the Giatec RCON electrical resistivity meter and manufacturer's recommendations were followed when testing concrete cylinders.

3.4.6 Resonant Frequency Test ASTM C215

Resonant frequency, using the transverse method, was measured every 36 cycles on cylinders undergoing F-T cycles per ASTM C215. Concrete's resonant frequency is directly related to the dynamic modulus of elasticity, which can decrease if there is degradation of the concrete during F-T testing.

4.0 EXPERIMENTAL RESULTS

4.1 BACKGROUND

This chapter reports the results of the experimental program. It is divided in two major sections. In the first section, the relationship between chloride ingress and electrical properties of concrete are investigated for reinforced concrete slabs that are exposed to several ponding cycles of the de-icing chemical. In the second part, the role of F-T action on such relationship is presented. In both cases, water-ponded slabs were used as control cases. The role of environment conditions during de-icing chemical application is discussed.

4.2 CHLORIDE INGRESS AND ELECTRICAL PROPERTIES

As discussed in the literature review, electrical properties of concrete (such as electrical resistivity of formation factor) are affected by the microstructure development, the degree of saturation of the pores, temperature, and the chemistry of the pore solution. During curing, and in the stages of service, it is expected that the electrical resistivity of concrete increases. During this stage, the electrical properties are also expected to be more sensitive to the changes in relative humidity and moisture content within concrete. When chloride-containing salts start penetrating into concrete, some is bound into the hardened matrix and the rest remains in the pore solution. The effect of chloride binding and presence of free chloride ions in the pore solution might affect the electrical properties differently. For example, the former would increase the electrical resistivity of the matrix, while the latter would decrease the electrical resistivity of the pore solution. However, in later stages, as the binding capacity of concrete is reached, the effect of chloride ingress into concrete should correspond to a decrease in overall electrical resistivity of the medium. This experimental investigation is intended to show these relationships for the reinforced concrete slabs investigated in this research program.

4.2.1 Compressive Strength

Compressive strength of cylindrical concrete specimens was measured after 28 days and 90 days following ASTM C39. Table 4.1 shows the compressive strengths of the six types of concrete used in this study.

Table 4.1: Compressive strengths of the six types of concrete at 28 days and 90 days.

	ST1-A	ST1-B	ST1-C	ST2	ST3	ST4
28 Day, MPa (psi)	12.3	24.4	20.9	28.3	27.8	24.6
	(1784.0)	(3539.0)	(3031.3)	(4104.6)	(4032.0)	(3567.9)
90 Day, MPa (psi)	17.1	27.5	28.3	37.3	34.0	33.1
	(2480.1)	(3988.5)	(4104.6)	(5409.9)	(4931.3)	(4800.7)

Overall, the compressive strengths of all the mixtures were lower than the design strengths. A reason for this can be attributed to the temperature at the time of casting which was 45°F (7.2°C)

and the temperature fluctuated at around 45°F (7.2°C) by ± 10°F (5.5°C) over their wet curing time since the slabs were cast outside. ST2 mixture had the highest compressive strength, even though its w/cm was 0.53 for ST2 and it did not contain any SCMs, which can be attributed to the fact that it contained no air- entrainment. The slabs with SCMs (ST3 and ST4) had greater compressive strengths than the ST1 mixtures that only contained OPC. Although ST4 was expected to have a higher strength than ST3 due to the addition of silica fume and fly ash, ST3 had a lower w/cm than ST4 (0.35 vs. 0.43), which controlled the strength.

4.2.2 Moisture Content

The evaporable moisture content of the concrete was determined first by using a wet core and a dry core to determine the effect that an outside water source has on the internal moisture of the samples. Table 4.2 shows the moisture content of samples cored with a wet and dry coring drill.

Table 4.2: Comparison of moisture content using a wet coring drill and a dry coring drill.

	Moisture Content (%)	
	Dry Cores	**Wet Cores**
1A 0-2" (0-5.1 cm)	5.6	5.5
1B 2-4" (5.1 – 10.2 cm)	5.6	5.6
1C 4-6" (10.2 – 15.2 cm)	5.0	5.9
Average	5.4	5.7
2A 0-2" (0-5.1 cm)	5.2	5.6
2B 2-4" (5.1 – 10.2 cm)	5.3	5.5
2C 4-6" (10.2 – 15.2 cm)	5.3	5.8
Average	5.3	5.6
3A 0-2" (0-5.1 cm)	5.4	5.9
3B 2-4" (5.1 – 10.2 cm)	5.2	5.7
3C 4-6" (10.2 – 15.2 cm)	-	5.8
Average	5.3	5.8

It can be observed from that the core extraction techniques did not significantly affect the moisture content of concrete significantly. The moisture content of the samples remained 5 to 6% regardless of the depth or the extraction method used. The difference between the two methods was negligible and it was determined that wet coring, being the most practical method, was an accurate and acceptable technique to use on the concrete slabs. Therefore, subsequent cores were taken from each type of concrete after five ponding cycles and after 14 ponding cycles using the wet coring method. The w/cm plays an important role in the porosity and transport properties of the concrete and this can be seen in Table 4.3, which shows the moisture content from six different types of concrete.

Table 4.3: Moisture content taken from extracted cores corresponding to each type of concrete that underwent 5 and 14 de-icing solution ponding cycles.

	Moisture content (%)	
	After 5 Cycles	After 14 Cycles
ST1-A	8.2	6.5
ST1-B	7.1	5.4
ST1-C	7.3	5.0
ST2	7.5	5.4
ST3	6.0	4.3
ST4	6.8	4.9

The moisture of the concrete after five ponding cycles decreased in order of w/cm for all cases except for ST4, the modern HPC concrete, which had the second lowest moisture content. ST1-A having a w/cm of 0.6, had the highest moisture at 8.2% and ST3, having a w/cm of 0.35, had the lowest at 6.0%. While the moisture content did decrease with decreasing w/cm, the difference between all the moistures of ST1 and ST2, which only contained OPC, is negligible. However, there is a clear difference when comparing the OPC mixtures with the mixtures containing SCMs, which show that the use of SCMs provide a less porous concrete matrix. The moisture of the concrete decreased in all cases as the concrete slabs continued to undergo cycling ponding, After 14 ponding cycles, the ST1-A specimen still contained the highest amount of moisture, and ST3 had the least amount of moisture, 6.5% and 4.9% respectively. The decrease of moisture is attributed partly to the continuing microstructure formation, high increasing ambient temperatures (owing to seasonal change) and the presence of Magnesium Chloride which absorbs water into its structure.

4.2.3 Chloride Profiles

Acid soluble chloride profiles were taken periodically throughout the ponding cycles. Figures 4.1 shows the acid soluble chloride profiles for all six types of concrete at the end of the 14th and the 20th ponding cycles. From this figure, it is clear how important of a role the w/cm and porosity have on chloride ingress: the higher the w/cm, the greater the chloride ingress. This can be supported by various studies which prove that a decrease in w/cm increases resistance to chloride penetration. Since the porosity of concrete is mainly governed by the w/cm, hence the effect of the observed w/cm on the amount of chlorides. Two types of concrete mixtures in this study contained SCMs. ST3 contained 20% replacement of cement with fly ash and ST4, the modern high performcen concrete mixture, contained 4% and 30% of silica fume and fly ash, respectively. From Figure 4.1, it is clear that both ST3 and ST4 have lower chloride contents than other mixtures which contained only ordinary portland cement (ST1 and ST2). The use of SCMs helped densify the concrete matrix by filling the voids in between the cement particles, increasing the resistance against penetrating chlorides. In this study, all the concrete slabs were air entrained except for ST2 and had the highest unit weight among the mxitures, which helped decrease the transport poporties and resulted in lower chloride ingress profils than ST1 mixtures.

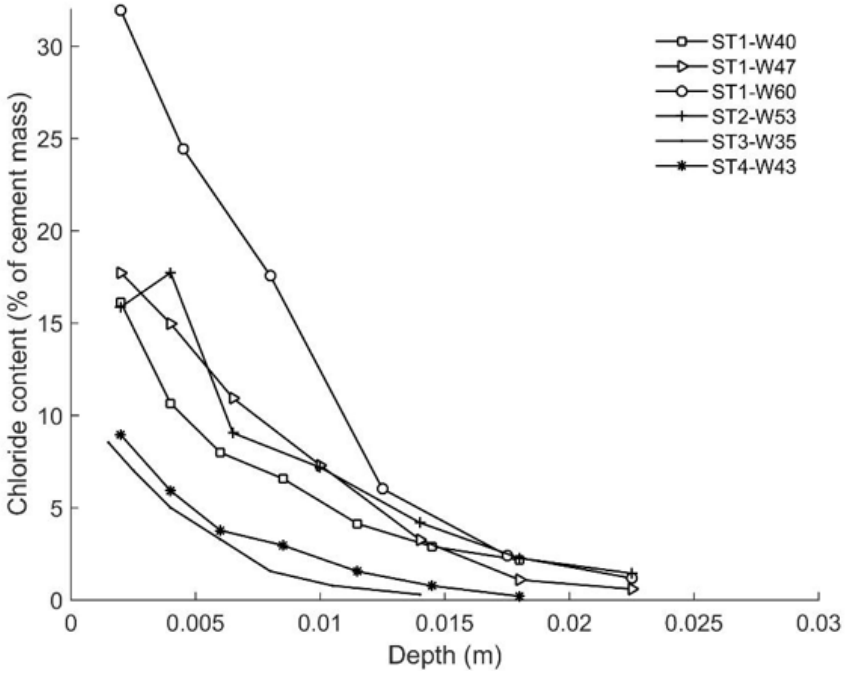

(a)

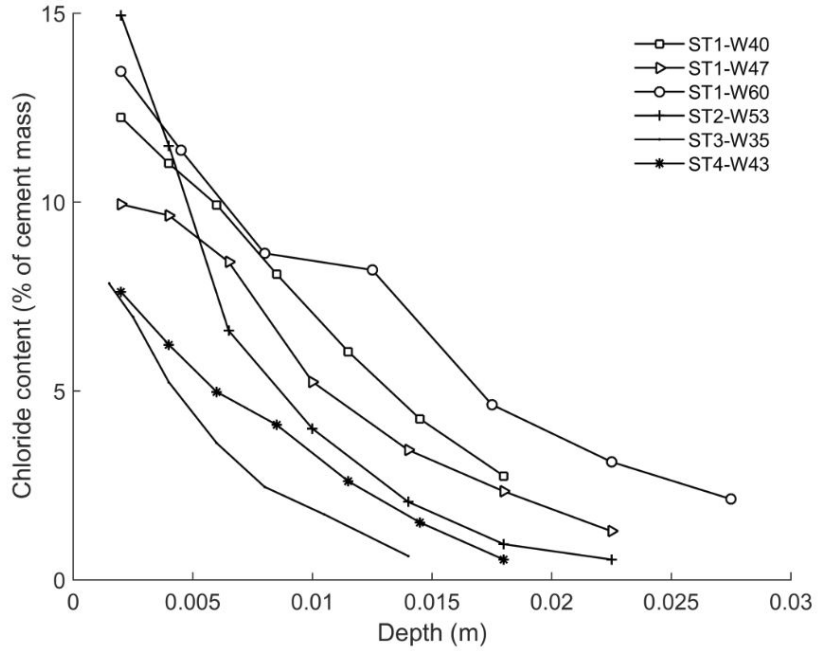

(b)

Figure 4.1: (a) Acid soluble chloride profiles are shown on the six types of concrete after (a) 14 ponding cycles; (b) 20 ponding cycles. ST1-W40 had a w/c ratio of 0.40, ST1 -W47 had a w/c ratio of 0.47, ST1-W60 had a w/c ratio of 0.60, ST2-W53 had a w/c ratio of 0.53, ST3 had a w/c ratio of 0.35 and ST4 had a w/c ratio of 0.43.

Figures 4.2 illustrates the chloride ingress into the slabs over time. Similar conclusions are observed here. It is evident that all the ST1 (Figures a, b and c) mixtures had a lower resistance to chloride penetration, and ST3 and ST4, as expected, due to the addition of SCMs, are more resistant to chloride penetration. It is interesting to note that after 24 days from ponding initiation, or 2 ponding cycles, the chlorides of all ST1 had already reached at least a concentration of total chlorides greater than 6% by weight of cement at 2 mm depth, and went on to reach a maximum of 32% by the end of the 14th cycle indicating high transport of chlorides of the concrete mixtures containing no SCMs. Figure 4.2(c) shows the type of concrete with the greatest amount of acid soluble chlorides in the system, which happens to be the concrete with the highest w/cm and the highest air content at 9%. When performing routine ponding of the slabs, surface cracking began showing on this type of concrete. The cracks presented themselves during the summer months. The combination of high temperatures, low relative humidity, high porosity, and chlorides was attributed to the presence of these cracks, which created a direct path for chlorides to enter. In neither of the two concrete mixtures containing SCMs (i.e., ST3 and ST4), chlirides reaced the reinforcement, which was embedded at 1 in (2.54 cm) and 2.5 in (6.35cm) from the concrete surface. If the concentration of chlorides that reach the surface of the reinforcement is high enough to disturb the passive layer, corrosion will initiate. This total chloride threshold can range from 0.2 to 0.6% by mass of cement. Figures 4.3(a-d) show that after abut 14 ponding cycles, these threshlds were exceeded in ST1 and ST2 slabs, suggesting possible corrosion initiation.

As a side investigation, comparison study was conducted to illustrate the acid and water soluble chloride contents in ST2 slab. Due to the low amount of powders collected from profile grinding, this study could not be expanded into other slabs. Figure 4.3 shows the water soluble (free) and acid soluble (bound) chliride contents at 0.394 in (10 mm) depth at different times. The concentration of acid soluble chlorides (which include both free and bound chlorides) increases over time at 0.394 inch (10 mm) depth. In the first 24 days of cyclic ponding, almost all chlorides at this depth were free chlorides. Over time, the amount of bound chlorides increased, however, the increase in free chloride concertation was larger. At 178 days, 25% of the total chlorides at this depth were bound chlorides. Since the binding capacity of the matrix is limited, the ratio of bound to free chloride concertation is expected to increase over time. As a result, in later stages of chloride exposure, it is also expected that chloride ingress would decrease the electrical resistivity of the pore solution, changing electrical properties of concrete.

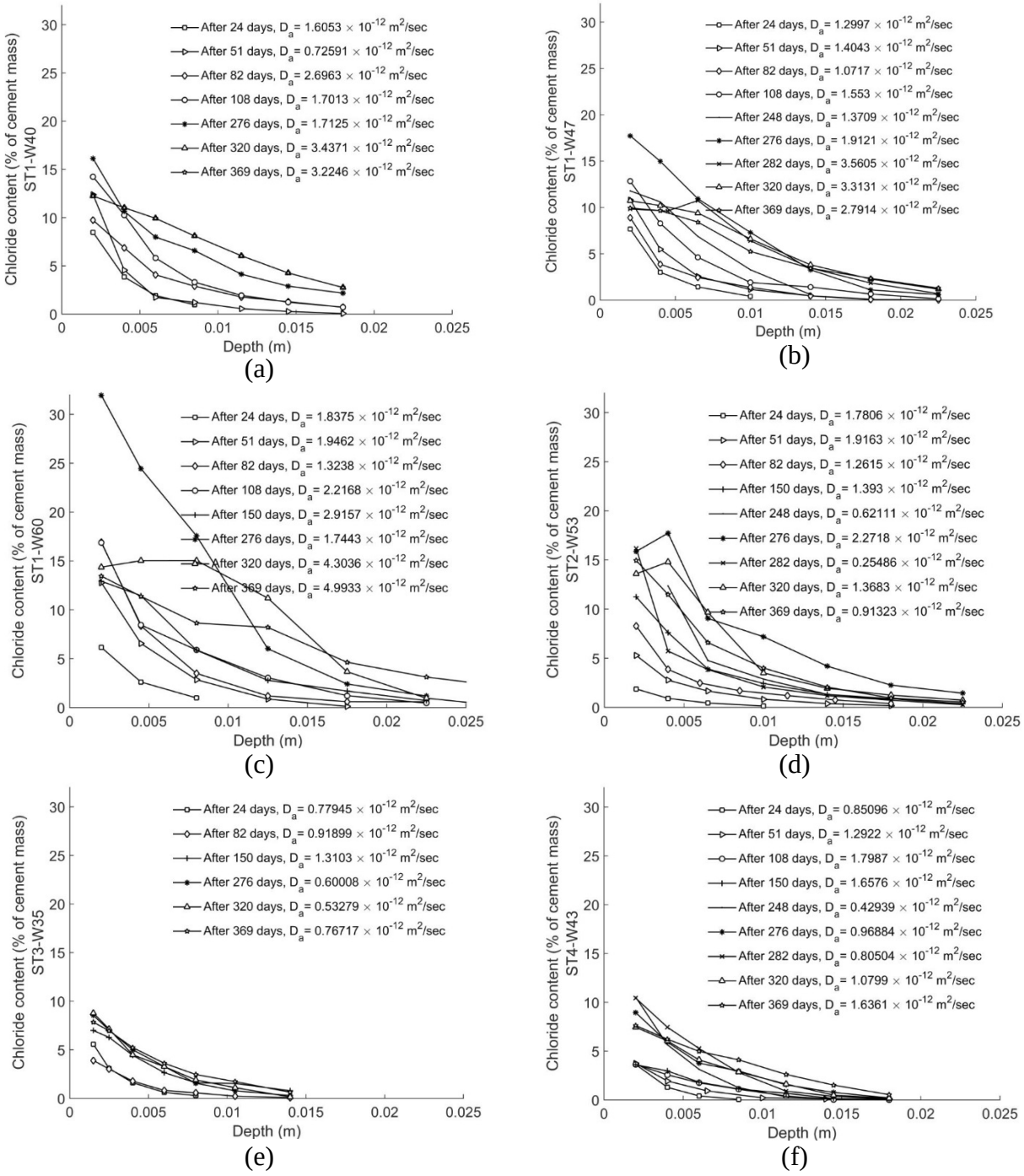

Figure 4.2: Acid-soluble chloride concentrations by weight of cement throughout 369 days of cyclic ponding with their respective apparent diffusion coefficients. (a) is ST1 with w/c ratio of 0.40, (b) is ST1 with w/c ratio of 0.47, (c) is ST1 with w/c ratio of 0.60, (d) is ST2 with w/c ratio of 0.53, (e) is ST3 with w/c ratio of 0.35 and (f) is ST4 with w/c ratio of 0.43.

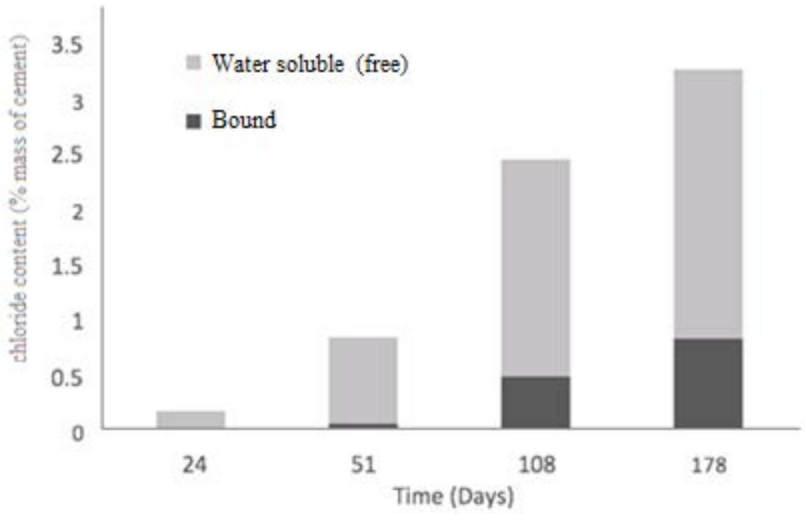

Figure 4.3: Free and bound chloride concentration of ST2 at 10 mm in depth over time.

4.2.4 Internal and Atmospheric Conditions

Because the concrete slabs were placed at an outdoor exposure site, they endured various ranges of temperature and relative humidity over the duration of the study, which played a key role in the development of concrete setting and chloride ingress so temperature and relative humidity were monitored both at the exposure site and within the concrete slabs. The internal, surface and air temperature changes are shown inn Figure 4.4 for all types of slabs. The increase and decrease in temperatures are due to the change in seasons. The internal and surface temperatures seem to follow a trend. It is noted note that, during the warm summer months, concrete retained heat due to its thermal mass — on average internal temperatures remained higher than the air temperatures. It is important to identify this increase in temperature, especially internally since it affects the chloride diffusion coefficients *(Qiang et al. 2008)*. It is observed in Figure 4.6 that the internal temperature of concrete can be easily predicted from the environmental temperature since temperature within concrete reaches equilibrium conditions relatively quickly. Therefore, in practice, the temperature effect on electrical resistivity measurements can be approximately accounted for using air temperature readings and existing resistivity-temperature relationships.

Figures 4.5 and 4.6 show the relative humidity changes (in the environment and in the slabs) of the water-ponded and de-icing chemical-ponded concrete slabs, respectively. Since the concrete slabs were relatively new when the ponding of de-icing solution began, the slabs had an internal relative humidity near 100%. The figures show a decrease of relative humidity over time, and correlates with the decrease in moisture content measured from core samples. The decrease in internal moisture and relative humidity is due to the hydration process of the concrete and the decrease of relative humidity in the air. The concrete type that contained no air entrainment had the smallest change in relative humidity. Since the concrete has no air-entrainment, the passageway for water vapor to move is very limited so the rate in which the relative humidity decreases is expected to be less than the rest of the concrete slabs. It is interesting to note that all six slabs, regardless of the type of concrete, continued to have a relative humidity that was close to 100% during the entire study. During the time that ponding stopped for 10 weeks, the relative humidity began to decrease. Once the ponding continued, the relative humidity increased once

again. The comparison between water-ponded and de-icing chemical ponded slabs shows some differences in internal relative humidity profiles. The relative humidity in water-ponded slabs remained relatively high, even during the dry period, while during the dry period, the relative humidity in the de-icing chloride-ponded slabs went below 80%.

The determination of internal relative humidity and the degree of saturation in concrete requires either measurement of these properties in-situ or simulating those using environmental data and concrete mixture design properties. The measurement of relative humidity requires installation of sensors within the concrete. Accurate measurement of the degree of saturation requires coring. Neither approaches are practical for regular bridge deck inspections; therefore, simulation approach is the most feasible and practical method for determining these parameters within concrete. Input data for these simulations can be obtained from public sources. In Oregon (and most of Pacific Northwest), current or historical environmental data such as temperature and relative humidity can be directly obtained from Cooperative Agricultural Weather Network (AgriMet). AgriMet provides weather data at every 15-minute intervals, hence, providing a very high resolution of environmental input data for typical virtual experiments on reinforced concrete structures.

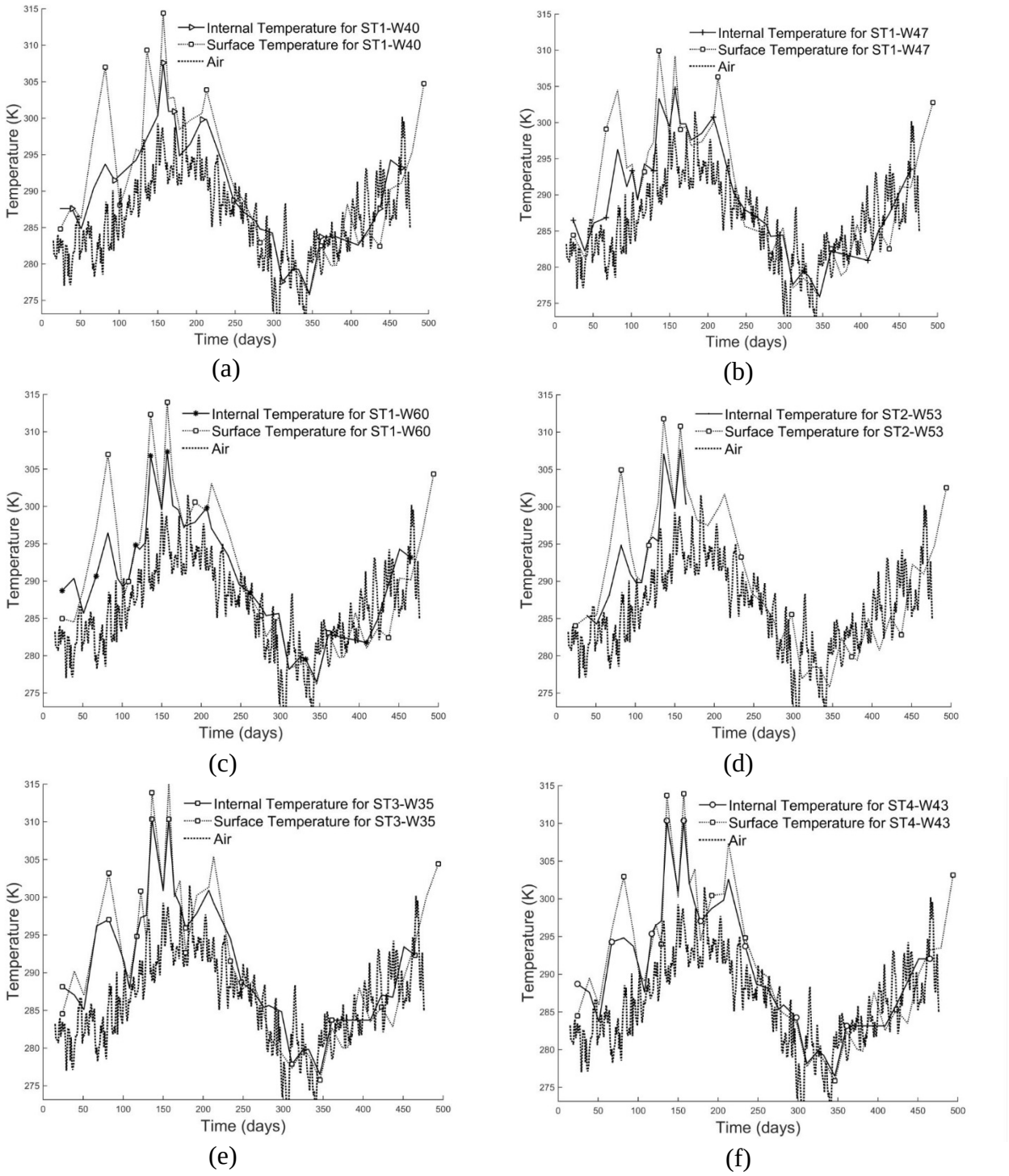

Figure 4.4: Air, surface and internal temperature for concrete slabs over the 15 months of chloride testing: (a) ST1-A, (b) ST1-B, (c) ST1-C, (d) is ST2, (e) ST3, and (f) ST4.

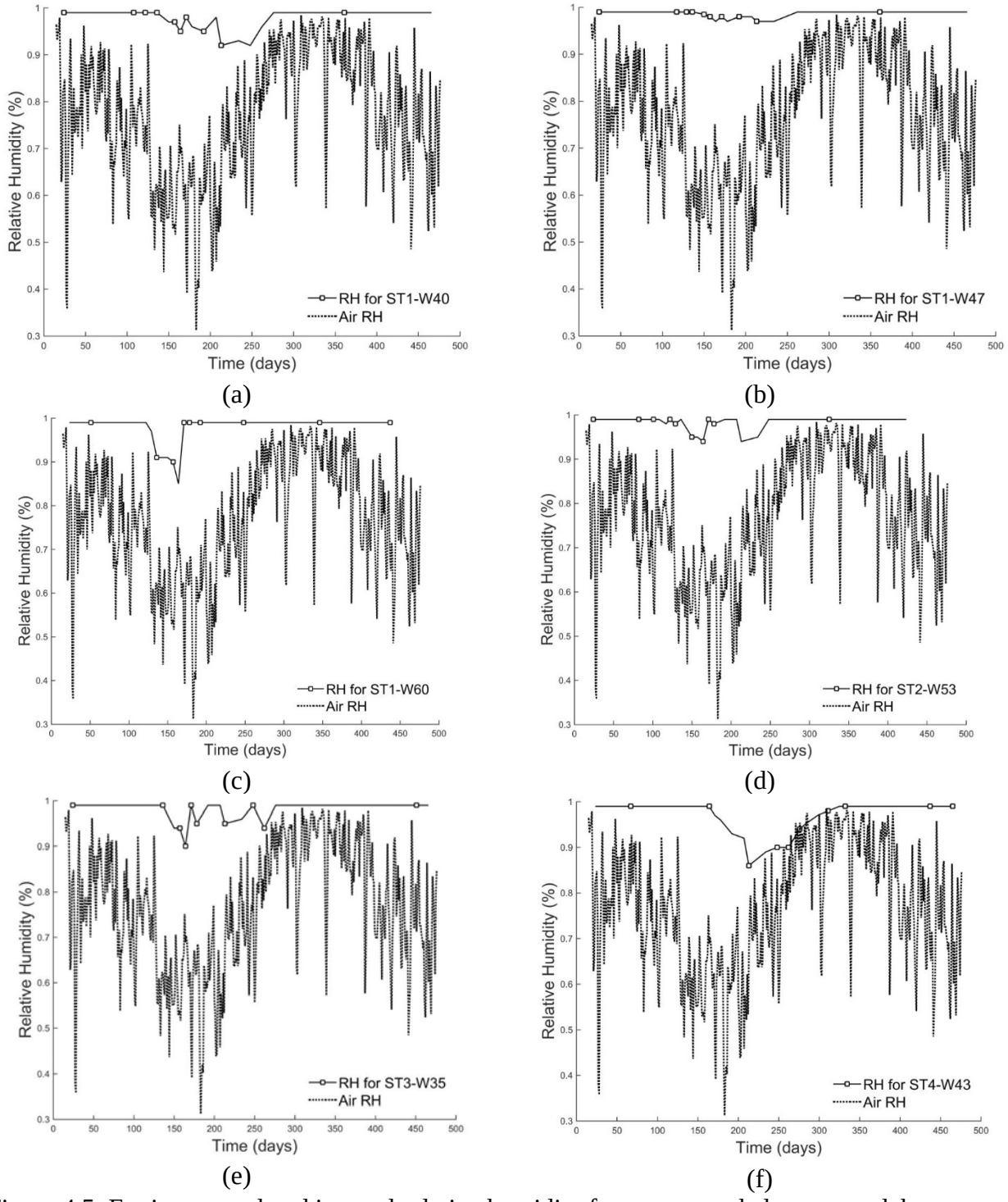

Figure 4.5: Environmental and internal relative humidity for water-ponded concrete slabs over the 15 months of chloride testing: (a) ST1-A, (b) ST1-B, (c) ST1-C, (d) is ST2, (e) ST3, and (f) ST4.

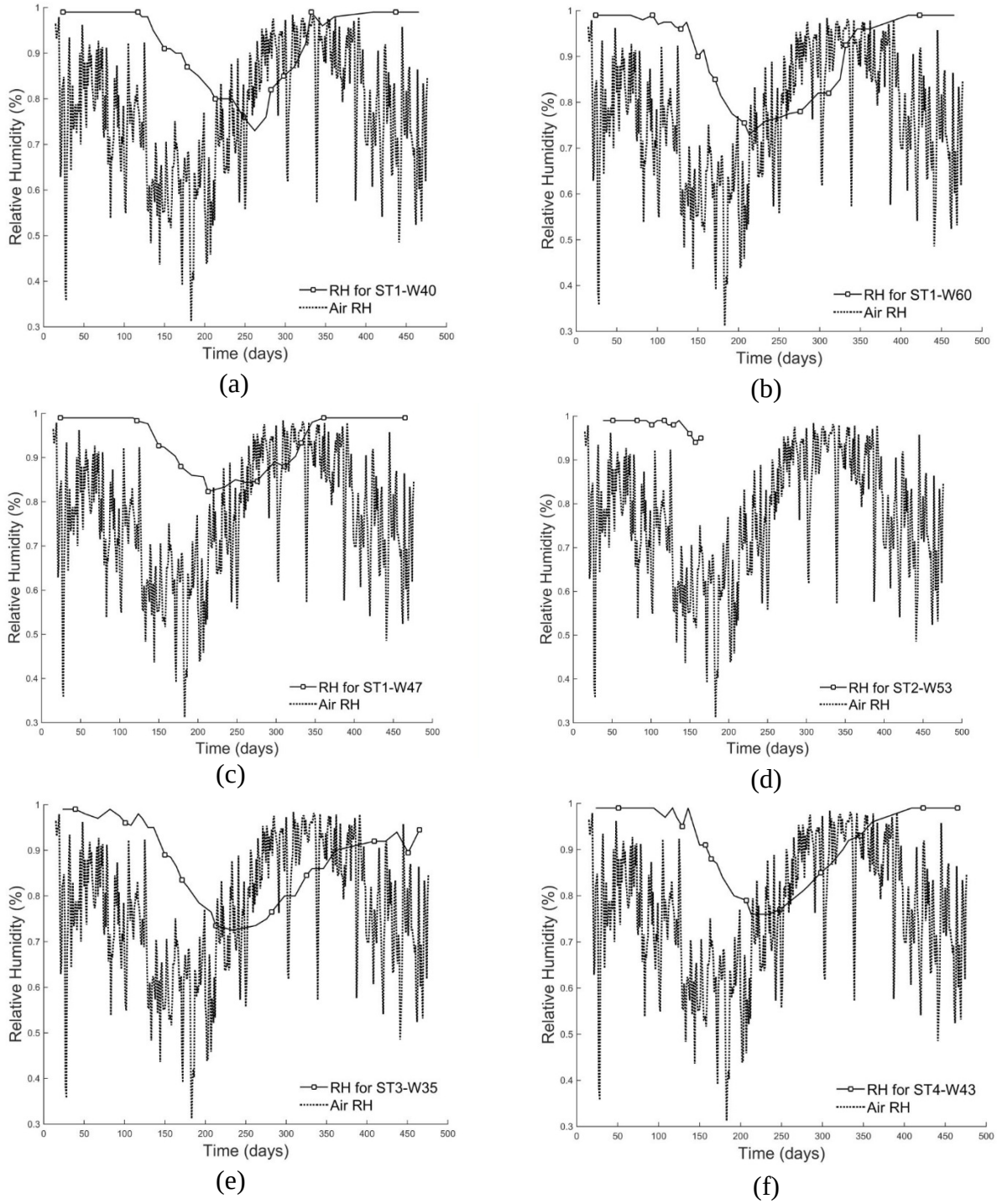

Figure 4.6: Environmental and internal relative humidity for de-icing solution-ponded concrete slabs over the 15 months of chloride testing: (a) ST1-A, (b) ST1-B, (c) ST1-C, (d) is ST2, (e) ST3, and (f) ST4.

4.2.5 Surface Resistivity

Surface resistivity was measured every week or bi-weekly throughout this study. The measurements were taken on both slabs that were ponded with the de-icing solution and the

control slabs that were ponded with water to assess the effect of chloride ingress on SR measurements. The SR measurements were taken on both reinforced sections and un-reinforced sections of the slabs. Since SR measurements are influenced greatly by temperature, all measurements were normalized by a temperature of 77°F (25°C) using Hinrichsen-Rasch law *(Hope 1987)*. Figure 4.7 shows a comparison of SR measurements taken over the reinforcement and the unreinforced section on both the control slabs and the de-icing solution ponded slabs. Note that Figure 4.7€ contains no error bars because only one slab was ponded with de-icing solution and the other slab was ponded with water. The measurements between the unreinforced and reinforced were nearly identical and fall well within the error bars, validating the techniques used to measure SR over the concrete reinforcement.

Avoiding early corrosion initiation was imperative in this study so that the relationship between SR and chloride ingress could be monitored for an extended period, hence the ponding cycles were stopped temporarily after 7 cycles due to the high concentration of chlorides in the system. Figure 4.7 also shows the period during which ponding cycles did not occur. Before the ponding cycles stopped, the SR was increasing in all the concrete types. The type of concrete influenced the SR measurements greatly. ST1 and ST2 slabs in Figures 4.7(a-d) all started with SR values much lower than SCM-containing ST3 and ST4 slabs in Figure 4.7(e and f). As time progressed, the SR measurements increased in all cases even after ponding stopped. The initial increase in resistivity can be attributed to a combination of factors including the changes in microstructure of concrete during and decrease in relative humidity observed during the dry period. Since chloride ingress was limited to only the top layers from the concrete surface during these initial stages, the effect (that would reduce electrical resistivity) is not prominent. These figures clearly show that the water-ponded control slabs also had an increase of SR measurements during this period. This suggests that the microstructure changes and relative humidity governed the SR measurements in the early stages of chloride exposure.

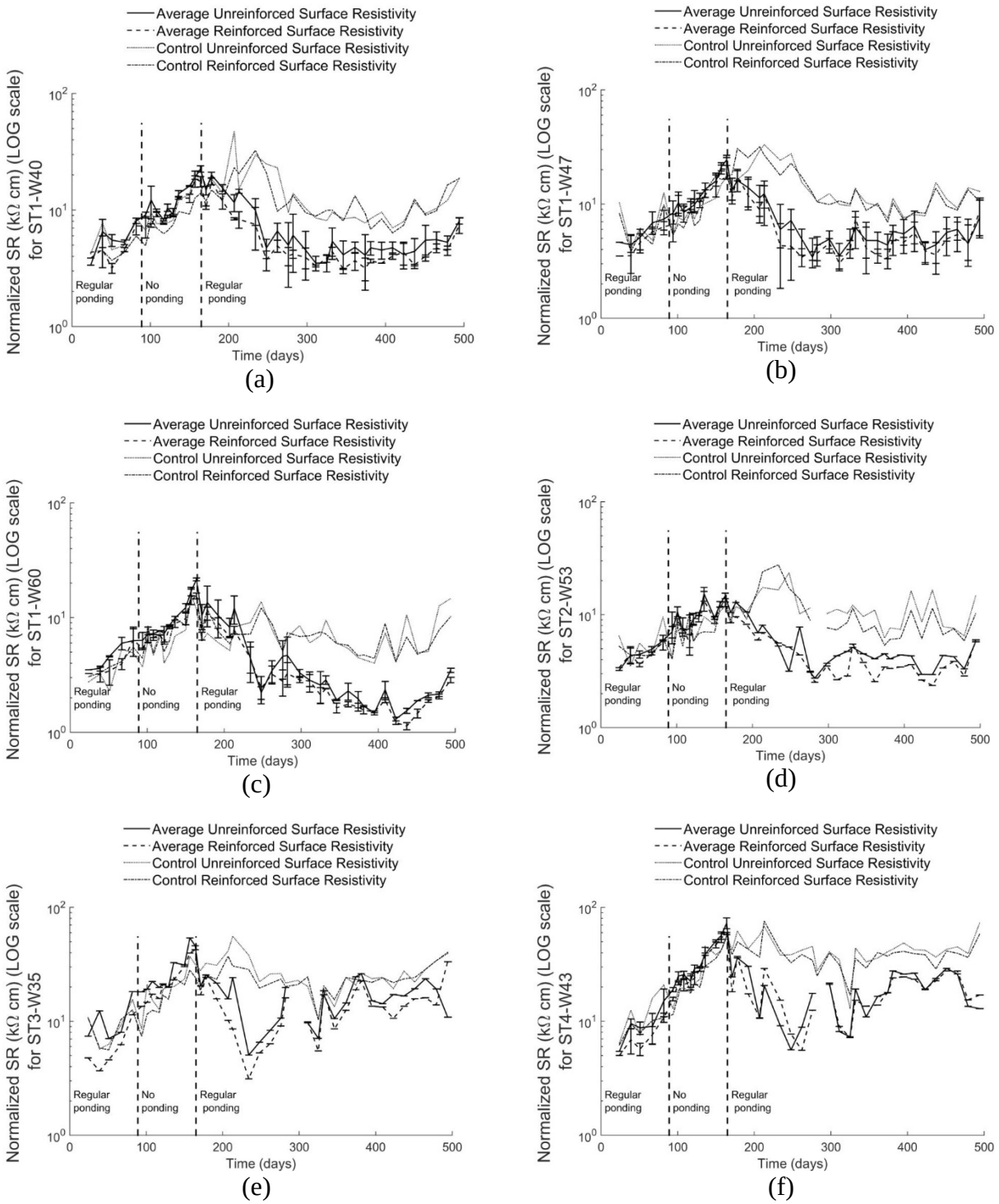

Figure 4.7: Surface resistivity measurements taken over the unreinforced section of the control slabs and the de -icing solution ponded slabs. (a) ST1-A, (b) ST1-B, (c) ST1-C, (d) is ST2, (e) ST3, and (f) ST4. Measurements are normalized for 77°F (25 °C).

In later stages of chloride explore, as the chloride penetration depths increased, the effect of chloride ingress on SR measurements became clear. During these later stages, there were no

significant changes in the microstructure of concrete, and relative humidity remained high (more so in water ponded samples than de-icing chemical ponded samples). Comparison of de-icing chemical ponded slabs with water ponded control slabs clearly show that chloride ingress results in lower SR measurements in all slabs. As shown in Figure 4.8, this relationship is dependent on the slab type. The ST1 slab with a high w/cm of 0.6 had significantly larger chloride ingress than the modern HPC mixture slabs, ST4, with w/cm of 0.43. The decrease in SR is larger in the former than the decrease in the HPC slab. These observations provide significant support for the ultimate objective of this research to provide a quantitative relationship between the electrical properties of concrete (e.g. SR or formation factor) and chloride ingress in concrete bridge decks.

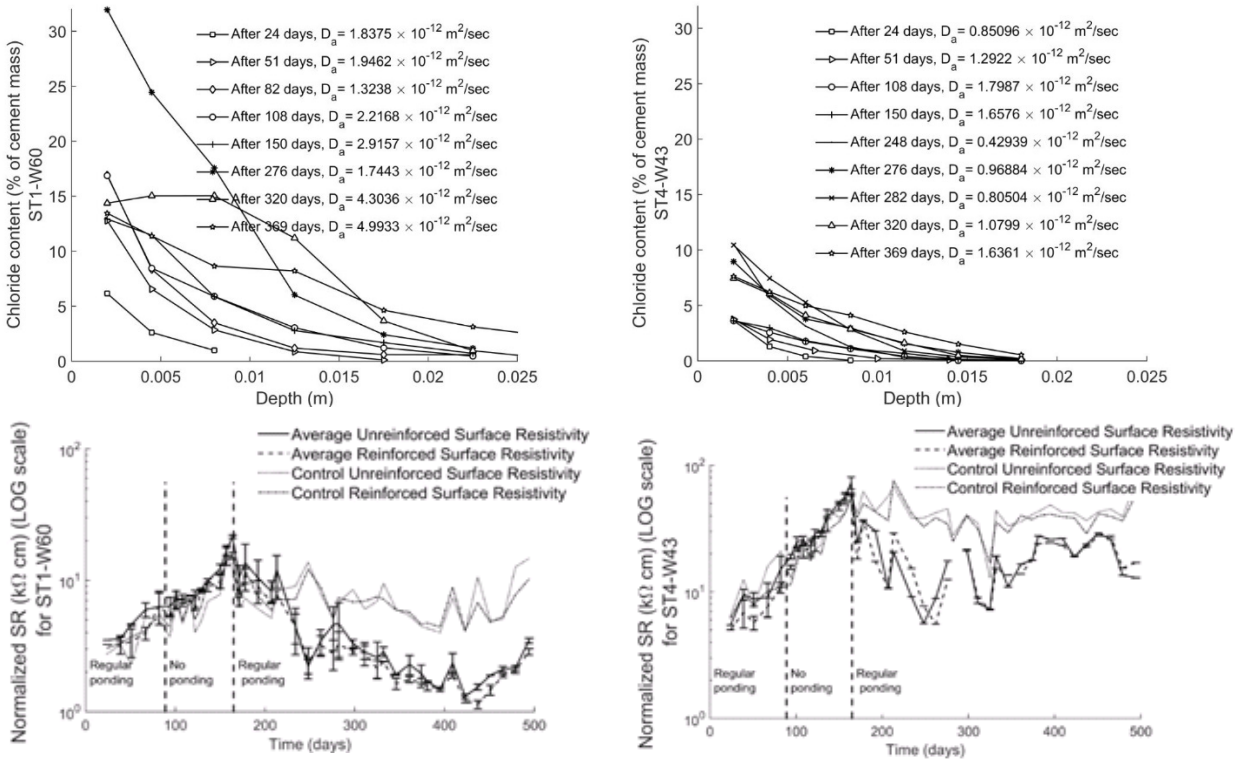

(a) (b)

Figure 4.8: The effect of chloride ingress on SR measurements (a) ST1 slab with w/cm 0.60, (b) ST4 slab with w/cm 0.43.

It is challenging to differentiate the effect of chloride ingress in concrete using electrical properties of concrete during the first couple of months after pouring the concrete bridge-deck. This is because the electrical properties of concrete are governed by multiple processes that take place in concrete during curing and the early stages of service. These include such things as microstructure development and evolution of the composition of the pore fluids. However, after concrete matures the changes in electrical properties of concrete (e.g. SR or formation factor) are mainly due to changes in pore solution composition, hence, they can be used as an indicator for chloride ingress. Since most bridge decks in Oregon are typically exposed to de-icing chemicals months after casting, the observed relationship between electrical properties of concrete (e.g. SR) and chloride ingress can be expedited to help predict chloride profiles in concrete. However, since SR measurements depend on the type of concrete mixture (e.g. w/cm, connectivity of

pores, and pore solution composition) and environmental parameters (e.g. relative humidity, degree of saturation and temperature) within concrete, they need to be corrected/normalized for these factors.

4.3 THE EFFECT OF FREEZE AND THAW (F-T) ACTION

The purpose of this study was to develop a better understanding of the electrical resistivity of concrete when reinforced concrete slabs are exposed to deicer solution underwent F-T cycles. The de-icing solution selected is the commercial product used by ODOT and is composed of a 30% magnesium chloride solution with a corrosion inhibitor. While de-icing chemicals are effective at reducing freezing points, they are also known to damage the concrete bridge decks *(Julio-Betancourt 2009)*. A study performed by the Michigan Tech Transport Institute *(2008)*, determined that the use of magnesium chloride and calcium chloride deicer solutions cause expansive cracking, increase in permeability, and loss of strength. A report by ODOT also showed that the use of magnesium chloride deicer decreased the strength of concrete *(Shi et al. 2013, Huang et al. 2014)*. Hardened air void analysis were performed on the cores following ASTM C457, taken from twelve bridges in Oregon and showed that half of the cores had a spacing factor of over .008 in. (200 microns), proving to be inadequate for good F-T resistance. ODOT concluded that the magnesium chloride de-icing solution combined with F-T action deteriorated the concrete both physically and chemically. Interestingly, a survey taken by ODOT indicated that their winter maintenance managers did not agree on the severity of the damage that their magnesium chloride de-icing solution had on their bridge decks. The report noted that some managers however, did believe that this solution caused a high level of risk to the structures so changes were made on concrete mixture designs and rehabilitation practices to address this risk *(Shi et al. 2013, Huang et al. 2014)*.

This background demonstrates that combined effect of F-T action and chloride ingress can be a critical problem for reinforced concrete bridge decks. The question that is imposed by this problem for the current investigation is whether the F-T action has any effect on the relationship between the chloride ingress and electrical properties of concrete. If this relationship is significantly affected by the F-T action, then using electrical methods to predict chloride ingress will be less effective. This experimental investigation seeks answers to this question by studying the potential for electrical resistivity of concrete to serve as a non-destructive evaluation tool to assess the chloride ingress in concrete. It is also possible that overall deterioration due to F-T action could also be assessed. The study involved two stages: (1) investigation of the effect F-T action on concrete cylinders that are exposed to ASTM C666 Procedure B protocol, (2) investigation of the effect of F-T action on de-icing chemical and water ponded reinforced concrete slabs and accompanying concrete cylinders.

4.3.1 Concrete Cylinders under F-T Action

Surface and bulk electrical resistivity of concrete cylinders that underwent 300 F-T cycles following ASTM C666 Procedure B in a Scientempt F-T chamber were compared to additional cylinders that were placed in the F-T environmental chamber with the reinforced concrete slabs. The SR and the bulk resistivity of the cylinders are shown in Figures 4.9.

As illustrated in Figure 4.9, even before the F-T cycles, the electrical resistivity is well correlated with the type of concrete tested. The lower the electrical resistivity, the lower the concrete quality and the more prone the concrete is to various durability problems. The lowest resistivity before the F-T cycles was the OPC with w/cm ratio of 0.53 (ST2), which contained no air entrainment (air content was about 1% as reported in Chapter 3). These concrete cylinders did not perform well under F-T, as expected. All cylinders from this type of concrete began to deteriorate at about 72 F-T cycles and showed spalling at 108 F-T cycles. The surface of the entire cylinder of this type of mixture came off in chunks and only the core of the cylinder remained exposing the aggregates, as shown in Figure 4.10. The figure shows that for these mixtures the resistivity decreasing rapidly as the specimens deteriorated until the SR measurements could not be taken any more. The performance of the other concrete mixtures was significantly better when compared to the mixture with no air-entrainment. Based on SR measurements alone, it can be said that SR can be an indicator of F-T deterioration since the values decreased for the specimens that deteriorated below 5 kΩ-cm, however, SR measurements should be combined with other tests to verify the extent of deterioration.

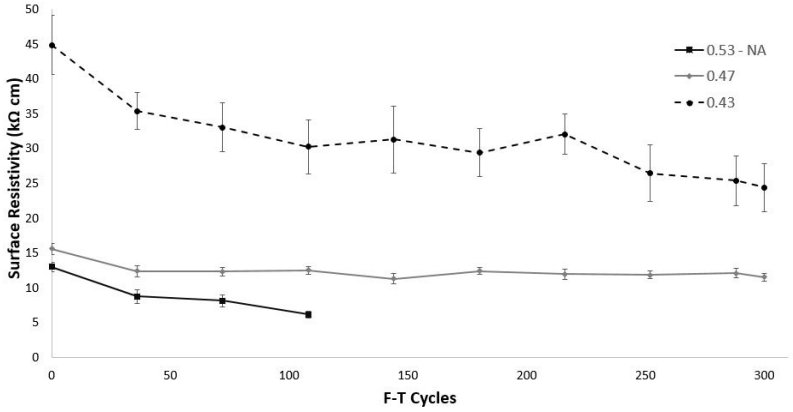

(a)

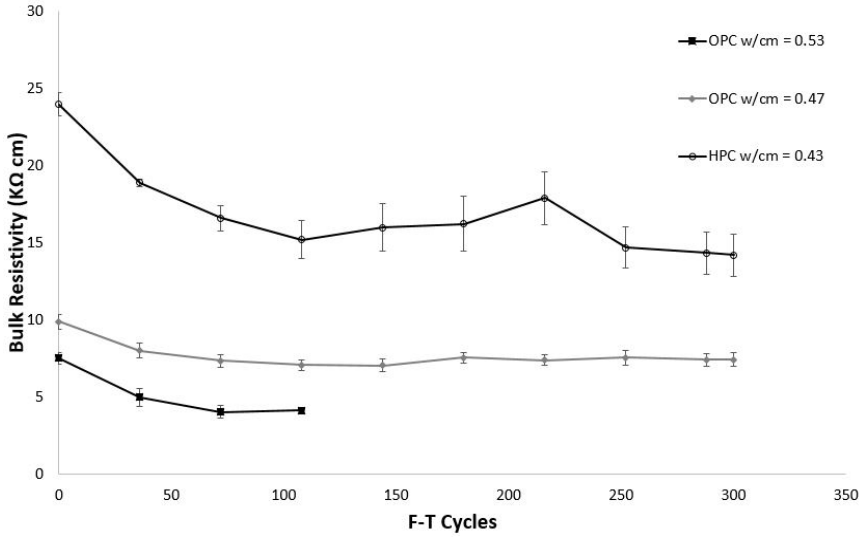

(b)

Figure 4.9: Surface (a) and bulk (b) resistivity taken on cylinders that underwent 300 F-T cycles according to ASTM C666 Procedure B. Three types of concrete were tested: 1) OPC concrete with w/c ratio of 0.53 and no air-entrainment (ST 2) an OPC concrete w/cm ratio of 0.47 with air-entrainment (ST1-C) and 3) a HPC with a w/cm ratio of 0.43 that contained silica fume, fly ash and air-entrainment (ST4). Measurements are normalized for 77°F (25 °C).

(a) (b)

Figure 4.10: Deterioration in ST2 cylinders (without air entrainment) after (a) 72 F-T cycles, (b) 108 F-T cycles under ASTM C666 Procedure B protocol.

From visual inspection, the ST1-C and ST4 specimens did not have any spalling or pop-outs. The air content of the OPC mixture with 0.47 w/cm (ST1-C) was 5% while the HPC mixture with w/cm of 0.43 (ST4) had an air content. It was expected that the HPC concrete would deteriorate at a faster rate than the OPC mixture due to a low percent of air content, however the specimens did not show any visual signs of deterioration. The SR of the OPC mixture with w/cm ratio of 0.47 (ST1-C) had a minimal change throughout the duration of the test. The SR measurements decreased by about 2 kΩ-cm, where the SR of the HPC mixture decreased by over 15 kΩ-cm throughout the duration of the test. The bulk resistivity of the OPC and HPC mixtures also decreased by about 2 and 10 kΩ-cm, respectively. The general trend for all measurements in both, bulk and SR seem to decrease over time, reflecting deterioration of concrete due to F-T action. Because both figures follow the same trend for all three types of concrete and since electrical resistivity has been used in the concrete industry as an aid for durability related studies, a comparison between the two methods was made to validate the results obtained. This comparison is important to establish since the use of bulk resistivity test may not always be the most convenient since it requires taking cores or cylinders from a structure and this may not always be an option. Bulk resistivity and SR were plotted against each other and can be seen in Figure 4.11.

Figure 4.11 shows the linear correlation coefficients (R^2) between bulk resistivity and SR. The coefficients are shown for each set of concrete samples as well as the overall group. The coefficient for the concrete mixtures with w/cm ratio of 0.47, 0.53, and 0.43 are 0.863, 0.905, and 0.940 respectively. The correlation coefficient for the overall set of points is 0.987. These coefficients support a strong correlation between bulk and SR and indicate that SR alone will provide accurate information. The ratio of the theoretical bulk resistivity to the SR of the data collected was calculated to be 0.576. A separate study done on the relationship between bulk and SR supports this finding. Ghosh and Tran showed that the two techniques were well correlated for different types of OPC, HPC and control mixtures over longer periods of time *(Ghosh et al. 2015).*

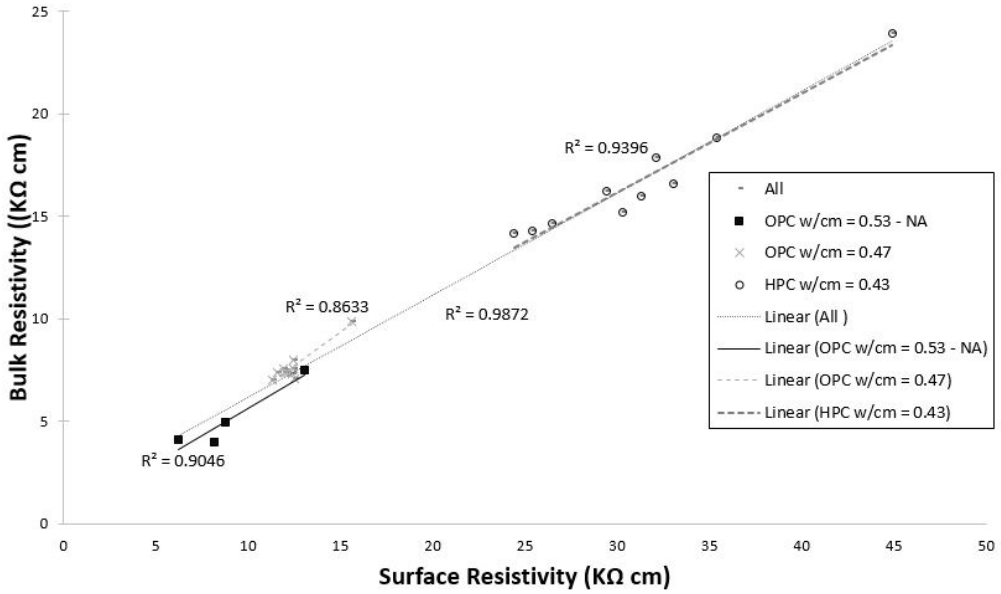

Figure 4.11: Linear regression relationship between SR and bulk resistivity taken on cylinders for each type of concrete.

To further investigate the behavior of the cylinders going through F-T cycles, and to better understand the results obtained from the electrical resistivity measurements, the mass over time and the relative dynamic modulus of the cylinders were monitored as shown in Figures 4.12 and 4.13, respectively.

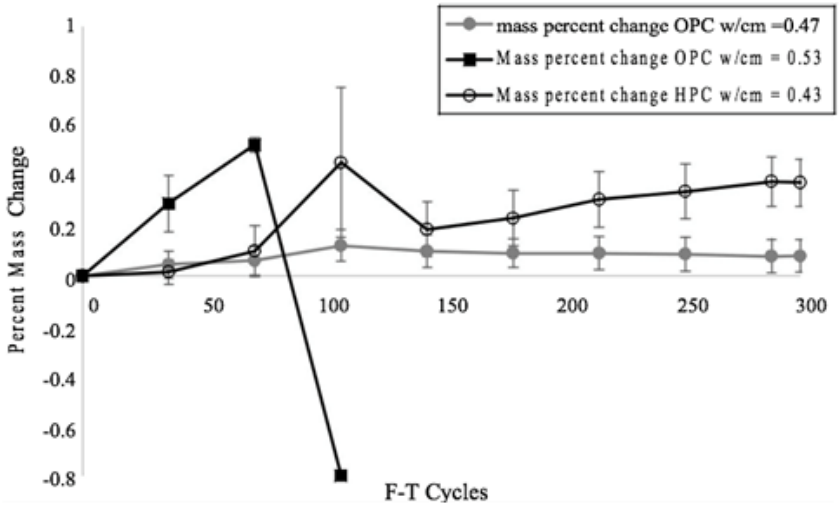

Figure 4.12: Percent mass change over time on cylinders that underwent 300 F-T cycles in the Scientempt chamber. Three types of concrete were tested: 1) OPC concrete with w/c ratio of 0.53 and no air-entrainment, 2) an OPC concrete w/cm ratio of 0.47 with air-entrainment and 3) a HPC with a w/cm ratio of 0.43 that contained silica fume, fly ash and air-entrainment.

Figure 4.12 shows that the three types of concrete increased in mass throughout the duration of the F-T cycles. The concrete mixture with no air (OPC w/cm = 0.53), while had a steep increase in mass compared to the other two mixtures, deteriorated under F-T cycles rather rapidly due to spalling. This gain in mass could be explained by an increase in water content in the concrete matrix, which caused expansion when the water froze to the point that it created the surface to spall off and separate from the aggregates. Literature shows contrary results when it comes to mass gain throughout the F-T cycles *(Wang et al. 2014)*. In these F-T studies, the concrete decreases in mass. This is attributed to the paste on the surface separating from the aggregate due to the expansion of water when frozen. However, most studies rely on procedure A from ASTM C666 standard.

Procedure A requires that the specimens undergo freezing and thawing submerged in water. Procedure B was used in this study, because it mimics the F-T cycles that the concrete slabs underwent. This provides a better understanding of what could be happening in the concrete matrix. While the F-T action is providing some damage to the microstructure of the concrete, the continuous cycles may also be driving water in the concrete further into the matrix during thawing phase, which is submerged in water, allowing more water to be absorbed by the cracks that are newly developed. Since Procedure A of the standard requires full submersion of the samples, it does not provide the concrete surface to go through a wet and dry period, and it is well understood that wet and dry cycles provide an increase of moisture ingress into the concrete matrix. This gain in moisture also helps understand why the electrical resistivity is decreasing over time. The conductivity will increase with an increase in water available in the system. The relative dynamic modulus (RDM) of the cylinders was also monitored in this study and can be found in Figure 4.13.

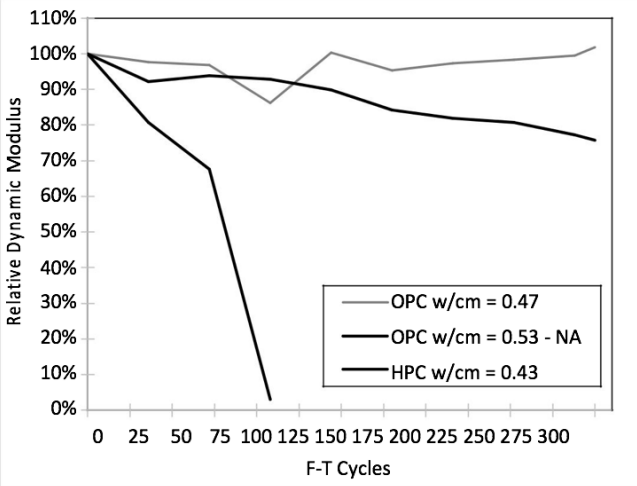

Figure 4.13: Relative dynamic modulus of elasticity on concrete cylinders after 300 F-T cycles in the in the Scientempt chamber.

The RDM of the air-entrained specimens essentially experiences no decrease. This indicates that these mixtures produce a properly air-entrained system. They should be expected to have excellent F-T resistance in the field. This further underscores the disconnect between the measured air content of the 0.43 mixture and the high dosage rate, which further supports the need to evaluate the samples for hardened air void analysis. The non-air entrained mixture on

the other hand performed poorly as was expected. The mixture experienced a very rapid decrease in RDM from the beginning and it was recorded in the first 36 cycles. After 108 cycles, the mixture was completely disintegrated due to the effects of F-T action.

4.3.2 Concrete Slabs under F-T Action

Surface resistivity measurements were taken on reinforced concrete slabs that went through 28 ponding cycles of deicer that contained 30% $MgCl_2$ solution with a corrosion inhibitor. The concrete slabs underwent five sets of 60 F-T cycles, which started after the seventh ponding cycle. A total of 300 F-T cycles were performed. Figures 4.14 and 4.15 show the SR measurements taken on the reinforced and unreinforced section of the slabs, respectively. These two figures show that the effect of the presence of reinforcement was negligible. SR measurements were also taken on the control slabs, which were only ponded with water. The control slabs did not go through F-T action. Each set of 60 F-T cycles are illustrated with vertical dotted lines labeled FT1, FT2, FT3, etc. All SR measurements are corrected for temperature and normalized to a 25°C reference temperature so that it did not have an effect on the measurements.

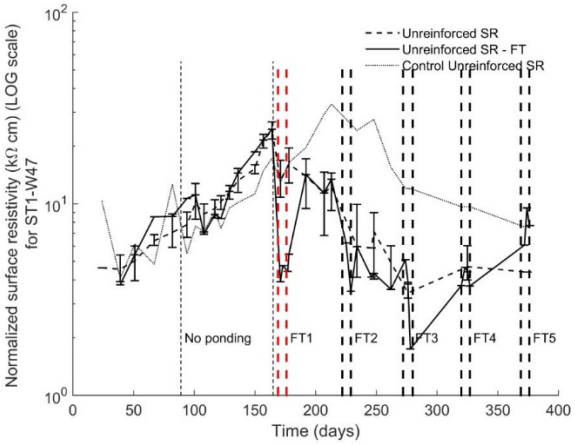

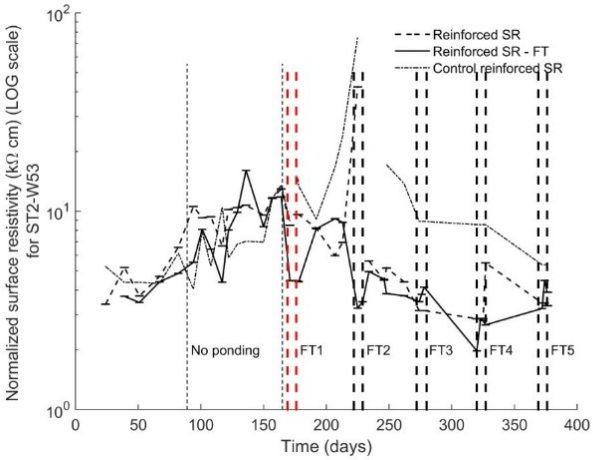

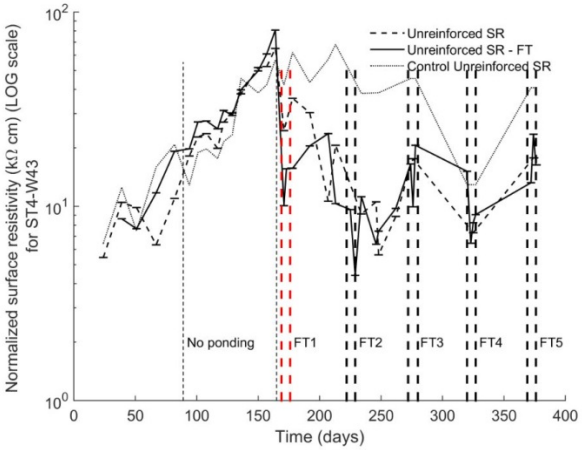

Figure 4.14: Surface resistivity measurements taken on unreinforced slabs throughout 28 ponding cycles. Each D-T cycles is shown with vertical doted lines labeled FT1, FT2, FT3, etc. Figure (a) ST1-C, (b) ST2, (c) ST4.

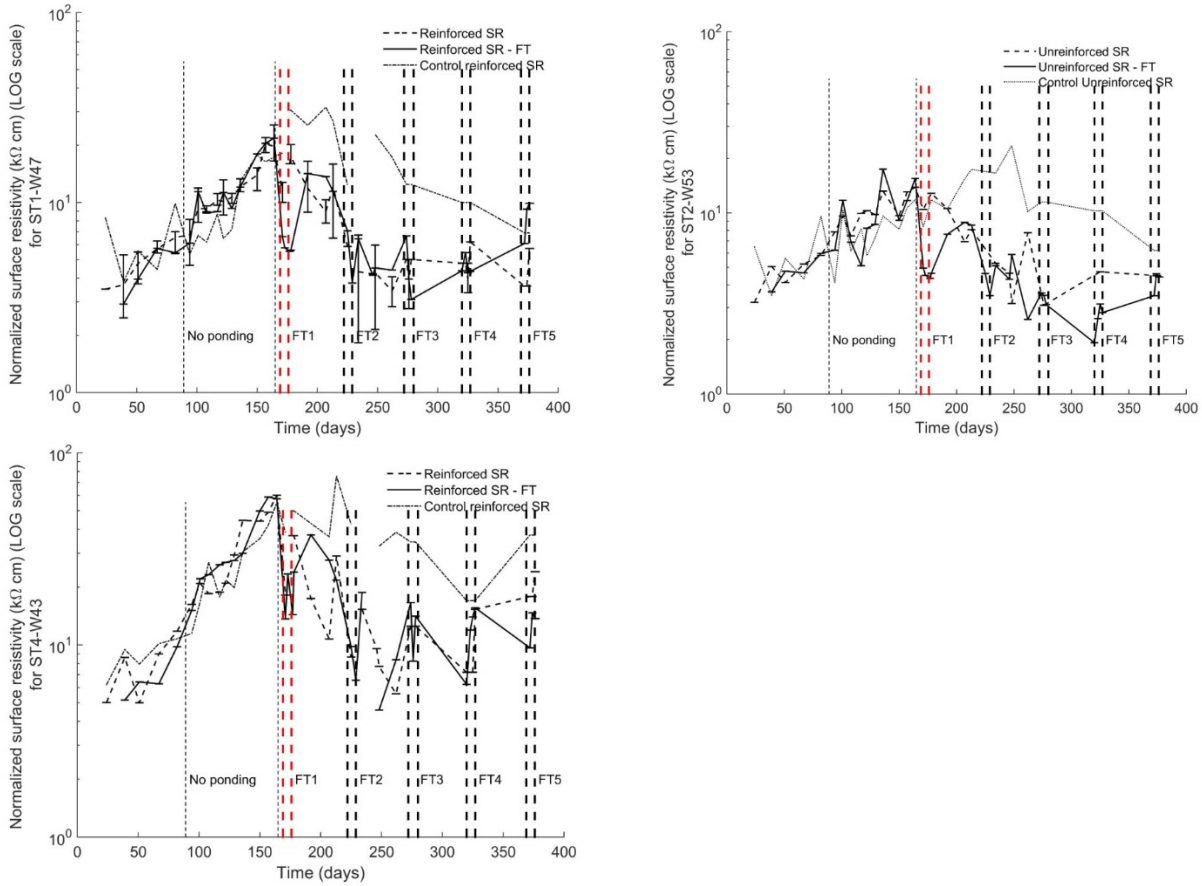

Figure 4.15: Surface resistivity measurements taken on reinforced slabs throughout 28 ponding cycles. Each D-T cycles is shown with vertical doted lines labeled FT1, FT2, FT3, etc. Figure (a) ST1-C, (b) ST2, (c) ST4.

Figure 4.14 (or 4.15) shows the section in which the F-T cycles occurred. The slab with no air entrainment had severe deterioration on the surface of the concrete after the initial 60 F-T cycles. The surface of the concrete had pop-outs and concrete paste particles on the surface had begun to separate from the slab, as shown in Figure 4.16(a). SST4 slabs produced with HPC mixtures did not show any deterioration due to F-T action as shown in Figure 4.16(b).

From Figure 4.13, it is evident that SR measurements are affected by the F-T cycles. The measurements decreased while the slabs underwent F-T cycles. The measurements take a steep decrease commensurate with F-T, however, the measurements recovered once the F-T action ended and then followed the trend of the slabs that did not go through F-T action. It indicates that the microstructure may experience some level of recovery after F-T. Another possibility is that the internal temperature decreases low enough that the correction factor for temperature may not appropriately normalize the readings taken. In all three sets of F-T cycles, regardless of the type of concrete, the SR measurements decreased and once the cycles stopped, the measurements increased once again suggesting that SR measurements are not affected by the F-T action. Since

the behavior observed is not conclusive, it is suggested that additional F-T cycles continue in this study. The cycles should be continued until the concrete with no air-entrainment starts to fail. This will show how the SR values are impacted by the deterioration. It would also show if the decrease in SR remains a permanent feature or if a different trend is observed once more widespread failure occurs.

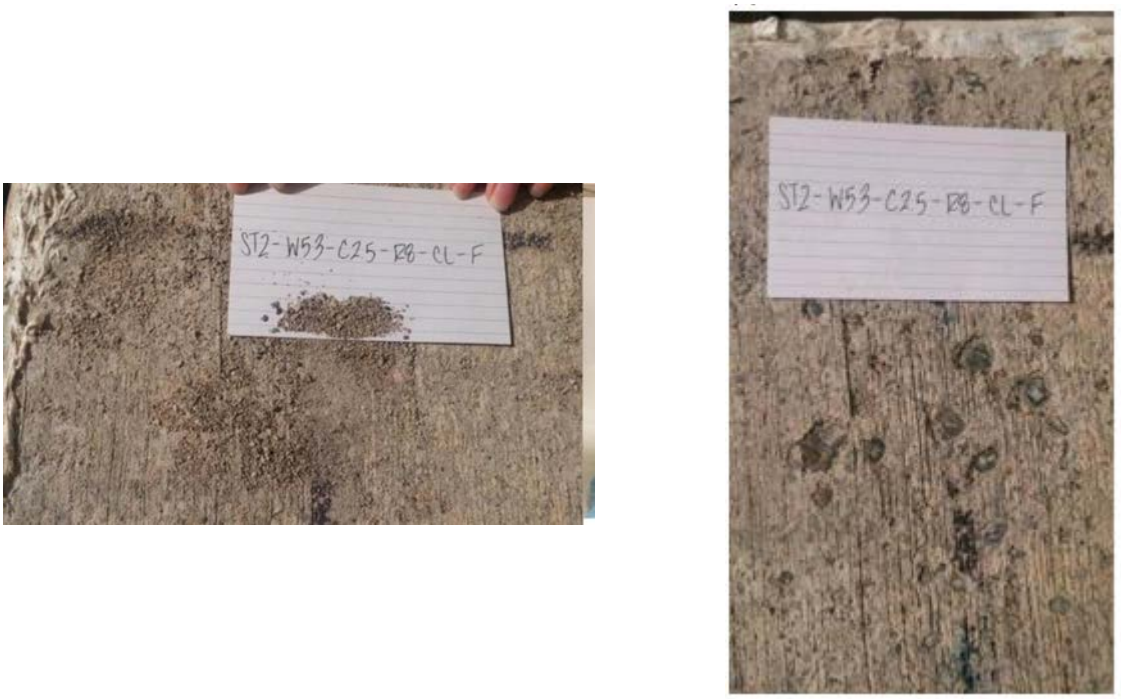

(a)

(b)

Figure 4.16: (a) Surface deterioration in ST2 slabs (without air entrainment) after 60 F-T cycles, (b)ST4 slab and accompanying concrete cylinder after the completion of the F-T study.

Figure 4.17 shows the SR measurements that were taken while the cylinders went through F-T cycles with the concrete slabs. The figure shows an increase in SR measurements in the two types of concrete that had air entrainment, which is the opposite behavior of the measurements from the cylinders that followed ASTM C666 in a Scientempt F-T chamber. This can be attributed to the fact that the cylinders were never fully submerged under water like the ones in the Scientempt F-T chamber. The increase in SR could indicate microstructural damage due to F-T action. However, it may be too early to tell until the cylinders undergo the full 300 cycles.

The measurements on the concrete cylinders with no air entrainment seem to be consistent but once again, it is too early in the F-T cycle test to conclude anything.

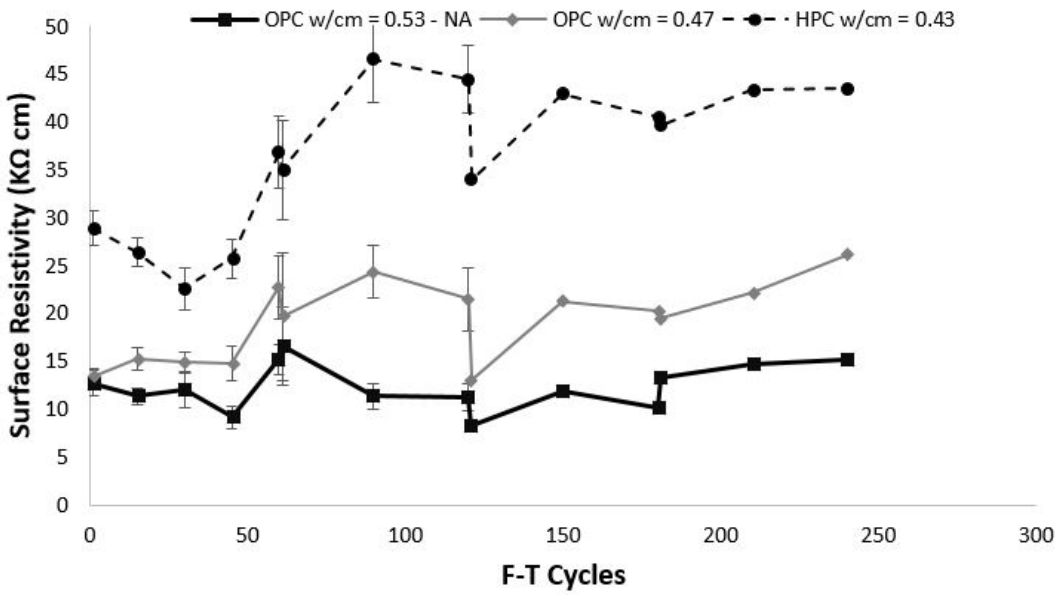

Figure 4.17: Surface resistivity taken on cylinders that underwent two sets of 60 F-T cycles in a controlled environmental chamber. An OPC concrete with w/c ratio of 0.53 and no air-entrainment, an OPC concrete w/cm ratio of 0.47 with air-entrainment and a HPC with a w/cm ratio of 0.43 that contained silica fume, fly ash and air-entrainment.

Figure 4.18 shows four chloride profiles for each type of concrete. The control slab, which is the slab that did not go through F-T action, is shown with a solid black line. After three ponding cycles, chloride profiles were taken and are depicted with a grey solid line. This shows the amount of chloride ingress after three ponding cycles. The same procedure was repeated for the slabs that underwent F-T action. These slabs underwent 60 F-T cycles, and was then ponded for three cycles. Chloride profiles were taken before any F-T action occurred and after the three ponding-cycles had ended. These slabs are represented with a dotted line and are labeled FT in the legend.

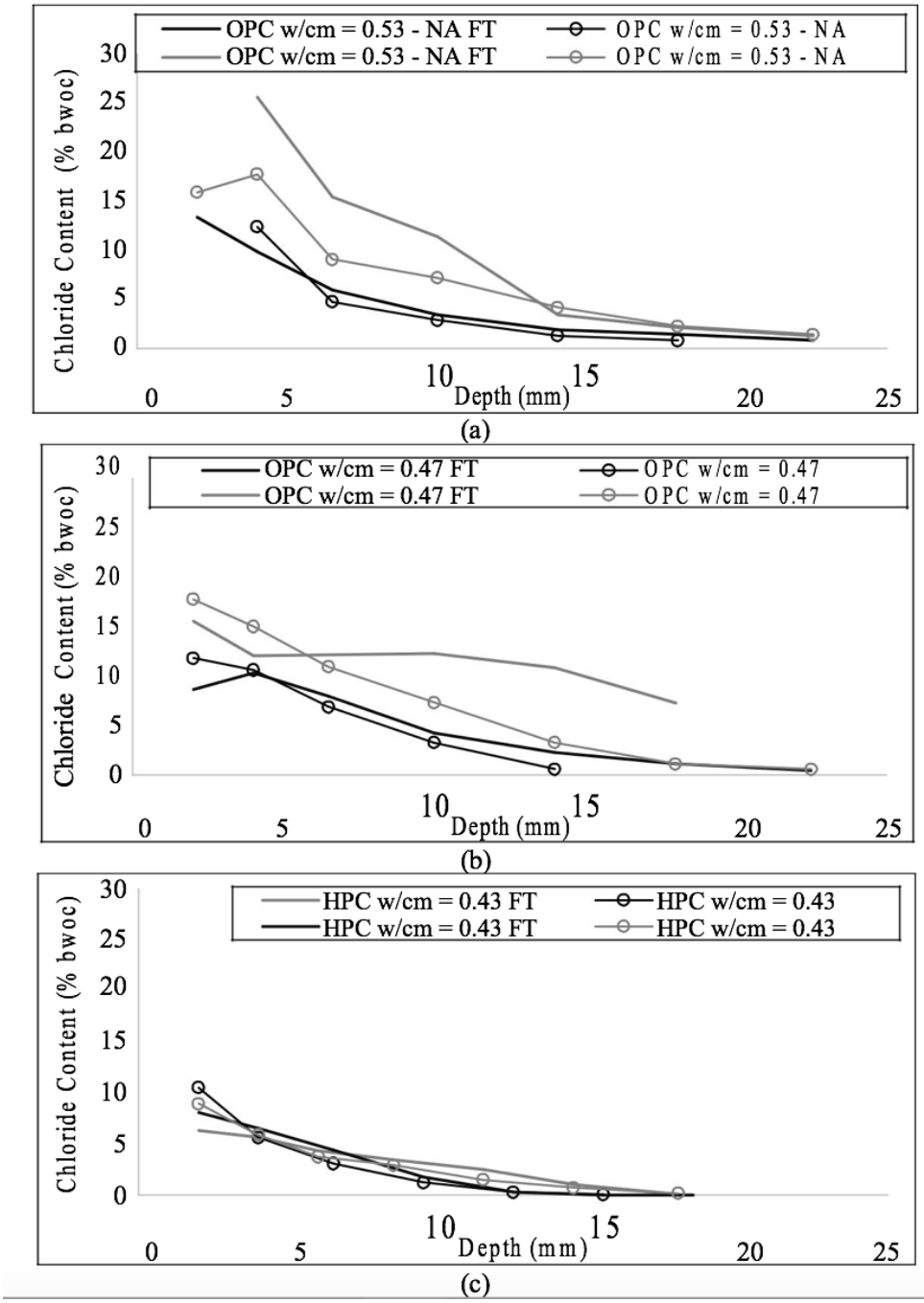

Figure 4.18: Two chloride profiles for three types of concrete are showing the effect of F-T action on chloride ingress. An OPC concrete with w/c ratio of 0.53 and no air-entrainment, an OPC concrete w/cm ratio of 0.47 with air-entrainment and a HPC with a w/cm ratio of 0.43.

From Figure 4.18 it is seen that F-T action has an impact on the amount of chlorides penetrating the slab with no air entrainment (ST2). This impact was not as clear for the ST1-C. It is seen that chlorides near the surface layers penetrated further into the deeper layers of concrete after F-T cycles, but no increase in chloride content near the surface was observed. The F-T action, on the other hand, did not affect the chloride ingress in the HPC slab (ST4). The fact that SR

measurements did not show significant difference between control and F-T specimens for ST4 slabs support this observation.

4.4 SUMMARY

This chapter reported the results of the experimental program in two sections. In the first section, the relationship between chloride ingress and electrical properties of concrete were presented for reinforced concrete slabs that are exposed to several ponding cycles of the de-icing chemical. The role of environmental conditions during de-icing chemical application was also discussed. In the second part the role of F-T action on such the relationship between electrical properties of concrete and chloride ingress and concrete deterioration were presented. The following summary represents the major outcomes of this experimental investigation.

- Electrical properties of concrete are affected by the microstructure development and compositional changes in pore solution of concrete during curing and early stages of service. As the concrete becomes more mature, the electrical resistivity of concrete increases, indicating stabilization of the pore solution composition and microstructure development (i.e., connectivity of the pores).

- Temperature, degree of saturation, and relative humidity of concrete affect its electrical properties such as resistivity. Among these factors, the temperature of concrete can be easily predicted from the environmental temperature since temperature within concrete reaches equilibrium conditions relatively quickly. Therefore, in practice, the temperature effect on electrical resistivity measurements can be approximately accounted for using air temperature readings and existing resistivity-temperature relationships.

- The determination of relative humidity and the degree of saturation in concrete, on the other hand, requires either measurement of these properties in-situ or simulating those using environmental data and concrete mixture design properties. The measurement of relative humidity requires installation of sensors within the concrete. Accurate measurement of the degree of saturation requires coring. Neither approaches are practical for regular bridge deck inspections; therefore, simulation approach is the most feasible and practical method for determining these parameters within concrete.

- It is challenging to differentiate the effect of chloride ingress in concrete using electrical properties of concrete during the first couple of months after pouring the concrete bridge-deck. This is because the electrical properties of concrete are governed by multiple processes that take place in concrete during curing and the early stages of service. These include such things as microstructure development and evolution of the composition of the pore fluids. However, after concrete matures the changes in electrical properties of concrete (e.g. SR or formation factor) are mainly due to changes in pore solution composition, hence, they can be used as an indicator for chloride ingress.

- Since most bridge decks in Oregon are typically exposed to de-icing chemicals months after casting, the observed relationship between electrical properties of concrete (e.g. SR) and chloride ingress can be expedited to help predict chloride profiles in concrete. However, since SR measurements depend on the type of concrete mixture (e.g. w/cm, connectivity of pores, and pore solution composition) and environmental parameters (e.g. relative humidity, degree of saturation and temperature) within concrete, they need to be corrected/normalized for these factors.

- Deterioration due to F-T action can be observed through the electrical properties of concrete, particularly in low quality mixtures. However, for HPC mixtures as in the case of ODOT's current mixture used for bridge decks, little to no damage was observed due F-T action. In these slabs, chloride ingress was not significantly affected by F-T action. Therefore, electrical resistivity measurements were still related to chloride ingress. Even in slabs produced with concrete that represent ODOT mixtures that were used in the past that experience, the SR measurements were affected during and right after the F-T cycles, but they returned to their natural trends shortly after. This observation needs to be studied further with additional F-T studies on the same slabs, especially until the concrete with no air-entrainment starts to fail to see how SR is impacted by the deterioration and to see if the damage indicators remain after the end of the F-T cycles.

- The HPC mixture that is currently used by ODOT provides significant protection against chloride ingress and F-T action. Despite the fact that both chloride exposure F-T regimes were rather aggressive, these mixtures performed well in comparison to other mixtures that represent ODOT mixtures that were used in the past. In particular, mixtures that did not contain any SCMs showed significant chloride ingress. The bridge decks that have been built using similar mixtures should be examined in the field more closely.

5.0 MODEL DEVELOPMENT

5.1 BACKGROUND

This chapter describes the theoretical background of the finite element (FEM) model development for relating SR measurements to chloride ingress in reinforced concrete bridge decks. The FEM models developed in this project are intended for use as virtual experiments. They can be used to represent bridges in different geographical areas in Oregon. The results can be used to derive practical, closed-form equations to be used by ODOT. A demonstration case study of such an application is presented in Chapter 6.

Since the resistivity of hydrated cement phases and of aggregate in concrete are orders of magnitude larger than the resistivity of concrete pore solution, the electrical resistivity of concrete is mainly controlled by the resistivity (or conductivity) of the concrete pore solution. The connectivity and the degree of saturation of the pore structure in the concrete matrix affect the overall conductivity; therefore, modeling electrical resistivity of concrete requires consideration of these parameters. In addition, the actual resistivity (or conductivity) of the concrete pore solution is related to the type and amount of ionic species and temperature. As a result, modeling electrical resistivity of concrete requires that we know the types and concentrations (or activities) of the ionic species in the matrix. These complex dependencies require that relating electrical resistivity of concrete to chloride ingress should include coupled modeling of SR measurements with heat and moisture transfer analyses as well as multi-species ionic transport in concrete. The following sections provide the details of the modeling theory that was used in this research.

5.2 MODELING OF SURFACE RESISTIVITY MEASUREMENTS

The electrical resistivity measurements of concrete using a Wenner probe are modeled through the solution of Laplace's equation:

$$\nabla\left(\frac{\sigma}{FF}\nabla\varphi\right) = 0 \tag{5.1}$$

where σ is the conductivity of the concrete pore solution (S/m), φ is the electrical potential (V), and FF is the formation factor of concrete, which is defined as the ratio of the resistivity of a bulk concrete (r) and the resistivity of the pore solution (r_o), as shown in Equation 5.1 *(Archie 1942)*:

$$FF = \frac{r}{r_o} \tag{5.2a}$$

An alternative way of expressing the formation factor is by using Archie's Law, which establishes generic relationship for most porous materials via *(Archie 1942)*:

$$FF = Ae^{-m} \tag{5.2b}$$

where A and m are constants, and e is the porosity of the concrete that can be estimated by Equation 5.3. [Note that Eq. (5.2b) is the same as Eq. (2.5). Here we use e as the symbol for porosity because we are using φ for electrical potential.] The coefficient A is related to the tortuosity [assumed 1.0 in this study], while the coefficient m is related to the cementation of the concrete porous medium, hence, on the type of the porous medium studied. For example, it has been observed to be around 1.3 for unconsolidated sands, and between 1.8 and 2.0 for consolidated sandstone. For carbonate rocks, the exponent shows higher variance (e.g. 1.7 to 5.1) due to complex pore structures. Similarly, variability for concrete is also high (from 1.9 to 6); however, it is generally around 2.0. Due to the sensitivity of the formation factor to this coefficient, accuracy of modeling depends highly its value.

The porosity of concrete is approximated using a Powers-based approach *(Powers and Brownyard 1946)* to include the effect of the degree of hydration, as shown in Equation 5.3.

$$\mathbf{e} = \boldsymbol{e_0} - \Delta \boldsymbol{e} = \frac{\frac{\boldsymbol{\rho_c}}{\boldsymbol{\rho_w}}\frac{\mathbf{w}}{\mathbf{c}}\left(\mathbf{1}-\boldsymbol{\varepsilon_{air}}\right)}{\left(\mathbf{1}+\frac{\boldsymbol{\rho_c}}{\boldsymbol{\rho_w}}\frac{\mathbf{w}}{\mathbf{c}}+\frac{\boldsymbol{\rho_a}}{\boldsymbol{\rho_w}}\frac{\mathbf{a}}{\mathbf{c}}\right)} + \boldsymbol{\varepsilon_{air}} - \frac{\left[\mathbf{0.23}\ \frac{\boldsymbol{\rho_c}}{\boldsymbol{\rho_w}} - \mathbf{6.4}\cdot\mathbf{10^{-5}}\boldsymbol{\rho_c}\right]\boldsymbol{\alpha_c}}{\left(\mathbf{1}+\frac{\boldsymbol{\rho_c}}{\boldsymbol{\rho_w}}\frac{\mathbf{w}}{\mathbf{c}}+\frac{\boldsymbol{\rho_a}}{\boldsymbol{\rho_w}}\frac{\mathbf{a}}{\mathbf{c}}\right)} \qquad \textbf{(5.3)}$$

where e_o is the initial porosity before hydration, ρ_c is the density of cement, ρ_w is the density of water, ρ_a is the density of aggregate, w/c is the water-to-cement ration, a/c is the aggregate-to-cement ratio, and ε_{air} is the ratio of air entrapped and entrained in concrete. The coefficient α_c represents the degree of hydration of cement, which can be approximately predicted based on cement composition, age of the concrete and average temperature. In reality, the degree of hydration can be predicted as a function of time using the Parrot and Killoh model (Parrot and Killoh 1984). However, since the main goal of this study was to develop a modeling protocol for existing bridge decks, the change in porosity due to hydration is based on the maximum possible degree of hydration, which was related to w/c as per the Powers model and shown in Figure 5.1.

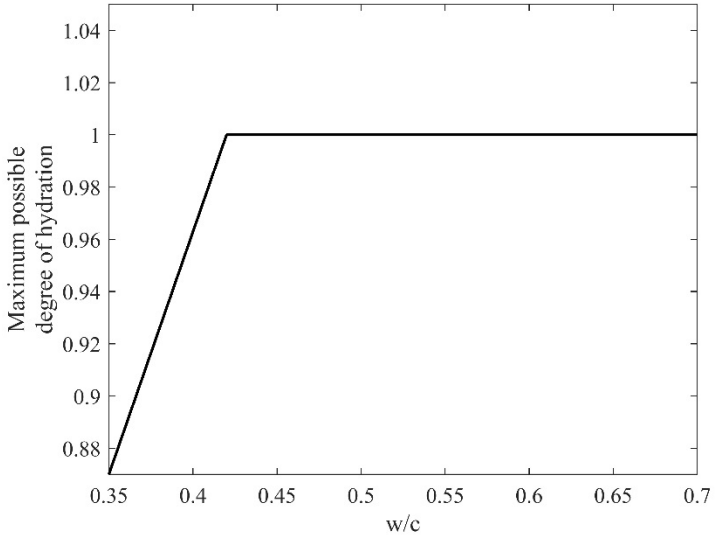

Figure 5.1: Maximum possible degree of cement hydration based on w/c.

It should be noted that Equation 5.2b assumes that pores are fully saturated with the liquid phase. When the pores are partially saturated, electrical resistivity of concrete is significantly affected by the water content of the medium. In this research, the effect of water content (or the degree of saturation) on formation factor is incorporated as a factor to modify Equation 5.2b such that

$$\mathbf{FF} = \left(\frac{\mathbf{w_e}}{\mathbf{w_{e,sat}}}\right)^{\mathbf{n_s}} \mathbf{A e^{-m}} \tag{5.4}$$

where w_e is the water content of concrete, $w_{e,sat}$ is the water content in saturated state of concrete, and n_s is the saturation coefficient (assumed 3.5 in this study) *(Weiss et al. 2012)*. Here the ratio $w_e/w_{e,sat}$ represents the degree of saturation of concrete. The determination of water content of concrete is discussed further in the following sections.

As shown in Equation 5.1, another important parameter that affects SR measurements of concrete is the conductivity of the concrete pore solution, σ, which depends on the type (e.g. (OH-, K+, Na+, Ca2+ and SO42-) and concentrations (or activities) of the ionic species in the solution. When the type and activities of the ionic species in the concrete pore solution are known, the conductivity of the pore solution can be obtained via *(Hovarth 1985, Snyder et al. 2003)*:

$$\sigma = \sum_{i=1}^{n} \frac{\mathbf{z_i \lambda_i c_i}}{\mathbf{1 + G_i I_{sol}}^{1/2}} \tag{5.5}$$

where n is the number of species considered, z_i is the valance number of the species i, c_i is the concentration (mol/m^3) of species i, λ_i is the equivalent conductivity of species i at infinite dilution, and I_{sol} is the ionic strength of the solution (mol/m^3), which is further discussed in detail later. The determination of the pore solution composition, c_i, can be achieved through thermodynamic modeling *(Azad et al. 2016)* or simplified approaches that are based on empirical data (Karadakis et al. 2016). In this study both approaches have been used; however, for practical reasons the latter is used in most simulations presented in this report. Table 1 provides $z_i\lambda_i$ values for different species that exist in typical concrete pore solutions *(Hovarth 1985)*. The empirical coefficients G_i are chosen for best agreement with published data for the electrical conductivity of solutions *(Snyder et al. 2003).*

Table 5.1: Equivalent conductivity at infinite dilution, zλ (cm^2/ Ω-mol) (Hovarth 1985).

Ion	0℃	18℃	25℃	50℃	75℃
Cl^-	41.4	66.3	76.4	117.2	162.4
Mg^{2+}	31.0	44.6	53.1	86.4	125.7
OH^-	105	174	197	281.1[1]	364.5[a]
Na^+	25.7	42.6	50.1	79.9	113.5
K^+	40.3	63.7	73.2	112	152.9
Ca^{2+}	30.5	50.4	59.8	96.6	138.2

[1] These values were calculated by linear interpolation.

The solution of Equation 5.1 results in the distribution of the electrical potentials, φ, in the analysis domain. Using the values of the electrical potentials on the surface, and assuming homogeneous, isotropic, and semi-infinite concrete domain, the SR based on the Wenner probe calculations can be performed via *(Telford et al. 1990, Salehi 2013)*:

$$SR=2\pi a\,\frac{\Delta\varphi}{I} \tag{5.6}$$

where Δφ is the potential difference between two internal electrodes of the Wenner probe (V), a is the distance between the electrodes (m) and I is the applied current in the domain through the outer probes (A) as shown in Figure 5.2.

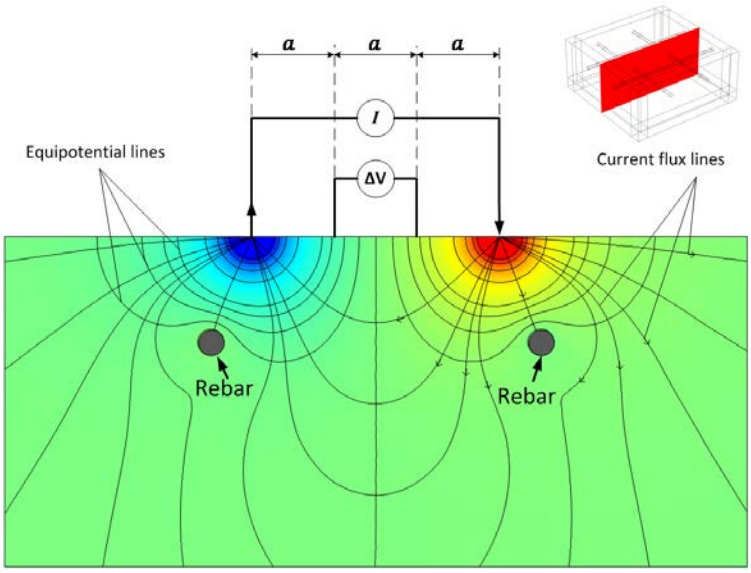

Figure 5.2: Typical configuration of Wenner probe resistivity measurement in reinforced concrete *(Salehi et al. 2016)*.

5.3 MODELING HEAT TRANSFER IN CONCRETE

The temperature distribution within concrete is modeled through the solution of the following governing equation *(Isgor and Razaqpur 2004)*:

$$\rho_{co}c_q\frac{\partial T}{\partial t}+\nabla(\lambda\nabla T)=0 \tag{5.7}$$

where ρ_{co} is the concrete density (kg/m^3), c_q is the specific heat capacity of concrete (840 J/kg-K), T (K) is the temperature in the slab and λ is the thermal conductivity in concrete (assumed as 1.4 W/m-K) *(Neville 1995)*. Boundary conditions of the heat transfer analysis are obtained from available weather station data or input manually.

5.4 MODELING MOISTURE TRANSFER IN CONCRETE

The moisture content of concrete is determined though the assumed equilibrium between relative humidity and water content in the pores of concrete *(Xi et al. 1994)*. The relative humidity

distribution, h, within concrete is obtained through the solution of the following governing equation:

$$\frac{\partial w_e}{\partial h}\frac{\partial h}{\partial t}+\nabla (D_h \nabla h)=0 \quad (5.8)$$

where w_e is the water content per unit volume of concrete (m^3/m^3) and D_h is the modified humidity diffusion coefficient (m^2/s). The effects of degree of concrete hydration, temperature and pore relative humidity of concrete are used to modify the humidity diffusion coefficient via *(Saetta et al. 1993)*:

$$D_h=D_{h0}\, f_1(t_e)\, f_2(T)\, f_3(h) \quad (5.9)$$

where D_{h0} is the reference-humidity diffusion-coefficient at 25°C and f_1, f_2 and f_3 are correction factors for the effects of concrete age, temperature and relative humidity, respectively, which are calculated as follows *(Bažant and Najjar 1972)*:

$$f_1(t_e) = 0.3 + \left(\frac{13}{t_e}\right)^{1/2} \quad (5.10)$$

$$f_2(T) = \exp\left(\frac{U}{R}\frac{1}{T_0}-\frac{1}{t}\right) \quad (5.11)$$

$$f_3(h) = \alpha_0 + \frac{1-\alpha_0}{1+\left(\frac{1-h}{1-h_c}\right)^6} \quad (5.12)$$

where t_e is the equivalent time of hydration, U is the activation energy of ionic diffusion (4×10^4 kJ/mol), T_0 is temperature of measurement of D_{c0} (K), R is gas constant (8.314 J/kmol), T is the temperature in concrete (K), T_{ref} is the reference temperature (296.15 K), α_0 is a parameter representing the ratio of the minimum and maximum value of the humidity diffusion coefficient (assumed as 0.05), h_c is the inflection point in the graph of $f_3(h)$ versus relative humidity (assumed as 0.75) *(Bažant and Najjar 1972)*. The equivalent time of hydration is calculated via *(Bažant and Najjar 1972)*:

$$t_e = t_0 + \int_{t_0}^{t} \beta_T\, \beta_h dt \quad (5.13)$$

$$\beta_T = \exp\left[4600\left[\frac{30}{T-263}\right]^{0.39}\left(\frac{1}{T_{ref}}-\frac{1}{T}\right)\right] \quad (5.14)$$

$$\beta_h = [1+(7.5-7.5h)^4]^{-1} \quad (5.15)$$

Boundary conditions of the heat transfer analysis are obtained from available weather station data or input manually.

5.5 MODELING IONIC TRANSPORT IN CONCRETE

The transport of ionic species in concrete (e.g. Cl^-, Mg^{2+}, OH^-, Na^+, K^+ and Ca^{2+}) is governed by the extended Nernst-Planck equation that couples diffusion, electrical migration, chemical activity and advection via *(Azad et al. 2016)*:

$$\mathbf{w_e \frac{\partial c_{i,aq}}{\partial t} + \frac{\partial c_{i,s}}{\partial t} = -\nabla(w_e D_{ci} \nabla c_i + w_e \frac{D_{ci} z_i F}{RT} c_i \nabla \varphi + w_e D_{ci} c_i \nabla \ln \gamma_i - D_h c_i \nabla w_e)} \quad \textbf{(5.16)}$$

where c_i is the ionic concentration of species (mol/m^3), $c_{i,s}$ is the mole amounts of solid species (if any) (mol/m^3 of pore solution), D_{ci} is the modified diffusion coefficient of species (m^2/s), w_e is the water content, z_i is the species valence number, F is the Faraday constant (96,488.46 C/mol), φ is the electrical potential (V), γ_i is the chemical activity of the species, D_h is the modified relative humidity coefficient (m^2/s). The ionic diffusion coefficient of species is modified with the effects of temperature, measurement time, and relative humidity *(Saetta et al. 1993)* as follows:

$$\mathbf{D_c = D_{c0} . f_2(T)\ f_4(t, w/c)\ f_5(h)} \quad \textbf{(5.17)}$$

where D_{c0} is the reference diffusion coefficient of each ion at 25^{o}C, f_4(t, w/c) is a factor for measurement time, and f_5(h) is a factor that incorporates the effect of relative humidity on D_c such that:

$$\mathbf{f_4(t, w/c) = (t_0/t)^{(2.5w/c - 0.6)}} \quad \textbf{(5.18)}$$

$$\mathbf{f_5(h) = [1 + (1 - h)^4 / ((1 - h_c)^4)]^{-1}} \quad \textbf{(5.19)}$$

where t_0 is the time of measurement of D_{c0}. In this research, the reference diffusion coefficient was assumed as an empirical function of w/c as:

$$\mathbf{D_{c0} = 10^{(-12.06 + 2.4(w/c))}} \quad \textbf{(5.20)}$$

To calculate the activity of all the ionic species, the approximation method proposed by Kumar et al. is used via *(Kumar et al. 2012)*:

$$\mathbf{\log \gamma_i = \frac{-A_g z_i^2 \sqrt{I_{sol} . 10^{-3}}}{1 + B_g a_i \sqrt{I_{sol} . 10^{-3}}} + b_i (I_{sol} . 10^{-3})} \quad \textbf{(5.21)}$$

where γ_i is the activity coefficient a_i and b_i are the ionic specific values and are reported in Table 5.2. A_g and B_g in Equation 5.21 are calculated as:

$$\mathbf{A_g = (2.74 \times 10^{-6}) T^2 + (-7.60 \times 10^{-4}) T^1 + (0.4916)} \quad \textbf{(5.22)}$$

$$\mathbf{B_g = (1.62 \times 10^{-4}) T^1 + (0.2799)} \quad \textbf{(5.23)}$$

Table 5.2: Parameters required for the calculation of activity of species using Equation 5.21.

Ion	z	a ($\times 10^{-10}$ (m))	b ($\times 10^{-10}$ (m))
Cl^-	-1	3.5	0.015
Mg^{2+}	+2	5.5	0.2
OH^-	-1	10.65	0.21
Na^+	+1	4	0.075
K^+	+1	3.5	0.015

The ionic strength, I_{sol} (mol/m^3) is calculated via *(Azad et al. 2016)*:

$$\mathbf{I_{sol} = 0.5 \sum_{i=1}^{n_s} c_i z_i^2} \tag{5.24}$$

The electric potential distribution within concrete (to be used in Equation 5.16) is determined through the solution of the Poisson's equation, which also requires the satisfaction of the electroneutrality within the system *(Samson and Marchand 1999)*:

$$\mathbf{\nabla(w_e \nabla \psi) + \frac{F}{\varepsilon} w_e \sum_{i=1}^{n_s} z_i c_i = 0} \tag{5.25}$$

where ε is the permittivity of the medium (7.092×10^{-10} C^2/N/m^2).

Chloride binding by hydrated phases in concrete is modelled using the Langmuir isotherm via *(Martin-Perez 1999)*:

$$\mathbf{c_{bi} = \frac{\alpha_{ci} c_{fi}}{1 + \beta_{ci} c_{fi}}} \tag{5.26}$$

where α_{ci} and β_{ci} are the binding coefficients of species, which are obtained from experimental data. c_{bi} is the concentration of bound specie and c_{fi} is the concentration of the free specie (mol/m^3).

The boundary conditions for salt exposure depend on the local region where the analyzed structure resides; therefore, they are defined manually for each analysis. In this research, the surface salt concentration (percent mass of concrete) is assumed as a bilinear function as shown in Figure 5.3. This assumption is consistent with other durability models/software *(Ehlen et al. 2009)*.

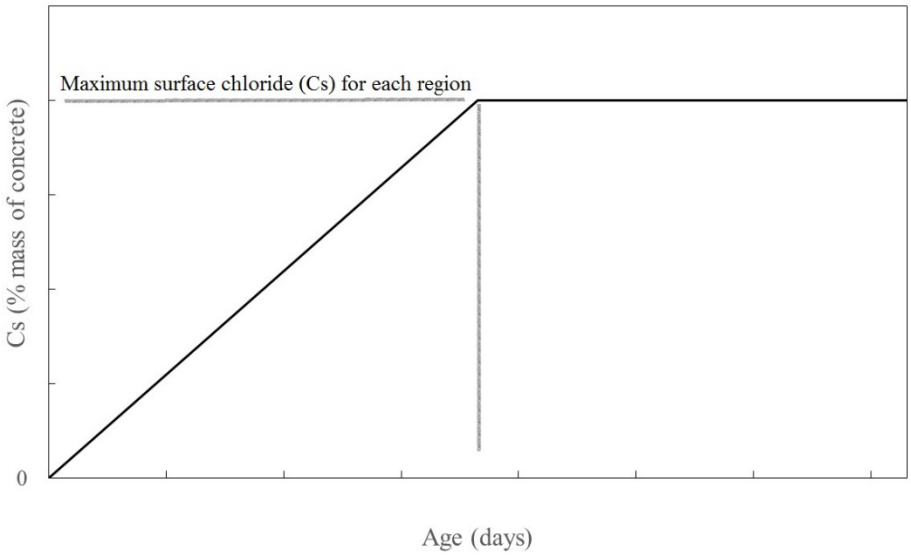

Figure 5.3: *The boundary condition for salt on bridge deck surface.*

5.6 ANALYSIS

The FEM models were developed and analyzed for concrete bridge decks with uniform material, boundary, and initial conditions. COMSOL Multiphysics™ was the tool used for the models. The coupled ionic transport and heat/moisture transfer analysis was conducted on a one-dimensional domain, while a three-dimensional model was developed for evaluating the SR in order to consider the effects of unsymmetrical positioning of Wenner probes on the concrete bridge deck slabs. Figure 5.4 shows the model geometry and FEM discretization of the analyzed zone. Typical domain had a 1.27 m diameter and 0.165m thickness, which eliminated the boundary effects on the simulation results. The electrode spacing of the Wenner probe was assumed to be 50 mm, which is typical in most commercial applications. The environmental (temperature, relative humidity) and deicing salt boundary conditions were applied on the top surface as Dirichlet boundaries. All other surfaces are assumed to have no-flux boundary conditions. Linear Lagrange elements were used to discretize the domain; the discretization was customized based on convergence rates, computational cost, and the level of accuracy needed for the analysis. All analysis cases were run to simulate 25 years of exposure, and the results were stored at 4-month intervals (i.e., three sets of results were saved for each year). Each set of results included ionic concertation, temperature, and moisture profiles as well as electrical resistivity calculations for concrete and concrete pore solution.

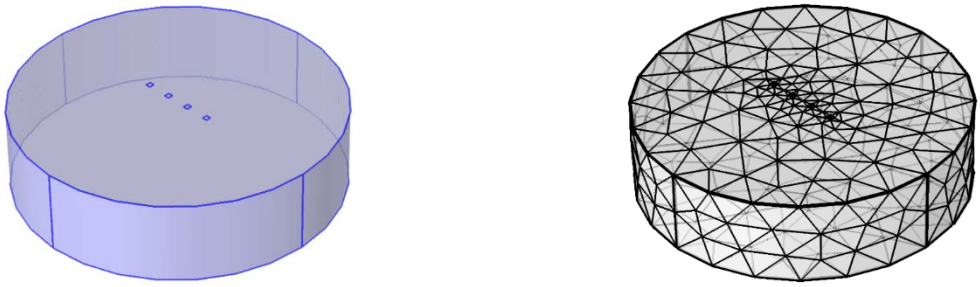

(a) (b)

Figure 5.4: (a) Domain geometry with the Wenner probe locations on top; (b) FEM discretization.

5.7 EXPERIMENTAL VALIDATION

The FEM modeling framework presented in this chapter was verified and validated by the data from this experimental program, other available experimental data from literature, and model benchmarking studies. It should be noted that the experimental program used a rather aggressive approach to increase the rate of chloride ingress in concrete, using chloride ponding and drying cycles to increase adjective transport of chlorides. The modeling framework was developed mainly for bridge decks that experience normal chloride exposure conditions, which typically have significantly a smaller, advective component. Therefore, it is expected that the modeling framework would likely perform better in simulating actual field conditions. Hence, the verification and validation of the developed transport model were conducted with experimental data from literature that is more representative of the field conditions as well as model benchmarking studies.

The verification and validation of the transport model are not presented here for the sake of brevity. Instead, the focus in this report is placed in the validation of SR predictions using the FEM modeling framework. For the validation of the SR predictions sing the developed modeling framework, the chloride profiles obtained from the concrete slabs tested in this experimental program were used as input. The SR predictions of the six different slabs (that did not go through F-T cycles) were computed and presented in Figure 5.5. Note that the simulations involved the validation of the temperature and relative humidity predictions of the model as well; however, these results are not presented for the sake of brevity.

The surface resistivity was calculated based on the input data from the experiments for each slab including concrete properties, temperature, relative humidity, and chloride profiles. The temperature and relative humidity boundary conditions were obtained from the installed weather station in the outdoor exposure site. While the concentrations of other ions in pore solution were assumed constant, Magnesium concentration was obtained from electro-neutrality. The maximum degree of hydration was considered based on w/c (i.e. 1.0 for w/c$\geq$0.42). Finally, a regression analysis was performed to obtain the formation factor of each slab with/out salt exposures. Table 5.7 shows the resulted “m” values from these regression analyses (see Equation 5.4).

Table 5.3: Regression analysis results for the calculation of formation factor coefficients m and A in Equation 5.2b.

Slab	Salt exposed slabs		Control slabs	
	m	**A**	**m**	**A**
ST1-W40	2.0141	0.9956	2.0119	0.8642
ST1-W47	2.1168	1.0794	2.3305	0.9115
ST1-W60	2.4429	1.1403	2.8572	0.9913
ST2-W53	1.7624	1.1848	1.8463	1.0098
ST3-W35	1.8957	1.0269	2.1266	0.9571
ST4-W43	1.9443	0.9872	2.1746	0.9169

The formation factors can be obtained from the parameters in Table 5.3 and using the input data from the experiments at each monitored time. Figure 5.5 shows the variations in formation factors from the model. The increase in the formation factor in the early stages is related to the microstructure development in concrete. During these early stages (first ~100-120 days) the formation factor increased similarly for both the deicing chemical exposed and water (control) exposed slabs. During dry period when relative humidity (and the degree of saturation) decreased within concrete, formation factor increased sharply, as expected. This illustrates the strength and potential of the formation factor (and other electrical based parameters) to capture microstructural and moisture-related changes within concrete.

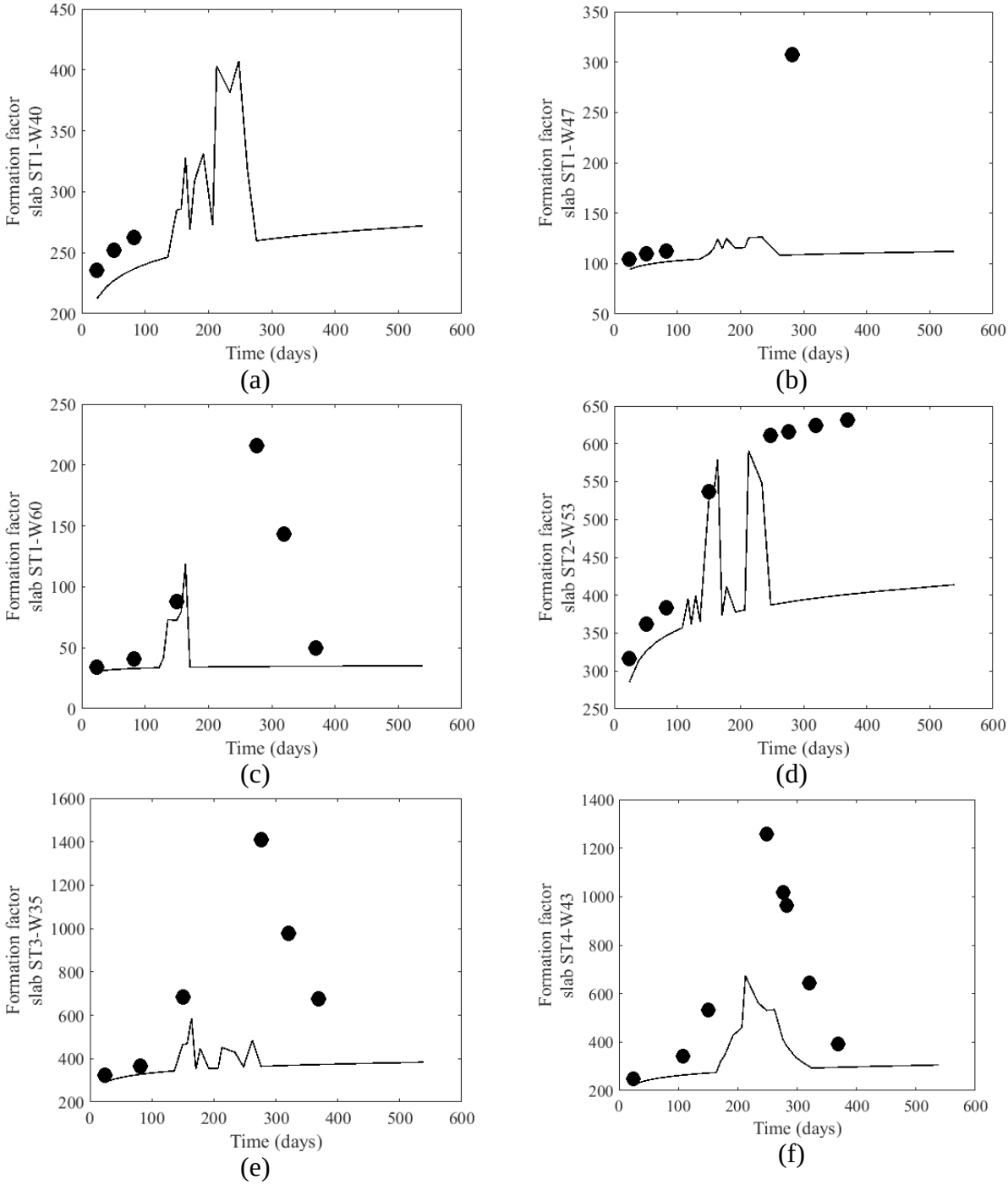

Figure 5.5: Comparison of the computed formation factors for the deicing chemical exposed and water exposed slabs (a) ST1-W40, (b) ST1-W47, (c) ST1-W60, (d) ST2-W53, (e) ST3-W35 and (f) ST4-W43.

More interestingly, in later stages, after chloride ingress became more prominent, formation factors for the deicing chemical exposed slabs were higher than those for the water exposed control slabs. This difference is due to the decrease in electrical resistivity of concrete pore solution due to new Mg^{+2} and Cl^{-} ions, as per Equation 5.2a. When chloride-containing salts start penetrating into concrete, some is bound into the hardened matrix and the rest remains in

the pore solution. The effect of chloride binding and presence of free chloride ions in the pore solution might affect the electrical properties differently. For example, the former would increase the electrical resistivity of the matrix, while the latter would decrease the electrical resistivity of the pore solution. However, in later stages, as the binding capacity of concrete is reached, the effect of chloride ingress into concrete should correspond to a decrease in overall electrical resistivity of the pore medium and an increase in formation factors.

As illustrated in Figure 5.6, the model predictions of SR follow capture the range and variation of SR measurements made on different types of slabs. For example the SR predictions and measurements of the ST1 and ST2 slabs, which represent ODOT's past mixtures, mostly range within 5-20 kΩ-cm, while the HPC slab, ST4, which represent ODOT's current mixtures for bridge decks, range within 10-40 kΩ-cm. the first STR measurements of hardened concrete (at about 28 days after casting) are marched very accurately for all slabs, which indicates that the develop SR prediction model can correctly incorporate concrete mixture design parameters. It is also important to note that the predictions also capture changes in SR due to temperature and relative humidity changes.

The FEM modeling framework developed in this project is to be used to conduct virtual experiments for bridges in different geographical areas in Oregon. The results will be used to derive practical, closed-form equations to be used by ODOT. A demonstration case study of such an application is presented in Chapter 6.

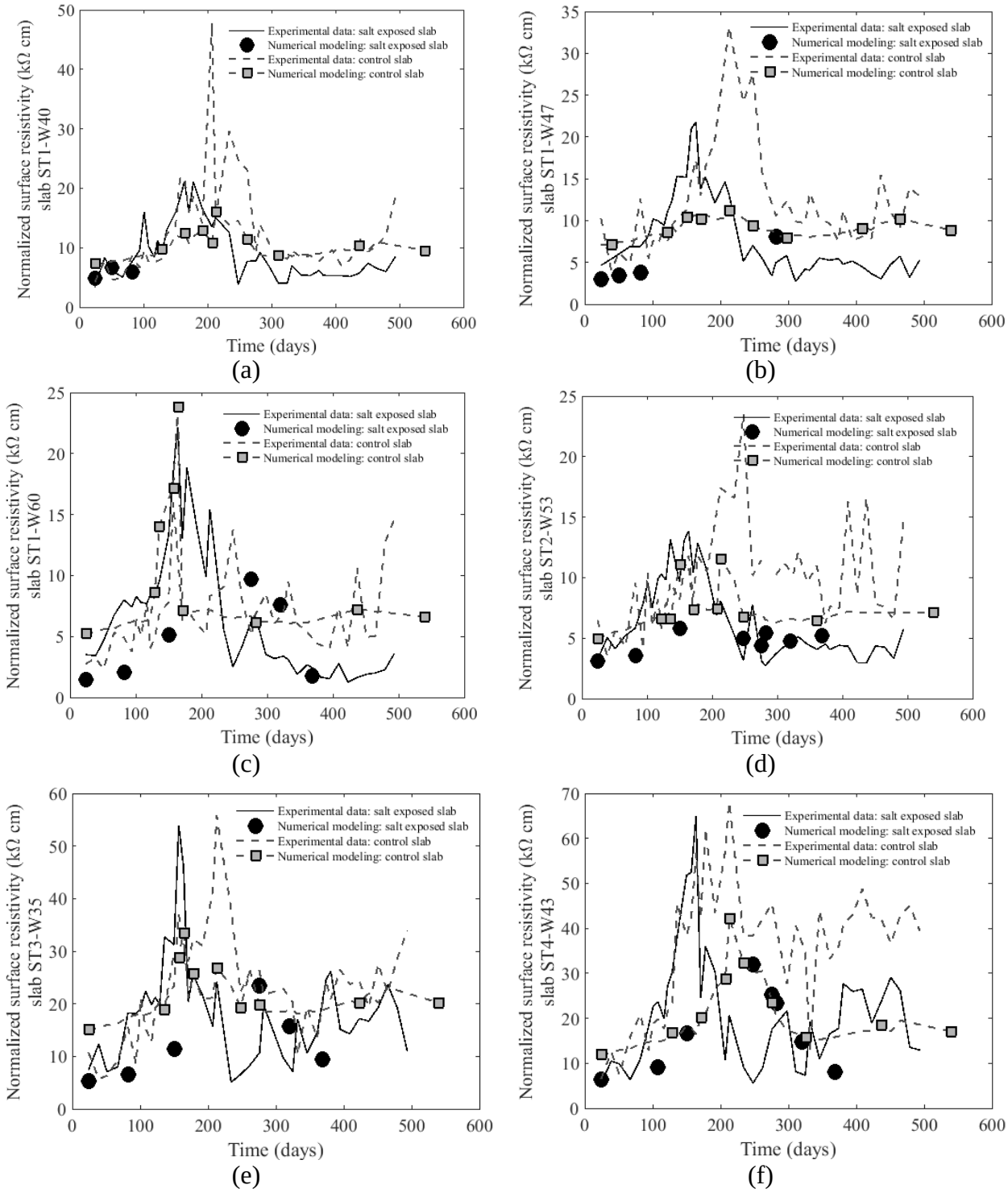

Figure 5.6: Comparison of the computed and experimental SR predictions for the deicing chemical exposed and water exposed slabs (a) ST1-W40, (b) ST1-W47, (c) ST1-W60, (d) ST2-W53, (e) ST3-W35 and (f) ST4-W43.

5.8 SUMMARY

This chapter presented the theoretical background of the finite element (FEM) model development for relating electrical properties of concrete to chloride ingress in reinforced concrete bridge decks. The following summary represents the major outcomes of this experimental investigation.

- Since the resistivity of hydrated cement phases and of aggregate in concrete are orders of magnitude larger than the resistivity of concrete pore solution, the electrical resistivity of concrete is mainly controlled by the resistivity (or conductivity) of the concrete pore solution. The connectivity and the degree of saturation of the pore structure in the concrete matrix affect the overall conductivity; therefore, modeling electrical resistivity of concrete requires consideration of these parameters. In addition, the actual resistivity (or conductivity) of the concrete pore solution is related to the type and amount of ionic species and temperature. As a result, modeling electrical resistivity of concrete requires that we know the types and concentrations (or activities) of the ionic species in the matrix. These complex dependencies require that relating electrical resistivity of concrete to chloride ingress should include coupled modeling of SR measurements with heat and moisture transfer analyses as well as multi-species ionic transport in concrete. In this research, such a modeling framework was developed, verified, and experimentally validated.

- The increase in the formation factor during curing and early stages of service is related to the microstructure development in concrete. During these early stages, formation factor increased similarly for both the deicing chemical exposed and water (control) exposed slabs. During the dry period when relative humidity (and the degree of saturation) decreased within concrete, formation factor increased sharply. This illustrates the strength and potential of the formation factor (and other electrical based parameters) to capture microstructural and moisture-related changes within concrete.

- In later stages, after chloride ingress became more prominent, formation factors for the deicing chemical exposed slabs were higher than those for the water exposed control slabs. This difference is due to the decrease in electrical resistivity of concrete pore solution due to new Mg^{+2} and Cl^{-} ions. When chloride-containing salts start penetrating into concrete, some is bound into the hardened matrix and the rest remains in the pore solution. The effect of chloride binding and presence of free chloride ions in the pore solution might affect the electrical properties differently. For example, the former would increase the electrical resistivity of the matrix, while the latter would decrease the electrical resistivity of the pore solution. However, in later stages, as the binding capacity of concrete is reached, the effect of chloride ingress into concrete should correspond to a decrease in overall electrical resistivity of the pore medium and an increase in formation factors.

6.0 DEMONSTRATION CASE STUDY

6.1 BACKGROUND

The potential practical use of the developed FEM modeling framework developed is presented in this chapter in the form of a case study. It is demonstrated in this chapter that the developed modeling framework can be used as a virtual test bed using to conduct statistically significant number of virtual experiments to generate data to obtain closed-form relationships between electrical properties of concrete (e.g. SR or formation factor), environmental data (e.g. temperature and relative humidity) and chloride ingress for bridge decks in different geographical areas in Oregon. For this demonstration, a hypothetical bridge near Bend, Oregon was selected. The chapter is concluded with a demonstration on how the developed closed-form equation can be used in a bridge-deck evaluation-protocol that can be used by ODOT in practice.

6.2 VIRTUAL EXPERIMENTS

The validated modeling framework allows the conducting large number of virtual experiments that would otherwise be unfeasible due to time, cost, and resource limitations. The generated data can be used to develop qualitative or quantitative relationships among several parameters and measurable properties of a reinforced concrete structure. As discussed in previous chapters, several factors affect electrical properties, chloride ingress and heat and moisture transport in concrete. Any effect of any these parameters on any of the properties can be investigated numerically using virtual experiments.

In this demonstration case study, a hypothetical bridge deck near Bend, Oregon was investigated. The following sections present some of the important parameters that affect electrical properties, ionic transport, and heat and moisture transport in concrete.

6.2.1 Concrete Mixture Design Parameters

As shown in Chapter 4, the type of concrete (i.e. mixture deign properties) significantly affects the electrical and transport properties of concrete. Most of these concrete mixture design properties are incorporated in the modeling framework; therefore, their effects on different electrical and transport properties can be studied though virtual experiments. These properties include (i) water-cement-ratio (w/cm), (ii) cement and SCM content, (iii) aggregate-cement ratio (a/cm), and (iv) air content. Since these properties have a direct effect on porosity and pore connectivity in concrete, as well as the chemical composition of the pore solution, they affect the electrical (e.g. formation factor and electrical resistivity) and transport properties (chloride diffusion coefficient, moisture transport coefficient, or heat conductivity) of concrete. In most cases, these data are known for investigated bridge decks. Reasonable, educated assumptions can be made even when some of these data are not known.

In this demonstration case study, a parametric study was conducted to study the effects of major concrete mixture design parameters on electrical and transport properties of concrete bridge deck. The ranges of parameters of this investigation are presented in Table 6.1.

Table 6.1: Concrete Mixture design parameters that are used in the virtual experiments.

Parameter	**Value(s)**
w/cm	0.35, 0.45, 0.55
a/cm	3
OPC content	350 kg/m^3
SCM content	0
Air content	0, 2%, 4%, 6%

6.2.2 Environmental Parameters and Deicing Chemical Exposure

Bridges in different geographical areas experience different temperature, relative humidity, moisture, and deicing chemical exposure profiles. Virtual experiments can be used to generate chloride ingress and/or SR data for any given bridge for a desired service life. In Oregon (and most of Pacific Northwest), current or historical environmental data such as temperature and relative humidity can be directly obtained from Cooperative Agricultural Weather Network (AgriMet). AgriMet provides weather data at every 15-minute intervals, hence, providing a very high resolution of environmental input data for typical virtual experiments on reinforced concrete structures. Figure 6.1 illustrates the locations of current AgriMet weather stations, which cover most regions of interest in Oregon and Pacific Northwest.

Although AgriMet database allows high resolution data (collected every 15 minutes), for a typical analysis for which the changes in chloride profiles and electrical properties within a concrete bridge deck over multiple years are investigated, lower resolution of the environmental data (e.g. hourly or daily) is more appropriate to minimize computational expense and uncertainties associated with high resolution data. For the current virtual experiments, the environmental data were obtained from BEWO weather station, which is located at 44.0475 N latitude, 121.32027 W longitude, 3620 ft. elevation. The BEWO weather station has been in operation since 5/1/2003; therefore, it has multiple year data at the location, allowing multi-year averages to be obtained. In this study, the environmental data resolution was 1 day, and periodic annual average environmental boundary conditions were used. The first day of the analysis was January 1, and the simulations were performed for 25 years of bridge deck service. Figures 6.2 presents the average annual temperature and relative humidity profiles obtained from the BEWO weather station.

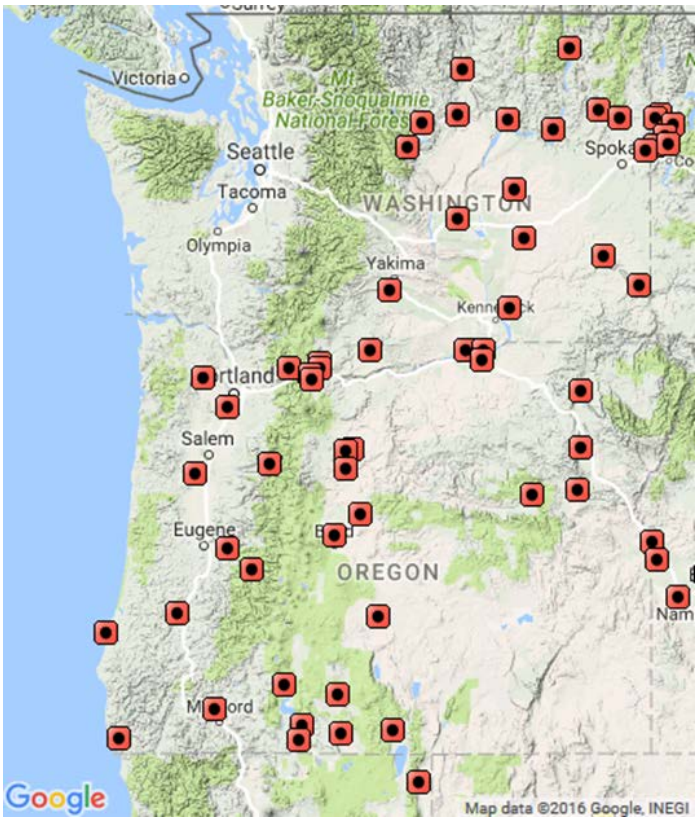

Figure 6.1: AgriMet weather station locations in Oregon and Washington. *(http://www.usbr.gov/pn/agrimet/)*

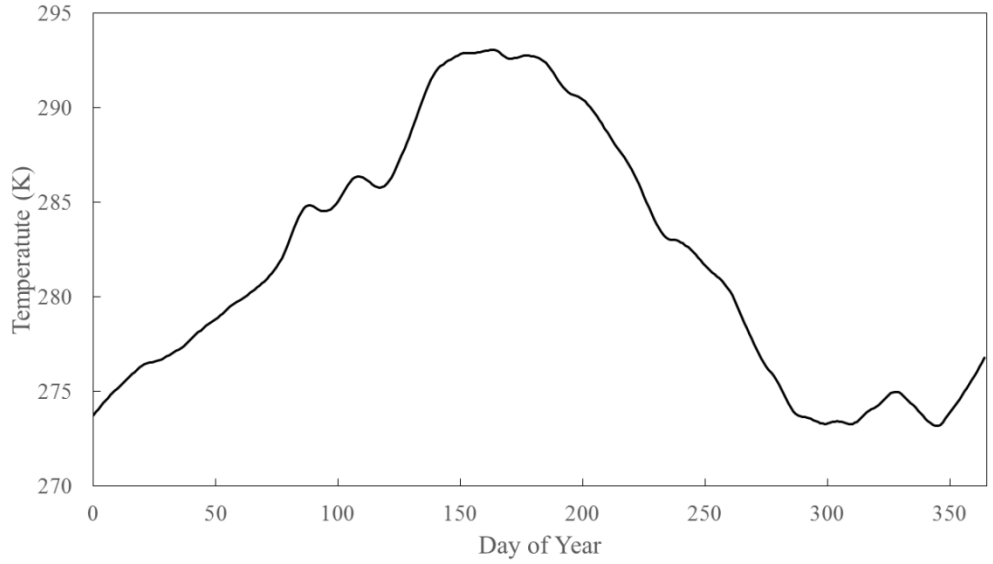

(a)

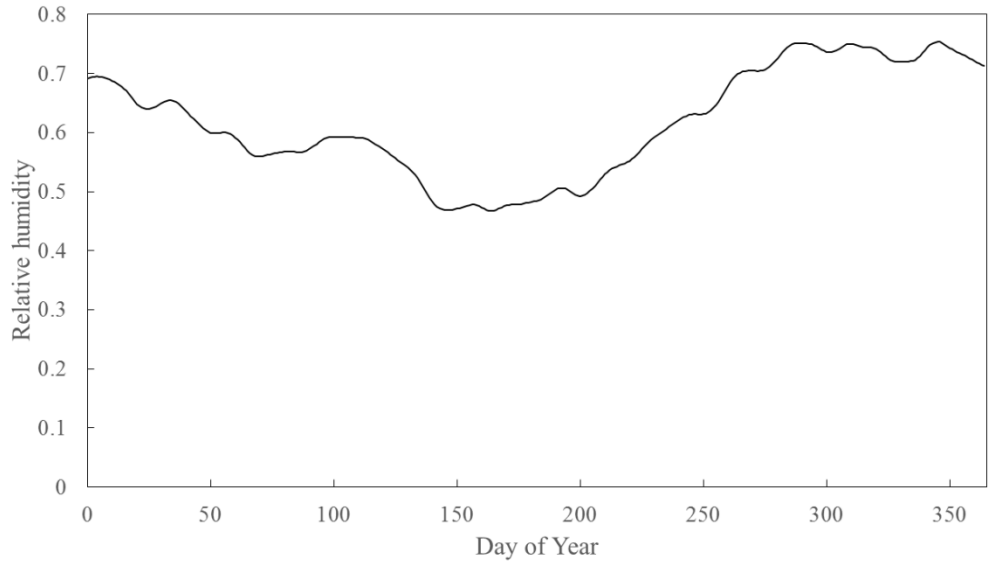

(b)

Figure 6.2: The average data for environmental boundary conditions from BEWO-AgriMet weather station (near Bend, Oregon): (a) average daily temperature and (b) average daily relative humidity. The first day of the year is January 1.

The amounts of de-icing chemical usage in different parts of Oregon are documented by ODOT *(Shi et al. 2013, Huang et al. 2014).* From this data, salt exposure profiles can be obtained for use in virtual experiments. In the present virtual experiments, the bilinear chloride exposure model as shown in Figure 5.3 was used. The maximum surface salt ($MgCl_2$) concertation, C_s, was selected for the location to range from 0.8 to 1.2 % (by mass of cement). The maximum salt concertation was assumed to be reached in 10 years.

6.2.3 Modeling Parameters

As described in Chapter 5, the FEM modeling framework has a number of modeling parameters that are needed as input. The modeling parameters that are listed in Table 6.2 were used in the virtual experiments. Note that the effect of changing the formation-factor porosity-coefficient, m, was investigated. It is documented in the literature that the formation factor is highly sensitive to this parameter and there is a relatively large variability in the reported values.

Table 6.2: Modeling parameters that are used in the virtual experiments.

Parameter	Value(s)
A, tortuosity coefficient (Eq. 5.2a)	1.0
m, cementation coefficient (Eq. 5.2b)	1.8, 2.9, 2.2
n_s, saturation coefficient (Eq. 5.4)	3.5
D_{h0}, reference humidity diffusion coefficient at 25°C	2×10^{-10} m^2/s
α_{ci}, chloride binding coefficient*	0
$\beta_{ci,}$ chloride binding coefficient*	0
$\rho_{co,}$ density of concrete	2,400 kg/m^3
ρ_c, density of cement	3,150 kg/m^3
ρ_a, density of aggregate	2,700 kg/m^3
ρ_w, density of water	1,000 kg/m^3
c_q, specific heat capacity of concrete	840 J/kg-K
λ, thermal conductivity in concrete	1.4 W/m-K

(*) For the present virtual experiments it was assumed that there was no chloride binding

6.2.4 Analysis and Parametric Investigation

Using the modeling framework, a total of 243 virtual experiments were performed to simulate chloride ingress and surface electrical resistivity measurements in the hypothetical reinforced concrete bridge located near Bend, Oregon. Simulations were performed to cover 25 years of service and exposure to the elements and deicing chemical. Figures 6.3 and 6.4 show the chloride profile and SR predictions, respectively, for a sample analysis case from one of the virtual experiments conducted in this study. The bridge deck in this case had a w/c of 0.35, and the surface $MgCl_2$ contrition, C_s, was 1.0% (by mass of cement).

Figure 6.3 shows the chloride profiles in the bridge deck after 5, 10 and 25 years of service/exposure. Figure 6.4 presents the SR for this case, which represent what an inspector would measure on the bridge surface. Note that these SR data are not temperature normalized; i.e., they show the seasonal fluctuations within each year. The yearly decrease in SR data, as shown by the dotted line in Figure 6.4, clearly shows the effects of chloride ingress in the bridge deck. While the SR has big periodic changes during a typical year, its average value decreases over time because of chloride ingresses.

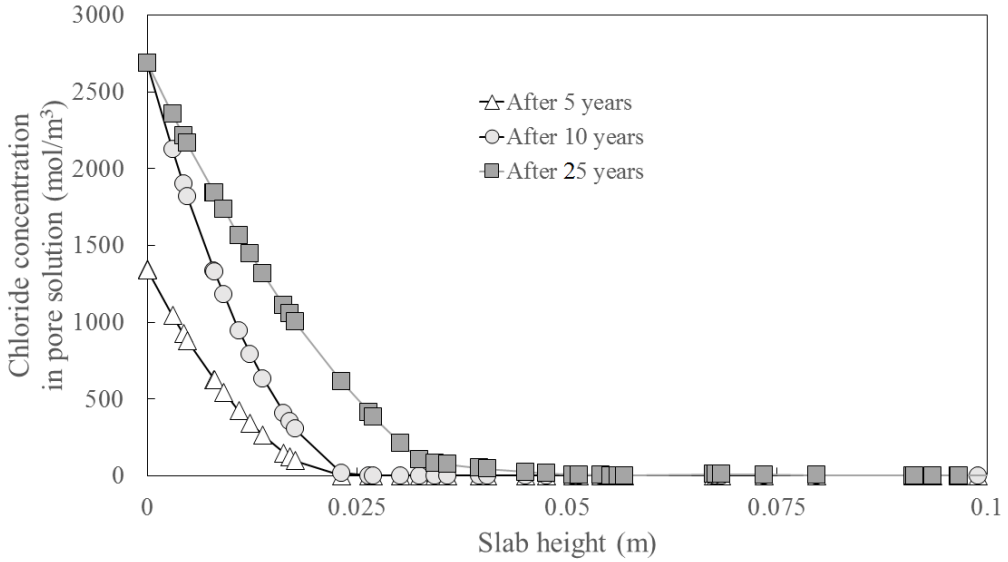

Figure 6.3: Chloride profiles of the example case over bridge deck thickness after 5, 10 and 25 years of exposure.

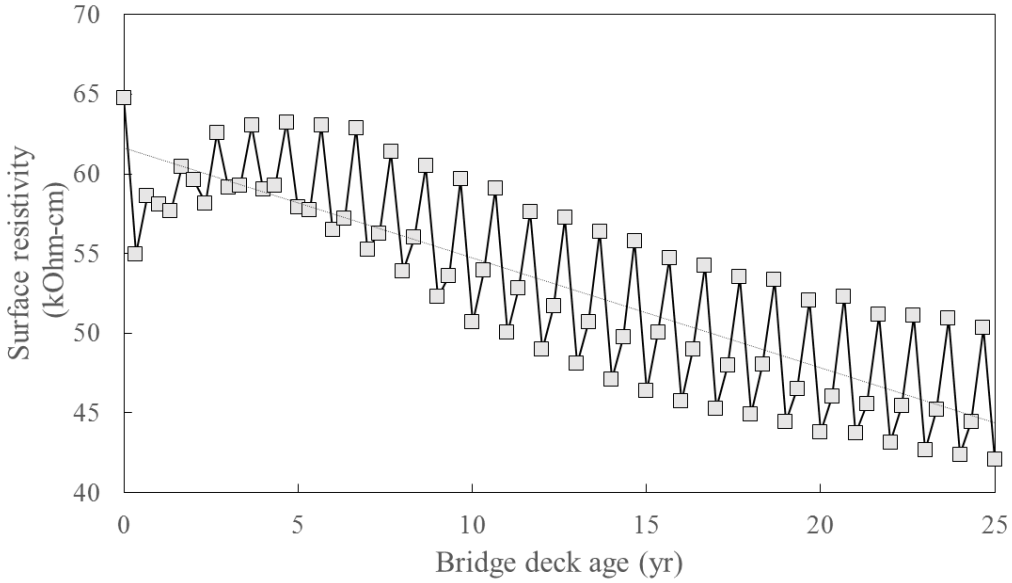

Figure 6.4: SR predictions of the example case over time (not normalized for temperature).

The results of the virtual experiments presented here can also be used to conduct a parametric study. Here this approach is used investigate the effects of a number of concrete mixture design parameters on SR. For example, Figure 6.5 shows the effect of w/c, air content on SR over time. As shown in the plot, the lower w/c and the air content leads to denser concrete and larger SR. From the Figure 6.5(a), it can be seen that the increase of w/c from 0.35 to 0.55 has decreased the average SR by approximately 50%. Figure 6.5(b) shows that change in air content from a theoretical 0% to 6% results in almost 100% change in SR measurements. In both cases, the

overall decrease in average SR resistivity is related to chloride ingress. The seasonal variations within each year due to changes in temperature and relative humidity are also clearly observed.

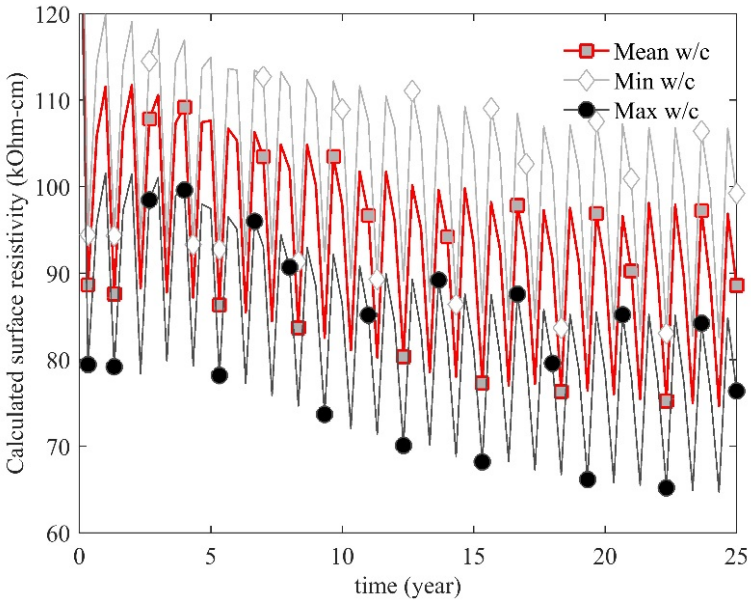

(a)

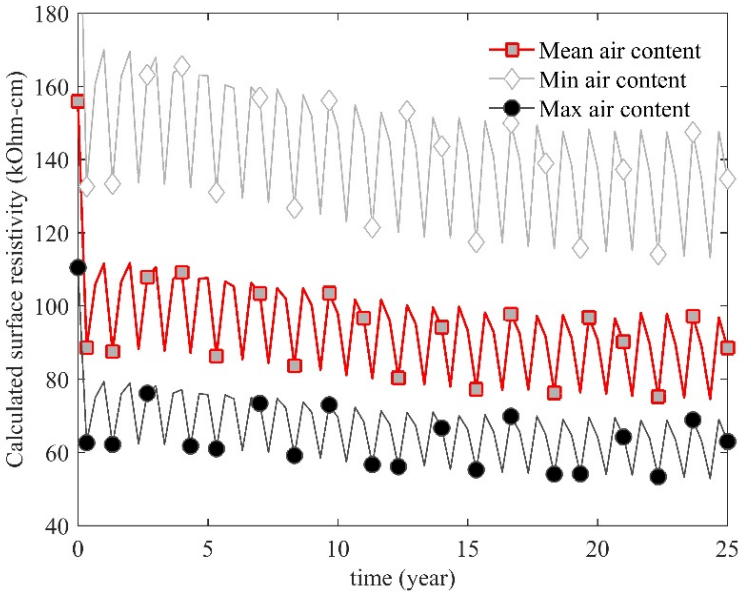

(b)

Figure 6.5: (a) Effect of w/c on SR over bridge deck age. (The considered values for w/c were 0.35, 0.45 and 0.55 for min, mean and max w/c, respectively); (b) Effect of air content on SR over bridge deck age. (The considered values for air content were 0%, 4% and 6% for min, mean and max air contents, respectively).

Similar parametric studies can also be conducted on modeling parameters. For example, Figure 6.6 shows the effect of the variations in the modeling parameter, m, which is used in the calculation of the formation actor, on SR. It is clear that a variation from 1.8 to 2.2 results in significant changes in SR predictions, as much as threefold increase in SR is observed. As before, the average decrease in SR is related to the chloride ingress, and seasonal variations are due to fluctuations in temperature and relative humidity within each year. This example shows another benefit of conducting virtual experiments in that modeling parameters that cannot be practically studied experimentally can be studied in virtual experiments rather easily.

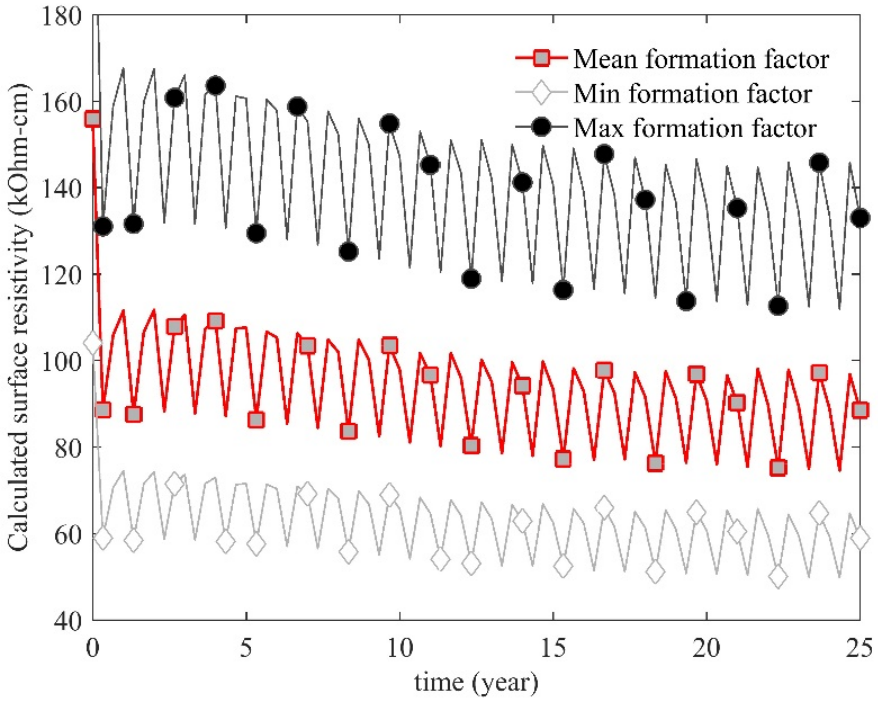

Figure 6.6: Effects of formation factor coefficient, m, on SR over bridge deck age. The considered values for m were 1.8, 2.0, and 2.2 for min, mean and max values, respectively.

Another benefit of virtual experiments shows itself in dealing with uncertainty. For example, if the surface chloride concertation, C_s, for a given bridge deck is not accurately known, as in the case of most bridges, but an assumption on the range can be made, the virtual experiments can be used to obtain a range of results to evaluate for better decision making. An example of such an approach is shown in Figure 6.7, where C_s is assumed to have a ±20% uncertainty over the average values. Similar uncertainty analysis can be performed for any other parameter, including weather station data.

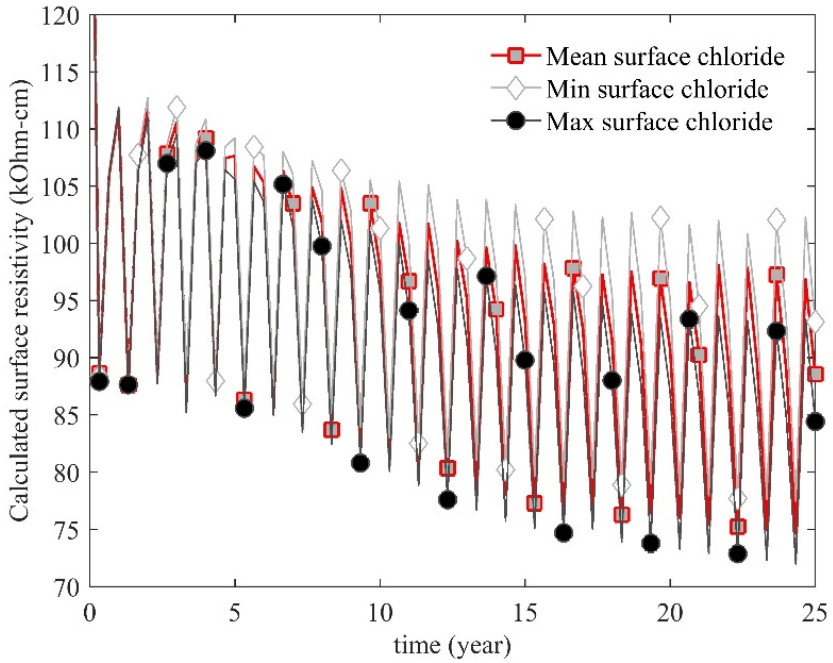

Figure 6.7: Effects of surface chloride concentration uncertainties on SR over bridge deck age. The surface chloride concertation was assumed to have ±20% uncertainty over the average values.

6.3 PROPOSED BRIDGE INSPECTION PROTOCOL

6.3.1 Closed-form Equation for Predicting Chloride Profiles

Chloride profiles along the depth of a concrete bridge deck can be calculated using the closed-form solution of the Fick's Second Law via:

$$C_{Cl}(x,t) = C_s + (C_s - C_o)\, erf\left[\frac{x}{\sqrt{4D_{app}\, t}}\right] \tag{6.1}$$

where C_{cl} is the chloride concentration at depth x and age t., C_s is the surface chloride concentration, C_o is the initial (background) chloride concentration in concrete, and D_{app} is the apparent chloride diffusion coefficient.

The developed modeling framework was used to conducts virtual experiments, as discussed in the previous section. These virtual experiments yielded chloride profiles (over a 25-year service life) for hundreds of virtual bridge decks with different mixture design properties. The collected data are analogous to data that could be collected from hundreds of real experiments that last 25 years, which is not a practically feasible. Conducting nonlinear regression analysis on the collected data from the virtual experiments, the flowing equation for apparent diffusion coefficient was obtained for the inspected bridge deck near Bend, Oregon:

$$D_{app} = \left[\left(a_{11}\ \frac{w}{c} + a_{12}\ SR + a_{13}\ \varepsilon_{air} + a_{14}\right)^3\ t_a{}^3 + \left(a_{21}\ \frac{w}{c} + a_{22}\ SR + a_{23}\ \varepsilon_{air} + a_{24}\right)^3 t_a{}^2 + \left(a_{31}\ \frac{w}{c} + a_{32}\ SR + a_{33}\ \varepsilon_{air} + a_{34}\right)^3\ t_a + \left(a_{41}\ \frac{w}{c} + a_{42}\ SR + a_{43}\ \varepsilon_{air} + a_{44}\right)^3\right] \times 10^{-12} \quad (6.2)$$

where D_{app} is the apparent chloride diffusion coefficient (m^2/s), w/c is the water-to-cement ratio, ε_{air} is the air content of concrete, SR is the temperature normalized surface resistivity of concrete bridge deck at 25°C, and t_a is the age of concrete (years), and a_{ij} are coefficients of the equation that were obtained from the regression analysis. The coefficients of the equation, a_{ij}, are provided in Table 6-3. The adjusted R^2 of the regression analysis was 0.897.

Table 6-3: aij values for the calculation of apparent diffusion coefficient for a bridge deck near Bend, Oregon.

i ↓, j→	1	2	3	4
1	0.2145	-0.1052	0.0446	-0.0851
2	6.74×10^{-6}	0.1176	-0.2378	-0.1487
3	0.0233	-5.02×10^{-6}	-1.1689	0.4977
4	0.0101	0.5308	-7.82×10^{-5}	1.2567

Equation (6.2) is to be used as part of a bridge-deck inspection-protocol, which includes SR measurements. During a typical bridge inspection several SR and surface temperature measurements and can be made within minutes. Average SR measurements can be normalized to 25°C using Eq. (2.2), Hinrichsen-Rasch Law (Hope 1987), to obtain the SR value to be used in Eq. (6.2). Since apparent diffusion coefficient, D_{app}, was obtained from regression analysis of the virtual experimental data, there are likely to include bridge-specific uncertainties that need to be accounted for by providing a maximum and minimum bounds such that

$$D_{app,min} = (1 - \propto_c) D_{app} \quad (6.3)$$

$$D_{app,max} = (1 + \propto_c) D_{app} \quad (6.4)$$

where $\propto_c$ is an uncertainty correction factor, which can be determined from:

$$\propto_c = (SR_{calc} - SR) \Big/ \left[-2.2794\left(-0.1308\frac{w}{c} + 0.4107\varepsilon_{air} - 4.1134\right)^2 t_a{}^3 + 0.0381\left(0.0271\frac{w}{c} - 0.608\ \varepsilon_{air} - 0.1101\right)^2 t_a{}^2 - 0.396\left(-0.0892\frac{w}{c} + 0.1931\ \varepsilon_{air} - 1.2290\right)^2 t_a - 14.33\left(-1.6536\frac{w}{c} + 3.9353\ \varepsilon_{air} - 26.0206\right)^2 + 1.2717\left(0.2069\ \frac{w}{c} - 0.4740\ \varepsilon_{air} + 3.0092\right)^2 \cos\left(\frac{2\pi}{365}\ DOY\right) - 0.1030\left(0.1109\frac{w}{c} - 0.1885\varepsilon_{air} + 2.3080\right)^2 \sin\left(\frac{2\pi}{365}\ DOY\right)\right] \quad (6.5)$$

where SR_{calc} is the calculated theoretical surface resistivity of the bridge deck, which is obtained from separate nonlinear regression analysis of the virtual experimental data. Therefore, ($SR_{calc} - SR$) represents the difference between theoretical (regression) and measured (during inspection) SR values. In Eq. (6.4), DOY is the day of the year when the SR inspection is made. The calculated theoretical surface resistivity of the bridge deck, SR_{calc}, can be calculated as:

$$\begin{aligned} SR_{calc} = {} & \left(b_{11}\frac{w}{c} + a_{12}\,\varepsilon_{air} + a_{13}\,Corr_D + a_{14}\,Corr_{C_s} + a_{15}\right)^3 t_a{}^3 \\ & + \left(b_{21}\frac{w}{c} + a_{22}\,\varepsilon_{air} + b_{23}\,Corr_D + b_{24}\,Corr_{C_s} + b_{25}\right)^3 t_a{}^2 \\ & + \left(b_{31}\frac{w}{c} + a_{32}\,\varepsilon_{air} + b_{33}\,Corr_D + b_{34}\,Corr_{C_s} + b_{35}\right)^3 \\ & + \left(b_{41}\frac{w}{c} + a_{42}\,\varepsilon_{air} + b_{43}\,Corr_D + b_{44}\,Corr_{C_s} + b_{45}\right)^3 \\ & + \left(b_{51}\frac{w}{c} + a_{52}\,\varepsilon_{air} + b_{53}\,Corr_D + b_{54}\,Corr_{C_s} + b_{55}\right)^3 \cos\left(\frac{2\pi}{365}\,DOY\right) \\ & + \left(b_{61}\frac{w}{c} + a_{62}\,\varepsilon_{air} + b_{63}\,Corr_D + b_{64}\,Corr_{C_s} + b_{65}\right)^3 \sin\left(\frac{2\pi}{365}\,DOY\right) \end{aligned} \tag{6.6}$$

where b*ij* are the coefficients that are obtained from the regression analysis, given in Table 6.4, and $Corr_D$ and $Corr_{Cs}$ are the correction factors on apparent diffusion coefficient and surface chloride concentrations. Note that if there is no uncertainty, they will be taken as 1.0. The adjusted R^2 of the regression analysis was 0.964.

Table 6-4: bij values for the calculation of SR_{calc} for a bridge deck near Bend, Oregon.

i ↓, j→	1	2	3	4	5
1	-0.1308	0.41067	-2.2794	-0.76151	-1.0725
2	0.0271	-0.060823	0.038056	-0.030681	-0.1175
3	-0.0892	0.19312	-0.39604	-0.5519	-0.2811
4	-1.6536	3.9353	-14.33	-7.3428	-4.3478
5	0.2069	-0.47401	1.2717	1.1205	0.6170
6	0.1109	-0.18851	-0.103	1.4508	0.9602

6.3.2 Demonstration Study

In order to illustrate the proposed bridge-deck inspection-protocol that includes the prediction of the chloride profile at the time of inspection, a hypothetical example is presented here. The sample bridge deck is considered to be close to Bend, Oregon, where the derived closed-form equations for apparent diffusion coefficient and surface resistivity are valid. The bridge deck concrete is known to have a w/c of 0.43 and air content of 6%. The bridge deck was inspected at the age of 10 years from casting. The filed inspector measured a number of SR measurements on the deck; the average of the measurements was 55 kΩ-cm, and the local temperature at the measurement time was 30°C. The temperature normalized SR was 40 kΩ-cm (at 25°C).

The procedure for determining the chloride profile is as follows:

(1) Calculate the apparent diffusion coefficient, D_{app}: From Eq. (6.2), the apparent diffusion coefficient is obtained as 6.307×10^{-12} m^2/s.

(2) Calculate the uncertainty coefficient, $\propto_c$: From Eq. (6.5), the uncertainty coefficient is calculated as 0.21.

(3) Determine the minimum and maximum apparent diffusion coefficients using Equations 6.3 and 6.4, respectively:

$$D_{app,min} = (1 - 0.21)6.307 \times 10^{-12} = 5.607\times10^{-12}\ m^2/s \quad \textbf{(6.3)}$$

$$D_{app,max} = (1 + 0.21)6.307 \times 10^{-12} = 6.93\times10^{-12}\ m^2/s \quad \textbf{(6.4)}$$

(4) Calculate the predicted chloride profiles at the time of the inspection (10 years): Use Eq. (6.1) with C_s = 1% (percent mass of cement) and C_o = 0%. These are assumed values for this bridge deck and can be modified as needed. Figure 6.8 shows the chloride maximum and minimum ranges of the chloride profiles.

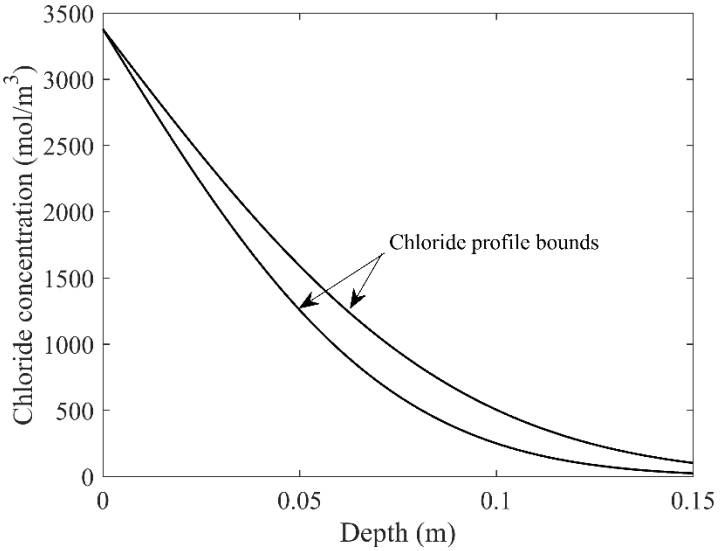

Figure 6.8: Chloride profiles at the time of the inspection (10 years from casting) for the demonstration study example for a hypothetical bridge near Bend, Oregon.

(5) Conduct service life predictions: Using a similar approach to Steps 1 through 4, inspectors can be used to obtain chloride profiles in the future years (e.g. at 20 years) as a tool for service life predictions or time-to-damage calculations.

It should be noted that due to the large number of bridges in Oregon, it is not practical or feasible to generate a closed-form equation for every single bridge. However, it is well known that Oregon is divided into several distinct climatic districts or zones, and bridges within each district/zone experience similar environmental conditions (temperature and relative humidity)

and deicing chemical exposure regimes. Therefore, separate closed-form equations can be developed for bridges in each climatic district/zone. These closed-form equations will also be functions of (a) concrete mixture properties of the deck (w/c, air content, and age) and (b) surface resistivity of concrete, which can be measured in rapidly in regular bridge inspections. Bridge inspectors can use these closed-form equations after bridge inspections to predict chloride profiles, make time-to-damage predictions, and decide if additional chloride profiling is necessary, and if so, at which locations on the deck it should be conducted. Such a future work plan is presented in Chapter 7.

7.0 CONCLUSIONS AND RECOMMENDATIONS

7.1 PROJECT SUMMARY

Corrosion of the steel in reinforced concrete bridge decks is a critical issue for structures that are exposed to chloride-containing de-icing chemicals or marine salts. Oregon Department of Transportation (ODOT) has a large number of bridges that are vulnerable to this form of deterioration. An obvious indicator of a corrosion problem is visible damage; unfortunately, if corrosion damage is visible, the window for preventive action is likely closed. Pre-emptive actions and early detection of potential problems are more cost effective than repair or replacement of bridge decks that have already experienced corrosion.

In recent years, electrical-based methods have emerged as durability-related performance indicators for reinforced concrete structures. Several investigations have shown the existence of relationships between electrical resistivity (or formation factor) of concrete and other durability-related parameters such as corrosion rate of steel reinforcement and transport properties of concrete. The main motivation of this research is to provide ODOT with a protocol to select bridges for its ongoing bridge deck treatment operations using quantitative tools that are practical and quick. Although rapid SR measurements are highly correlated with water and chloride transport properties of concrete, they do not directly provide the actual chloride depth profiling. However, transport properties that are revealed by SR measurements can be used in chloride ingress models that can be used to predict chloride profiles in concrete. The accuracy of the predictions improves with additional easily accessible quantitative information such as concrete mixture design properties (e.g. water-to-cement ratio), environmental data (e.g. temperature and relative humidity), and salt exposure histories. Most of these additional quantitative data are readily available for most locations in Oregon. These predictions, coupled with SR data, will also indicate if additional chloride profiling is necessary, and if so, at which locations on the deck it should be conducted.

To achieve the project goals, the following tasks have been performed:

(1) An experimental investigation was conducted to establish the relationship between electrical properties of concrete (e.g. SR or formation factor), environmental data (e.g. temperature and relative humidity), and chloride ingress in reduced-size reinforced concrete slabs simulating bridge decks commonly used in Oregon.

(2) The effect of F-T action on the observed relationship was investigated.

(3) A comprehensive modeling framework that relates the electrical properties of concrete, environmental data and chloride ingress was developed, verified, and validated.

(4) A virtual test bed using the validated modeling framework was developed to conduct statistically significant number of virtual experiments to obtain closed-form

relationships between electrical properties of concrete, environmental data and chloride ingress for bridge decks in different geographical areas in Oregon.

(5) A demonstration case study was performed. This case study showed the development of a closed-form equation. The use of the equation in a bridge-deck evaluation-protocol was also demonstrated.

7.2 MAJOR CONCLUSIONS

Major conclusions of this research can be summarized as follows.

- Electrical properties of concrete are affected by the microstructure development and compositional changes in pore solution during curing and early stages of service. As the concrete becomes more mature, the electrical resistivity of concrete increases, indicating stabilization of the pore solution composition and microstructure development (i.e., connectivity of the pores).

- Temperature, degree of saturation, and relative humidity of concrete affect its electrical properties such as resistivity. Among these factors, the temperature of concrete can be easily predicted from the environmental (air) temperature since temperature within concrete reaches equilibrium conditions relatively quickly. Therefore, in practice, the temperature effect on electrical resistivity measurements can be approximately accounted for using air temperature readings and existing resistivity-temperature relationships.

- The determination of relative humidity and the degree of saturation in concrete, on the other hand, requires either measurement of these properties in-situ or simulating those using environmental data and concrete mixture design properties. The measurement of relative humidity requires installation of sensors within the concrete. Accurate measurement of the degree of saturation requires coring. Neither approaches are practical for regular bridge deck inspections; therefore, simulation approach is the most feasible and practical method for determining these parameters within concrete.

- During the first couple of months of casting the concrete bridge deck, since the electrical properties of concrete are governed by a multiple processes that take place in concrete such as microstructure development and compositional changes in pore solution of concrete during curing and early stages of service, it is challenging to differentiate the effect of chloride ingress in concrete using electrical properties of concrete. However, after concrete matures the changes in electrical properties of concrete (e.g. SR or formation factor) are mainly due to changes in pore solution composition, hence, they can be used as an indicator for chloride ingress.

- Since most bridge decks in Oregon are typically exposed to de-icing chemicals months after casting, the observed relationship between electrical properties of concrete (e.g. SR) and chloride ingress can be expedited to help predict chloride profiles in concrete. However, since SR measurements depend on the type of concrete mixture (e.g. w/cm, connectivity of pores, and pore solution composition) and

environmental parameters (e.g. relative humidity, degree of saturation and temperature) within concrete, they need to be corrected/normalized for these factors.

- Deterioration due to F-T action can be observed through the electrical properties of concrete, particularly in low quality mixtures. However, for HPC mixtures as in the case of ODOT's current mixture used for bridge decks, little to no damage was observed due F-T action. In these slabs, chloride ingress was not significantly affected by F-T action. Therefore, electrical resistivity measurements were still related to chloride ingress. Even in slabs produced with concrete that represent ODOT mixtures that were used in the past that experience, the SR measurements were affected during and right after the F-T cycles, but they returned to their natural trends shortly after. Since the behavior observed is not conclusive, it is suggested that additional F-T cycles continue in this study. The cycles should be continued until the concrete with no air-entrainment starts to fail. This will show how the SR values are impacted by the deterioration. It would also show if the decrease in SR remains a permanent feature or if a different trend is observed once more widespread failure occurs.

- The HPC mixture that is currently used by ODOT provides significant protection against chloride ingress and F-T action. Despite the fact that both chloride exposure F-T regimes were rather aggressive, these mixtures performed well in comparison to other mixtures that represent ODOT mixtures that were used in the past. In particular, mixtures that did not contain and SCMs showed significant chloride ingress. The bridge decks that have been built using similar mixtures should be examined in the field more closely.

- Since the resistivity of hydrated cement phases and of aggregate in concrete are orders of magnitude larger than the resistivity of concrete pore solution, the electrical resistivity of concrete is mainly controlled by the resistivity (or conductivity) of the concrete pore solution. The connectivity and the degree of saturation of the pore structure in the concrete matrix affect the overall conductivity; therefore, modeling electrical resistivity of concrete requires consideration of these parameters. In addition, the actual resistivity (or conductivity) of the concrete pore solution is related to the type and amount of ionic species and temperature. As a result, modeling electrical resistivity of concrete requires that the types and concentrations (or activities) of the ionic species in the matrix are known. These complex dependencies require that relating electrical resistivity of concrete to chloride ingress should include coupled modeling of SR measurements with heat and moisture transfer analyses as well as multi-species ionic transport in concrete. In this research, such a modeling framework was developed, verified, and experimentally validated.

- During curing or early stages of service, it was observed that formation factor increased due to the microstructure development in concrete. During these early stages, formation factor increased similarly for both the deicing chemical exposed and water (control) exposed slabs. During the dry period when relative humidity (and the degree of saturation) decreased within concrete, formation factor increased sharply. This illustrates the strength and potential of the formation factor (and other electrical

based parameters) to capture microstructural and moisture-related changes within concrete.

- When chloride ingress becomes more prominent, formation factor increases further due to the decrease in electrical resistivity of concrete pore solution due to new ingresses ions. When chloride-containing salts start penetrating into concrete, some is bound into the hardened matrix and the rest remains in the pore solution. The effect of chloride binding and presence of free chloride ions in the pore solution might affect the electrical properties differently. For example, the former would increase the electrical resistivity of the matrix, while the latter would decrease the electrical resistivity of the pore solution. However, in later stages, as the binding capacity of concrete is reached, the effect of chloride ingress into concrete should correspond to a decrease in overall electrical resistivity of the pore medium and an increase in formation factors.

- The validated modeling framework allows the conducting large number of virtual experiments that would otherwise be unfeasible due to time, cost, and resource limitations. The generated data can be used to develop qualitative or quantitative relationships among several parameters and measurable properties of a reinforced concrete structure. Several factors affect electrical properties, chloride ingress and heat and moisture transport in concrete. Any effect of any these parameters on any of the properties can be investigated numerically using virtual experiments.

- It was demonstrated that the developed modeling framework can be used as a virtual test bed using to conduct statistically significant number of virtual experiments to generate data to obtain closed-form relationships between electrical properties of concrete (e.g. SR or formation factor), environmental data (e.g. temperature and relative humidity) and chloride ingress for bridge decks in different geographical areas in Oregon. For this demonstration, a hypothetical bridge near Bend, Oregon was selected. It was concluded with a demonstration on how the developed closed-form equation can be used in a bridge-deck evaluation-protocol that can be used by ODOT in practice.

7.3 RECOMMENDATIONS FOR FUTURE WORK

The following two thrusts of future work are recommended to ODOT in the form of problem statements.

7.3.1 Problem Statement 1

Development of improved bridge deck inspection protocols for different climatic districts/zones in Oregon

A comprehensive modeling framework that relates the electrical properties of concrete, environmental data and chloride ingress was developed, verified, and validated as part of SPR 780. This modeling framework can be used to develop improved bridge deck inspection protocols for any given bridge as long as (1) concrete mixture properties of the deck (w/c, air

content, and age), (2) environmental properties (temperature and relative humidity), which can be obtained from a nearby AgriMet weather station, and (3) amount of deicing chemical exposure are known or can be estimated. Once the required input (1-3) are collected, the modeling framework can be used to develop a closed-form equation for chloride diffusion coefficient for the bridge deck as a function of (a) concrete mixture properties of the deck (w/c, air content, and age) and (b) surface resistivity of concrete, which can be measured rapidly during regular bridge inspections. This chloride diffusion coefficient, which is specifically developed for the specific bridge under consideration (under the aforementioned environmental and deicing chemical exposure conditions), can be used to predict chloride profiles using the well-known solution of Fick's Law equation (also closed form) after each bridge inspection. These profiles can be used to make time-to-damage predictions and will indicate if additional chloride profiling is necessary, and if so, at which locations on the deck it should be conducted. This is a significant improvement in ODOT's bridge-deck inspection-protocol.

Due to the large number of bridges in Oregon, it is not practical or feasible to generate a closed-form equation for every single bridge. However, it is well known that Oregon is divided into several distinct climatic districts or zones, and bridges within each district/zone experience similar environmental conditions (temperature and relative humidity) and deicing chemical exposure regimes. Therefore, separate closed-form equations can be developed for bridges in each climatic district/zone. These closed-form equations will also be functions of (a) concrete mixture properties of the deck (w/c, air content, and age) and (b) surface resistivity of concrete, which can be measured in rapidly in regular bridge inspections. Similarly, bridge inspectors can use these closed-form equations after bridge inspections to predict chloride profiles, make time-to-damage predictions, and decide if additional chloride profiling is necessary, and if so, at which locations on the deck it should be conducted.

The following activities are the main tasks of this problem statement:

Task 1: Identify different climatic zones/districts in Oregon with similar environmental conditions (temperature and relative humidity) and deicing chemical exposure regimes. Note that a preliminary work toward this has already been performed by ODOT (Huang et al. 2014); however, a more refined zoning would be necessary so that developed closed-form chloride diffusion equations are representative of the environmental conditions and deicing chemical usage for all bridges in a given district/zone. It is expected that there will be fewer than 20 distinct climatic zones/districts within Oregon.

Task 2: For each district/zone, using the developed modeling framework, develop closed-form equations for making chloride-profile and time-to-damage predictions. These closed-form equations will be functions of concrete material properties, unique for each bridge, and surface resistivity measurement, which can be performed quickly during regular bridge inspections.

Task 3: Write a bridge-deck inspection-protocol that reflects the improved methodology for bridge inspections. It is anticipated that the Bridge Design and Drafting Manual will also be revised to identify corrosion mitigation actions for different levels of chloride exposure.

It is expected that these tasks can be completed within one year from the start date of the recommended work.

7.3.2 Problem Statement 2

Selected experimental studies on the existing reinforced concrete slabs representing ODOT's current bridge deck inventory

As part of the experimental program performed under *SPR 780,* several reinforced concrete slabs were cast. The slabs were designed to represent bridge decks commonly used by Oregon Department of Transportation (ODOT) in Oregon from 1960s to present. Based on concrete mixture properties from three different periods, twenty slabs were cast and investigated. Slab Type 1 (ST1) contained a Type I/II ordinary Portland cement (OPC) concrete mixture with no supplementary cementitious materials (SCMs) as per 1960s specifications. A range of w/cm values (ST1-A, ST1-B, ST1-C) were investigated for concrete of this era. Slab Type 2 (ST2) was also cast with the same OPC as the ST1 specimens but without air entrainment; these slabs represent non-air-entrained bridge decks from the 1960s. Slab Type 3 (ST3) represents bridges from the 1990s; this concrete mixture is an air-entrained concrete with 20% Class F fly ash replacement. Slab Type 4 (ST4) represent modern air-entrained high performance mixture (HPC) which contained 30% Class F fly ash and 4% silica fume.

During the experimental program of SPR 780, some of these slabs were exposed to ODOT's deicing chemical ($MgCl_2$ with corrosion inhibitor) for approximately two years. Control slabs were exposed to water and $MgCl_2$ (without corrosion inhibitor). Some of the slabs have started to corrode (1960s slabs) and some are still performing well (modern mixtures). Some of the deicing chemical exposed and water exposed (control) slabs were also subjected to 300 freeze-and-thaw (F-T) cycles.

With this setup already in place, ODOT has an opportunity to study many other aspects of bridge deck deterioration. The following activities are the main tasks for this problem statement:

Task 1: Investigate the role of deicing chemical application on the properties and durability of concrete. It is well known and documented that magnesium ions can deteriorate hydrated phases of concrete. This task will involve mechanical, spectroscopic and microscopic testing of concrete (both deicing chemical exposed and control) to investigate the reactivity of ODOT's deicing chemical with concrete.

Task 2: Investigate the effectiveness and side effects of the corrosion inhibitor used in ODOT's deicing chemical. This task will involve monitoring corrosion rates of steel in slabs that are exposed to ODOT's deicing chemical ($MgCl_2$ with corrosion inhibitor) and regular $MgCl_2$ solution. In this task, the differences in concrete properties from both exposure cases will also be compared to investigate if the corrosion inhibitor has any side effects on concrete.

Task 3: Investigate possible bridge-deck repair-strategies on slabs that are at different stages of deterioration. Since some of the slabs have already started to corrode (1960s slabs) and some are still performing well (modern mixtures), the effectiveness of different repair strategies can be explored for different levels of bridge deck deterioration. This task may include the study of the effectiveness of patch repairs, the use of sacrificial embedded anode systems or migrating corrosion inhibitors.

Task 4: Expand the F-T investigation of SPR 780 for slabs produced with ODOT's modern HPC mixture. As reported in SPR 780, modern HPC mixtures did experience significant deterioration due to F-T action. This task will expand the F-T study to develop a stronger understanding about the long-term performance of these mixtures and the effects of F-T action on chloride ingress.

It is expected that these tasks can be completed within one to two years from the start date of the recommended work. The duration of the work depends on which tasks are pursued and if additional slabs need to be cast.

8.0 REFERENCES

AASHTO TP 095-11-UL. *Standard Method of Test for Surface Resistivity Indication of Concrete's Ability to Resist Chloride Ion Penetration*. American Association of State Highway and Transportation Officials, Washington, D.C., 2011.

ACI Committee 222R. *Protection of Metals in Concrete against Corrosion*. Reapproved 2010. 2001.

Alonso, C., C. Andrade, and J.A. González. Relation between Resistivity and Corrosion Rate of Reinforcements in Carbonated Mortar made with Several Cement Types. *Cement and Concrete Research*, Vol. 18, No. 5, 1988, pp. 687-698.

Andrade, C., and C. Alonso. Test Methods for On-Site Corrosion Rate Measurement of Steel Reinforcement in Concrete by Means of the Polarization Resistance Method. *Materials and Structures*, Vol. 37, No. 9, 2004, pp. 623-643.

Andrade, C., M. Prieto, P. Tanner, F. Tavares, and R. d'Andrea. Testing and Modelling Chloride Penetration into Concrete. *Construction and Building Materials*, Vol. 39, 2013, pp. 9-18.

Angst, U.M., and B. Elsener. On the Applicability of the Wenner Method for Resistivity Measurements of Concrete. *ACI Materials Journal*, Vol. 111, No. 6, 2014, pp. 61-672.

Archie, G.E. The Electrical Resistivity Log as an Aid in Determining Some Reservoir Characteristics. *Transactions of the American Institute of Mining and Metallurgical Engineers*, Vol. 146, 1942, pp. 54-62.

ASTM. *Standard Test Method for Measuring the Surface Resistivity of Hardened Concrete Cylinders or Cores using the Wenner Four-Electrode Method* (Draft). ASTM International, West Conshohocken, PA, 2012.

ASTM C39. *Standard Test Method for Compressive Strength of Cylindrical Concrete Specimens*. ASTM International, West Conshohocken, PA, 2015.

ASTM C215. *Standard Test Method for Fundamental Transverse, Longitudinal, and Torsional Resonant Frequencies of Concrete Specimens*. (2014). ASTM International, West Conshohocken, PA, 2014.

ASTM C457. *Standard Test Method for Microscopical Determination of Parameters of the Air-Void System in Hardened Concrete*. ASTM International, West Conshohocken, PA, 2012.

ASTM C597. *Standard Test Method for Pulse Velocity through Concrete*. ASTM International, West Conshohocken, PA, 2010.

ASTM A615. *Standard Specification for Deformed and Plain Carbon-Steel Bars for Concrete Reinforcement.* ASTM International, West Conshohocken, PA, 2015.

ASTM C666/C666M. *Standard Test Method for Resistance of Concrete to Rapid Freezing and Thawing*. ASTM International, West Conshohocken, PA, 2015.

ASTM C856. *Standard Practice for Petrographic Examination of Hardened Concrete*. ASTM International. West Conshohocken, PA, 2014.

ASTM C876. *Standard Test Method for Corrosion Potentials of Uncoated Reinforcing Steel in Concrete*. ASTM International. West Conshohocken, PA, 2012.

ASTM C1152. *Standard Test Method for Acid-Soluble Chloride in Mortar and Concrete*. ASTM International, West Conshohocken, PA, 2012.

ASTM C1202. *Standard Test Method for Electrical Indication of Concrete's Ability to Resist Chloride Ion Penetration*. ASTM International. West Conshohocken, PA, 2012.

ASTM C1218/C1218M. *Standard Test Method for Water-Soluble Chloride in Mortar and Concrete*. ASTM International, West Conshohocken, PA, 2015.

ASTM C1556. *Standard Test Method for Determining the Apparent Chloride Diffusion Coefficient of Cementitious Mixtures by Bulk Design*. ASTM International, West Conshohocken, PA, 2012.

ASTM C1760. *Standard Test Method for Bulk Electrical Conductivity of Hardened Concrete*. ASTM International. West Conshohocken, PA, 2012.

ASTM WK37880. *New Test Method for Measuring the Surface Resistivity of Hardened Concrete Using the Wenner Four-Electrode Method*. ASTM International, West Conshohocken, PA, 2014.

Azad, V.J., C. Li, C. Verba, J.H. Ideker, and O.B. Isgor. A COMSOL–GEMS Interface for Modeling Coupled Reactive-Transport Geochemical Processes, *Computers and Geosciences*, Vol. 92, 2016, pp. 79-89.

Azad, V.J., and O.B. Isgor. A Thermodynamic Perspective on Chloride Limits of Concrete Produced with SCMs. *ACI Special Publication*, Vol. SP-308, 2016, pp. 1-18.

Backus, J., D. McPolin, A. Long, M. Basheer, and N. Holmes. Exposure of Mortars to Cyclic Chloride Ingress and Carbonation. *Advances in Cement Research*, Vol. 25, No. 1, 2013, pp. 3-11.

Basheer, P., P. Gilleece, A. Long, and W. Mc Carter. Monitoring Electrical Resistance of Concretes Containing Alternative Cementitious Materials to Assess Their Resistance to Chloride Penetration. *Cement and Concrete Composites*, Vol. 24, No. 5, 2002, pp. 437-449.

Bažant, Z., and L. Najjar. Nonlinear Water Diffusion in Nonsaturated Concrete. *Matériaux et Construction*, Vol. 5, No. 1, 1972, pp. 3-20.

Bentz, D.P., K.A. Snyder, and A. Ahmed. Anticipating the Setting Time of High-Volume Fly Ash Concretes Using Electrical Measurements: Feasibility Studies Using Pastes. *Journal of Materials in Civil Engineering*, Vol. 27, No. 3, 2014.

Blackburn, R., D. Amsler, and K. Bauer. Snow Removal and Ice Control Technology. Sixth International Symposium on Snow Removal and Ice Control Technology, Transportation Research Board of the National Academies, Spokane, WA, 2004.

Brencich, A., G. Cassini, D. Pera, and G. Riotto. Calibration and Reliability of the Rebound (Schmidt) Hammer Test. *Civil Engineering and Architecture*, Vol.1, No. 3, 2013, pp. 66-78.

CAN/CSA. *Concrete Materials and Methods of Concrete Construction/Test Methods and Standard Practices for Concrete* (A23.2). Toronto, ON, Canadian Standards Association. 2009.

Carino, N.J. Nondestructive Techniques to Investigate Corrosion Status in Concrete Structures. *Journal of Performance of Constructed Facilities*, Vol. 13, No. 3, 1999, pp. 96-106.

Chen, C.-T., J.-J. Chang and W.-C. Yeih. The Effects of Specimen Parameters on the Resistivity of Concrete. *Construction and Building Materials*, Vol. 71, No. 0, 2014, pp. 35-43.

Chouteau, M., and S. Beaulieu. An Investigation on Application of the Electric Resistivity Tomography Method to Concrete Structures. Geophysics 2002. The 2nd Annual Conference on the Application of Geophysical and NDT Methodologies to Transportation Facilities and Infrastructure. 2002.

Conciatori, D., H. Sadouki, and E. Brühwiler. Capillary Suction and Diffusion Model for Chloride Ingress into Concrete. *Cement and Concrete Research*, Vol. 38, No. 12, 2008, pp. 1401-1408.

Di Bella, C., C. Villani, N. Phares, E. Hausheer, and J. Weiss. Chloride Transport and Service Life in Internally Cured Concrete. *American Society of Civil Engineers Structures Congress*. 2012.

du Plooy, R., S. Palma Lopes, G. Villain, and X. Dérobert. Development of a Multi-Ring Resistivity Cell and Multi-Electrode Resistivity Probe for Investigation of Cover Concrete Condition. *NDT and E International*, Vol. 54, No. 0, 2013, pp. 27-36.

Dunn, M., A. Abu-Hawash, R. Feldmann, S. Kruschwitz, F. Romero, and N. Gucunski (2010). Multiple Complementary Nondestructive Evaluation Technologies for Condition Assessment of Concrete Bridge Decks. In *Transportation Research Record: Journal of the Transportation Research Board, No.* 2201(-1), Transportation Research Board of the National Academies, Washington, D.C., 2010, pp. 34-44.

Ehlen, M.A., M.D. Thomas, and E.C. Bentz. Life-365 Service Life Prediction Model™ Version 2.0. *Concrete International*, Vol. 31, No. 05, 2009, pp. 41-46.

FDOT FM 5-578. *Florida Method of Test for Concrete Resistivity as an Electrical Indicator of Its Permeability*. Department of Transportation Florida, FL, USA. 2004.

Ferraro, J., and A. Bentivegna. *Modified Damage Rating Index (DRI) Analysis of Concrete Cores from Oregon State University Resistivity Project.* CTL Group, Skokie, IL, 2015.

Garzon, A. J., J. Sanchez, C. Andrade, N. Rebolledo, E. Menéndez, J. Fullea. Modification of Four Point Method to Measure the Concrete Electrical Resistivity in Presence of Reinforcing Bars. *Cement and Concrete Composites*, Vol. 53, 2014, pp. 249-257.

Ghosh, P., and Q. Tran. Correlation Between Bulk and Surface Resistivity of Concrete. *International Journal of Concrete Structures and Materials*, Vol. 9, No. 1, 2015, pp. 119-132.

Goueygou, M., O. Abraham, and J.-F. Lataste. A Comparative Study of Two Non-Destructive Testing Methods to Assess Near-Surface Mechanical Damage in Concrete Structures. *NDT and E International*, Vol. 41, No. 6, 2008, pp. 448-456.

Gowers, K.R., and S.G. Millard. Measurement of Concrete Resistivity for Assessment of Corrosion Severity of Steel Using Wenner Technique. *ACI Materials Journal*, Vol. 96, No. 5, 1999, pp. 536-541.

Gucunski, N., A. Imani, F. Romero, S. Zanarian, D. Yuan, H. Wiggenhauser, P. Shokouhi, A. Taffe, and D. Kutrubes. *Nondestructive Testing to Identify C oncrete Bridge Deck Deterioration*. Washington, D.C., 2013.

Gulikers, J. Theoretical Considerations on the Supposed Linear Relationship between Concrete Resistivity and Corrosion Rate of Steel Reinforcement. *Materials and Corrosion*, Vol. 56, No. 6, 2005, pp. 393-403.

Hamilton, H., A.J. Boyd, E. Vivas, and M. Bergin. *Permeability of Concrete - Comparison on Conductivity and Diffusion Methods.* No. 00026899. Gainesville, FL, University of FL, 2007.

Hansson, C., A. Poursaee, and A. Laurent. Macrocell and Microcell Corrosion of Steel in Ordinary Portland Cement and High Performance Concretes. *Cement and Concrete Research*, Vol. 36, No. 11, 2006, pp. 2098-2102.

Hornbostel, K., C.K. Larsen, and M.R. Geiker. Relationship Between Concrete Resistivity and Corrosion Rate–A Literature Review. *Cement and Concrete Composites*, Vol. 39, 2013, pp. 60-72.

Hong, K. Cyclic Wetting and Drying and Its Effects on Chloride Ingress in Concrete. National Library of Canada, Ottawa, ON, 1999.

Hooton, R.D., A. Shahroodi, and E. Karkar. Evaluating Concretes Using Rapid Test Methods for Fluid Penetration Resistance, ACI Fall Convention in Toronto, presented in the Emerging Technologies (Part 2), 2012; available at aci-int.org.

Hope, B., and A. Ip. Chloride Corrosion Threshold in Concrete. *Materials Journal*, Vol. 84, No. 4, 1987, pp. 306-314.

Hovarth, A. Handbook of Aqueous Electrolyte Solutions: Physical Properties, Estimation, and Correlation Methods. Ellis Horwood, New York, NY, 1985.

Huang, J., W. Shaowei, J. Chaudhari, S. Soltesz, and X. Shi. Deicer Effect on Concrete Bridge Decks: Practitioners Perspective and a Method of Developing Exposure Maps. Transportation Research Board Annual Meeting: 1-13. Washington, D.C., 2014.

Hussain, R.R. Effect of Moisture Variation on Oxygen Consumption Rate of Corroding Steel in Chloride Contaminated Concrete. *Cement and Concrete Composites*, Vol. 33, No. 1, 2011, pp. 154-161.

Hussain, S., E., Rasheeduzzafar, A. Almusallam, A. S. Algahtani. Factors Affecting Threshold Chloride for Reinforcement Corrosion in Concrete. *Cement and Concrete Research*, Vol. 25, No. 7, 1995, pp. 1543-1555.

Icenogle, P.J., and T.D. Rupnow. Development of Precision Statement for Concrete Surface Resistivity. In *Transportation Research Record: Journal of the Transportation Research Board*, No. 2290-1, Transportation Research Board of the National Academies, Washington, D.C., 2012, pp. 38-43.

Isgor, O.B., and A.G. Razaqpur. Finite Element Modelling of Coupled Heat Transfer, Moisture Transport and Carbonation Processes in Concrete Structures. *Cement and Concrete Composites*, Vol. 26, 2004, pp. 57-73.

Isgor, O.B. Chapter 13: *Modelling of Corrosion of Steel in Concrete Structures*. In Corrosion of Steel in Concrete Structures, edited by Amir Poursaee, Woodhead Publishing. 2016.

Jackson, L. Surface Resistivity Test Evaluation as an Indicator of the Chloride Permeability of Concrete. *Tech Brief*. Publication no. FHWA-HRT-13-024, McLean, VA, 2013.

Jaegermann, C. Effect of Water-Cement Ratio and Curing on Chloride Penetration into Concrete Exposed to Mediterranean Sea Climate. *Materials Journal*, Vol. 87, No. 4, 1990, pp. 333-339.

Jenkins, A. *Surface Resistivity as an Alternative for Rapid Chloride Permeability Test of Hardened Concrete*. Kansas Department of Transportation Bureau of Research, 2015, p. 39.

Ji, Y., T. Zan, and Y. Yuan. Chloride Ion Ingress in Concrete Exposed to a Cyclic Wetting and Drying Environment. *American Society of Agricultural and Biological Engineers*, Vol. 52, No. 1, 2009, pp. 239-245.

Jiang, J.H. Relationship of Moisture Content with Temperature and Relative Humidity in Concrete. *Magazine of Concrete Research*, Vol. 65, No. 11, 2013, pp. 685-692.

Jianhong, C., B. Dylan, J. Frank, and H. Dryver. *Concrete bridge deck condition assessment with automated Multisensor Techniques*. Bridge Maintenance, Safety Management, Health Monitoring and Informatics. Burlington, VT, Taylor and Francis. 2008.

Julio-Betancourt, J.A. *Effect of De-icer and Anti-icer Chemicals on the Durability Microstructure, and Properties of Cement-Based Materials*. Graduate of Civil Engineering. Toronto, Canada, University of Toronto. Doctor of Philosophy. 2009. 854 pp.

Karadakis, K., V.J. Azad, P. Ghods, and O.B. Isgor. Numerical Investigation of the Role of Mill Scale Crevices on the Corrosion Initiation of Carbon Steel Reinforcement in Concrete. *Journal of the Electrochemical Society*, Vol.163, No. 6, 2016, pp. C306-C315.

Kessler, R., R. Powers, and M. Paredes. Resistivity Measurements of Water Saturated Concrete as an Indicator of Permeability. NACE International. 2005.

Khalim, A.R., D. Sagar, M.D. Kumruzzaman, and A.S.M.Z. Hasan. Combination of Nondestructive Evaluations for Reliable Assessment of Bridge Deck. Facta universitatis - series: *Architecture and Civil Engineering*, Vol. 9, No. 1, 2011, pp. 11-22.

Koch, G.H., M. Brongers, N. Thompson, Y. Virmani, and J. Payer. *Corrosion Costs and Preventive Strategies in the United States*. FHWA-RD-01-156 (Final Report), 2002. 773 pp.

Kosmatka, S.H., and M.L. Wilson. *Design and Control of Concrete Mixtures*." 15th Edition: 444, Portland Cement Association, Washington, D.C., 2011.

Kulik, D., T. Wagner, S. Dmytrieva, G. Kosakowski, F. Hingerl, K. Chudnenko, and U. Berner. GEM-Selektor Geochemical Modeling Package: Revised Algorithm and GEMS3K Numerical Kernel for Coupled Simulation Codes. *Computational Geosciences*, Vol. 17, No. 1, 2013, pp. 1-24.

Kumar, A., S. Bishnoi, and K.L. Scrivener. Modelling Early Age Hydration Kinetics of Alite. *Cement and Concrete Research*, Vol. 42, No. 7, 2012, pp. 903-918.

Lataste, J., C. Sirieix, D. Breysse, and M. Frappa. Electrical Resistivity Measurement Applied to Cracking Assessment on Reinforced Concrete Structures in Civil Engineering. *NDT and E International*, Vol. 36, No. 6, 2003, pp. 383-394.

Lingen, R.T. *Concrete in Coastal Structures.* Thomas Telford Limited , London, U.K., 1998.

López, W., and J.A. González. Influence of the Degree of Pore Saturation on the Resistivity of Concrete and the Corrosion Rate of Steel Reinforcement. *Cement and Concrete Research*, Vol. 23, No. 2, 1993, pp. 368-376.

Lord, B.N. *Program to Reduce Deicing Chemical Usage*. Federal Highway Administration, McLean, VA, 1988.

Mahmoodian, M., and A. Alani (2015). *Time-Dependent Reliability Analysis of Corrosion Affected Structures. Numerical Methods for Reliability and Safety Assessment*. Springer International Publishing, Switzerland, 2015, pp. 459-498.

Mancio, M., J.R. Moore, Z. Brooks, P.J.M. Monteiro, and S.D. Glaser. Instantaneous In-Situ Determination of Water-Cement Ratio of Fresh Concrete. *ACI Materials Journal*, Vol. 107, No. 6, 2010.

Martin-Perez, B. *Service Life Modelling of R.C. Highway Structures Exposed to Chlorides*. Ph.D. Thesis. Department of Civil Engineering, University of Toronto. 1999.

Meyer, C. The Greening of the Concrete Industry. *Cement and Concrete Composites*, Vol. 31, No. 8, 2009, pp. 601-605.

Millard, S. Reinforced Concrete Resistivity Measurement Techniques. ICE Proceedings, Thomas Telford. 1991.

Millard, S., J. Harrison, and K. Gowers. Practical Measurement of Concrete Resistivity. *British Journal of Non-Destructive Testing*, Vol. 33, No. 2, 1991, pp. 59-63.

Millard, S.G. Reinforced-Concrete Resistivity Measurement Techniques. Proceedings of the Institution of Civil Engineers. Vol. 91, 1991, pp. 71-88.

Moore, W. *Table 1-28: Condition of US Highway Bridges*. National transportation Statistics. 2011.

Morales, M.T. *Experimental Investigation of the Effects of Embedded Rebar, Cracks, Chloride Ingress and Corrosion on Electrical Resistivity Measurements of Reinforced Concrete.* Thesis. Oregon State University. 2015.

Morris, W., A. Vico, and M. Vázquez. Chloride Induced Corrosion of Reinforcing Steel Evaluated by Concrete Resistivity Measurements. *Electrochimica Acta*, Vol. 49 No. 25, 2004, pp. 4447-4453.

MTO. *Method of Test for Determination of Electrical Resistivity of Concrete*. Ministry of Transportation, Ontario, Toronto, ON, 2013.

Mussato, B.T., O.K. Gepraegs, and G. Farnden. Relative Effects of Sodium Chloride and Magnesium Chloride on Reinforced Concrete: State of the Art. In *Transportation Research Record: Journal of the Transportation Research Board*, No. 1866, Transportation Research Board of the National Academies, Washington, D.C., 2004, pp. 59-66.

Mutale, L. *An Investigation into the Relationship between Surface Concrete Resistivity and Chloride Conductivity Tests*. Thesis. Department of Civil Engineering, University of Cape Town. 2014.

Neville, A.M. *Properties of Concrete*. Pitman Publising Limited, London, UK, 1981.

Neville, A.M. *Properties of Concrete*. Fourth Edition. 844. Wiley, Hoboken, NJ, 1996.

ODOT. *Oregon Standard and Specifications for Construction*. Oregon Department of Transportation, Salem, OR, 2008.

ODOT. *ODOT Bridge Inspection Program Manual 2013*, Oregon Department of Transportation, Salem, OR, 2013.

O'Keefe, K., and X. Shi. Anti-icing and Pre-wetting: Improved Methods for Winter Highway Maintenance in North America. Proceedings of the Transportation Research Board Annual Meeting. 2006.

Parrot, L., and D. Killoh. Prediction of Cement Hydration. British Ceramic Proceedings. Vol. 35, 1984, p.41-53

Polder, R.B. Test Methods for On Site Measurement of Resistivity of Concrete—a RILEM TC-154 Technical Recommendation. *Construction and Building Materials*, Vol. 15, No. 2, 2001, pp. 125-131.

Polder, R.B., and W.H.A. Peelen. Characterisation of Chloride Transport and Reinforcement Corrosion in Concrete under Cyclic Wetting and Drying by Electrical Resistivity. *Cement and Concrete Composites*, Vol. 24, No. 5, 2002, pp. 427-435.

Powers, T., and T. Brownyard. Studies of the Physical Properties of Hardened Portland Cement Paste. *ACI Journal Proceedings*, Vol. 43, No. 9, 1946, pp. 469-504.

Presuel-Moreno, F., A. Suarez, and Y. Lio. *Characterization of New and Old Concrete Structures Using Surface Resistivity Measurements*. Florida DOT - Research Center. 2010, p. 263.

Presuel-Moreno, F., Y. Liu, M. Paredes. Understanding the Effect of Rebar Presence and/or Multilayered Concrete Resistivity on the Apparent Surface Resistivity Measured Via the Four-Point Wenner Method. Corrosion Conference 2009. Atlanta, GA, NACE International, 2009.

Presuel-Moreno, F., Y. Liu, and Y.Y. Wu. Numerical Modeling of the Effects of Rebar Presence and/or Multilayered Concrete Resistivity on the Apparent Resistivity Measured via the Wenner Method. *Construction and Building Materials*, Vol. 48, 2013, pp. 16-25.

Proceq, S. *Resipod Operating Instructions*. Schewerzenbach, Switzerland, 2011.

Qiang, Y., A. Katrien, S. Caijun, and S. Geert De. *Effect of Temperature on Transport of Chloride Ions in Concrete. Concrete Repair, Rehabilitation and Retrofitting II*, CRC Press. 2008, pp. 159-160.

Reichling, K., M. Raupach, J. Broomfield, J. Gulikers, V. L'Hostis, S. Kessler, K. Osterminski, I. Pepenar, U. Schneck, G. Sergi, and G. Taché. Full Surface Inspection Methods Regarding Reinforcement Corrosion of Concrete Structures. *Materials and Corrosion*, Vol. 64, No. 2, 2013, pp. 116-127.

Rupnow, T., and I. Patrick. *Evaluation of Surface Resistivity Measurements as an Alternative to the Rapid Chloride Permeability Test for Quality Assurance and Acceptance*. Louisiana Transportation Research Center. 2011.

Ryu, D.,W. Ko, and T. Noguchi. Effects of Simulated Environmental Conditions on the Internal Relative Humidity and Relative Moisture Content Distribution of Exposed Concrete. *Cement and Concrete Composites*, Vol. 33, No. 1, 2011, pp. 142-153.

Sadowski, L. Methodology for Assessing the Probabilty of Corrosion in Concrete Structures on the Basis of Half-Cell Potential and Concrete Resistivity Measurements. *Scientific World Journal*, Vol. 2013, Article ID 714501, 2013.

Saetta, A.V., R.V. Scotta, and R.V. Vitaliani. Analysis of Chloride Diffusion into Partially Saturated Concrete. *ACI Materials Journal*, Vol. 90, No. 5, 1993.

Salehi, M. *Numerical Investigation of the Effects of Cracking and Embedded Reinforcement on Surface Concrete Resistivity Measurements using Wenner Probe*. Civil and Environmental Engineering. Master of Applied Science in Civil Engineering. Carleton University, Ottawa, ON, 2013.

Salehi, M., P. Ghods, and O.B. Isgor. Numerical Investigation of the Role of Embedded Reinforcement Mesh on Electrical Resistivity Measurements of Concrete using the Wenner Probe Technique, *Materials and Structures*, 2014. DOI 10.1617/s11527-014-0498-x, 1-16.

Salehi, M., P. Ghods, O.B. Isgor. Numerical Study on the Effect of Cracking on Surface Resistivity of Plain and Reinforced Concrete Elements, *ASCE Journal of Materials*, Vol. 49, No. 1-2, 2016, pp. 301-316.

Samson, E., and J. Marchand. Numerical Solution of the Extended Nernst–Planck Model. *Journal of Colloid and Interface Science*, Vol. 215, No. 1, 1999, pp. 1-8.

Sengul, O., and O.E. Gjorv. Effect of Embedded Steel on Electrical Resistivity Measurements on Concrete Structures. *ACI Materials Journal*, Vol. 106, No. 1, 2009, pp. 11-18.

Sengul, O., and O.E. Gjorv. Electrical Resistivity Measurements for Quality Control during Concrete Construction. *ACI Materials Journal*, Vol. 105, No. 6, 2008, pp. 541-547.

Shah, A.A., and Y. Ribakov. Non-Destructive Measurements of Crack Assessment and Defect Detection in Concrete Structures. *Materials and Design*, Vol. 29, No. 1, 2008, pp. 61-69.

Shariati, M., H. Sulong, M. Arabnejad, P. Shafigh, and H. Sinaei. Assessing the Strength of Reinforced Concrete Structures Through Ultrasonic Pulse Velocity and Schmidt Rebound Hammer Tests. *Scientific Research and Essays*, Vol. 6, No. 1, 2011, pp. 213-220.

Shi, X. *Understanding and Mitigating Effects of Chloride Deicer Exposure on Concrete.* Western Transportation Institute. Montana State Univerity, Bozeman, MT, 2011.

Shi, X., L. Yajun, M. Mooney, M. Berry, L. Fay, and A.B. Leonard. *Effect of Chloride-Based Deicers on Reinforced Concrete Structures*. Montana State University, Bozeman, MT, 2010, pp. 1-74.

Shi, X., Y. Li., S. Jungwirth, Y. Fang, N. Seeley, and E. Jackson. *Identification and Laboratory Assessment if Best Practices to Protect DOT Equipment from the Corrosive Effect of Chemical Deicers*. ODOT Technical Report, Oregon Department of Transportation, Salem, OR, 2013.

Simon, T.K., and V. Vass. The Electrical Resistivity of Concrete. *Concrete Structures Annual Technical Journal*, Vol. 13, 2012, pp. 61-64.

Sirivivatnanon, V., W.A. Thomas, and K. Waye. Determination of Free Chlorides in Aggregates and Concrete. *Australian Journal of Structural Engineering*, Vol. 12, No. 2, 2012, pp. 151-158 .

Snyder, K., X. Feng, B. Keen, and T.O. Mason. Estimating the Electrical Conductivity of Cement Paste Pore Solutions from OH−, K+ and Na+ Concentrations. *Cement and Concrete Research*, Vol. 33, No. 6, 2003, pp. 793-798.

Song, H., and V. Saraswathy. Corrosion Monitoring of Reinforced Concrete Structures - A Review. *International Journal of Electrochemical Science*, Vol. 2, 2007, pp. 1-28.

Spragg, R.P., J. Castro, T. Nantung, M. Paredes, and J. Weiss. *Variability Analysis of the Bulk Resistivity Measured Using Concrete Cylinders*. Joint Transportation Research Program, Indiana Department of Transportation and Purdue University West Lafayette, IN, 2011.

Spragg, R., C. Villani, and J. Weiss. Electrical Properties of Cementitious Systems: Formation Factor Determination and the Influence of Conditioning Procedures. *Advances in Civil Engineering Materials*, Vol. 5, 2016, pp. 124-148.

Sutter, L., K Peterson, G. Julio-Betancourt, D. Hooton, T.J. Van Dam, and K. Smith. *The Deleterious Chemical Effects of Concentrated Deicing Solutions on Portland Cement Concrete*. SD2002-01. Federal Highway Administration: 1-198, Houghton, MI, 2008.

Swanstrom, J., T. Rogers, G. Bowling, and S. Tuttle. *ODOT Bridge Inspection Program Manual 2013*. Oregon Department of Transportation, 2013.

Taillet, E., J.F. Lataste, P. Rivard, and A. Denis. Non-Destructive Evaluation of Cracks in Massive Concrete using Normal DC Resistivity Logging. *NDT and E International*, Vol. 63, No. 0, 2014, pp. 11-20.

Telford, W.M., L.P. Geldart, and R.E. Sheriff. *Applied Geophysics*. Cambridge university Press, 1990.

Torres-Luque, M., E. Bastidas-Arteaga, F. Schoefs, M. Sánchez-Silva, and J.F. Osma. Non-Destructive Methods for Measuring Chloride Ingress into Concrete: State-of-the-Art and Future Challenges. *Construction and Building Materials*, Vol. 68, No. 0, 2014, pp. 68-81.

Transportation for America. One in 9 Bridges Still Structurally Deficient. 2013.

Wagner, T., D.A. Kulik, F.F. Hingerl, S.V. Dmytrieva. Gem-Selektor Geochemical Modeling Package: TSolMod Library and Data Interface for Multicomponent Phase Models. *Canadian Mineralogist*, Vol. 50, No. 5, 2012, pp. 1173-1195.

Wang, Z., Q. Zeng, L. Wang, Y. Yao, and K. Li. Effect of Moisture Content on Freeze–Thaw Behavior of Cement Paste by Electrical Resistance Measurements. *Journal of Materials Science*, Vol. 49, No. 12, 2014, pp. 4305-4314.

Wang, Z., Q. Zeng, L. Wang, Y. Yao, and K. Li. Electrical Resistivity of Cement Pastes Undergoing Cyclic Freeze-Thaw Action. *Journal of Materials in Civil Engineering*, Vol. 27, No. 1, 2015, pp. 1-8.

Weydert, R., and C. Gehlen. Electrolytic Resistivity of Cover Concrete: Relevance, Measurement and Interpretation. Proceedings of the 8th International Conference on Durability of Building Materials and Components. 409-419. NRC Research Press, Vancouver, Canada. 1999.

Wei, X., and L. Xiao. Influence of the Aggregate Volume on the Electrical Resistivity and Properties of Portland Cement Concretes. *Journal of Wuhan University of Technology-Mater. Sci. Ed.*, Vol. 26, No. 5, 2011, pp. 965-971.

Weiss, J., K. Snyder, J. Bullard, and D. Bentz. Using a Saturation Function to Interpret the Electrical Properties of Partially Saturated Concrete. *Journal of Materials in Civil Engineering*, Vol. 25, No. 8, 2012, pp. 1097-1106.

Weiss, J. Relating Transport Properties to Performance in Concrete Pavements, in MAP - Moving Advancements into Practice. S. Shields-Cook, Editor. Federal Highway Admininstration, 2014, pp. 1-6.

Weiss, W.J., Barrett, T.J., Qiao, C., Todak, H. (2016). “Toward A Specification for Transport Properties of Concrete Based on the Formation Factor of A Sealed Specimen.” Advances in Civil Engineering Materials, in press (2016).

Whittington, H., J. McCarter, and M. Forde. The Conduction of Electricity through Concrete. *Magazine of Concrete Research*, Vol. 33, No. 114, 1981, pp. 48-60.

Wiwattanachang, N., and P. Giao. Monitoring Crack Development in Fiber Concrete Beam by Using Electrical Resistivity Imaging. *Journal of Applied Geophysics*, Vol. 75, No. 2, 2011, pp. 294-304.

Xi, Y., Z.P. Bažant, L. Molina, and H.M. Jennings. Moisture Diffusion in Cementitious Materials Moisture Capacity and Diffusivity. *Advanced Cement Based Materials*, Vol. 1, No.6, 1994, pp. 258-266.

Zhu, Z., S. German, and I. Brilakis. Detection of Large-Scale Concrete Columns for Automated Bridge Inspection. *Automation in Construction*, Vol. 19, No. 8, 2010, pp. 1047-1055.

APPENDIX A

CHEMICAL ANALYSIS DATA SHEETS OF OPC AND SCMS

CHEMICAL ANALYSIS DATA SHEETS OF OPC AND SCMS

WYOMING ANALYTICAL LABORATORIES, INC.
14035 W. 44th Avenue
Golden, CO 80403
www.wal-lab.com
Email: wallab@rad.com
(303) 278-2446
Fax: (303) 278 2439

November 5, 2014

Chang Li
Oregon State University
220 Owen Hall
Corvallis, OR 97331-3212

WAL #1409[illegible]-1
Sample ID: Type I/II Cement
PO#:

CHEMICAL ANALYSIS
Wt%, as Rec'd Basis

Silicon Dioxide	SiO_2	19.93	
Aluminum Oxide	Al_2O_3	4.77	
Iron Oxide	Fe_2O_3	3.50	
Calcium Oxide	CaO	63.47	
Magnesium Oxide	MgO	0.87	
Sodium Oxide	Na_2O	0.29	
Potassium Oxide	K_2O	0.33	
Total Alkalies as Na_2O			0.51
Titanium Dioxide	TiO_2	0.27	
Manganic Oxide	Mn_2O_3	0.17	
Phosphorus Pentoxide	P_2O_5	0.07	
Strontium Oxide	SrO	0.18	
Barium Oxide	BaO	0.11	
Sulfur Trioxide	SO_3	3.11	
Loss on Ignition		3.09	
Total		100.00	

Tricalcium Silicate	C_3S	61.33
Tricalcium Aluminate	C_3A	6.51
Dicalcium Silicate	C_2S	10.86
Tetracalcium Aluminoferrite	C_4AF	10.64

*TiO_2 and P_2O_5 not included in Al_2O_3
*No correction has been made for the possible use of limestone.
Analysis per ASTM C 114

Charles R. Wilson,
Division Manager

MEMBER ACIL

Figure 9-1: Chemical analysis of Type I/II OPC

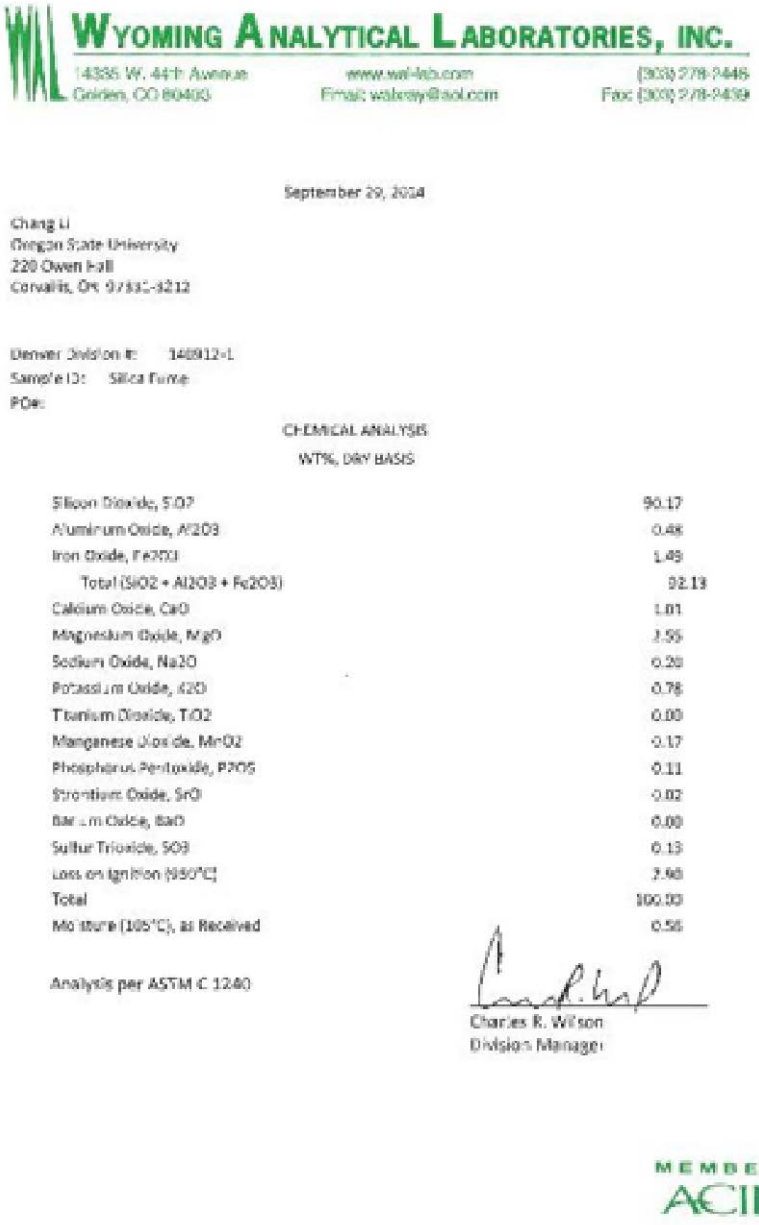

WYOMING ANALYTICAL LABORATORIES, INC.

14335 W. 44th Avenue
Golden, CO 80403

www.wal-lab.com
Email: walray@aol.com

(303) 278-9446
Fax: (303) 278-9439

September 29, 2014

Chang Li
Oregon State University
220 Owen Hall
Corvallis, OR 97331-4212

Denver Division #: 140912-L
Sample ID: Silica Fume
PO#:

CHEMICAL ANALYSIS
WT%, DRY BASIS

Silicon Dioxide, SiO2	90.17
Aluminum Oxide, Al2O3	0.48
Iron Oxide, Fe2O3	1.49
Total (SiO2 + Al2O3 + Fe2O3)	92.13
Calcium Oxide, CaO	1.01
Magnesium Oxide, MgO	1.55
Sodium Oxide, Na2O	0.20
Potassium Oxide, K2O	0.78
Titanium Dioxide, TiO2	0.00
Manganese Dioxide, MnO2	0.17
Phosphorus Pentoxide, P2O5	0.11
Strontium Oxide, SrO	0.02
Barium Oxide, BaO	0.00
Sulfur Trioxide, SO3	0.13
Loss on Ignition (950°C)	3.98
Total	100.00
Moisture (105°C), as Received	0.56

Analysis per ASTM C 1240

Charles R. Wilson
Division Manager

MEMBER ACIL

Figure 9-2: Chemical analysis of silica fume

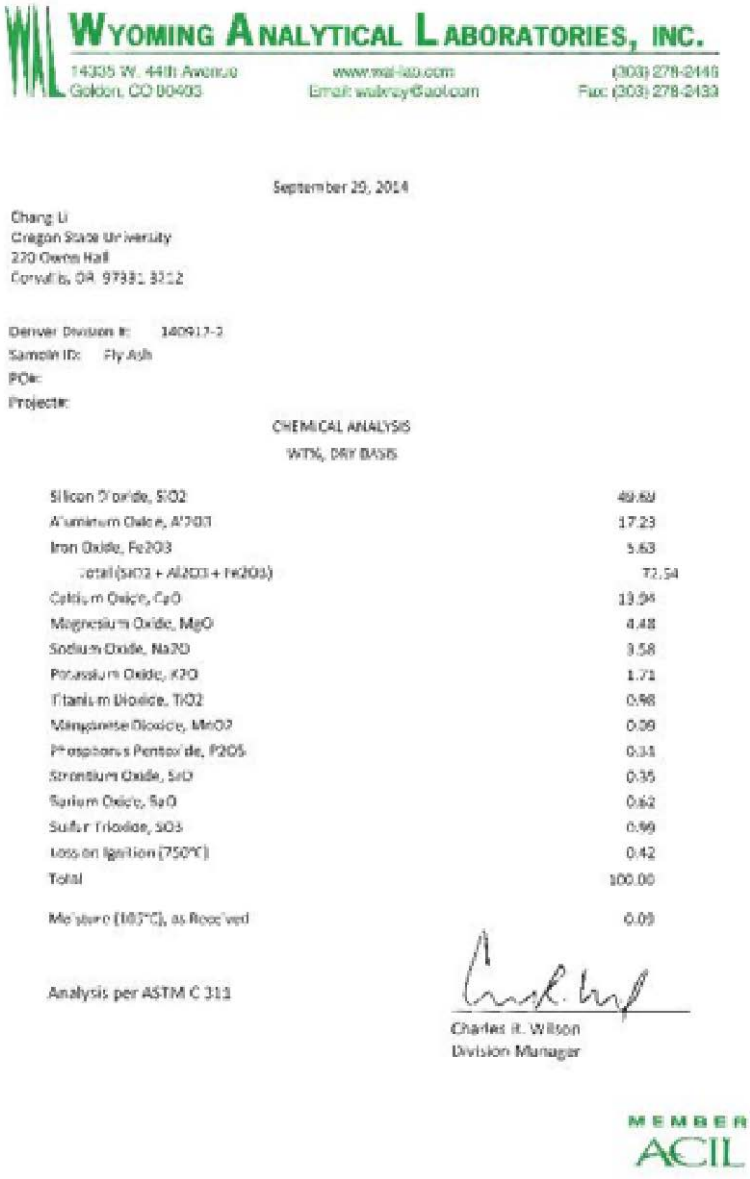

WYOMING ANALYTICAL LABORATORIES, INC.

14035 W. 44th Avenue
Golden, CO 80403

www.wal-lab.com
Email: walinsy@aol.com

(303) 278-2446
Fax: (303) 278-2433

September 25, 2014

Chang Li
Oregon State University
220 Owens Hall
Corvallis, OR 97331-3212

Denver Division #: 140917-2
Sample ID: Fly Ash
PO#:
Project#:

CHEMICAL ANALYSIS
WT%, DRY BASIS

Silicon Dioxide, SiO2	49.69
Aluminum Oxide, Al2O3	17.23
Iron Oxide, Fe2O3	5.63
Total (SiO2 + Al2O3 + Fe2O3)	72.54
Calcium Oxide, CaO	13.94
Magnesium Oxide, MgO	4.48
Sodium Oxide, Na2O	3.58
Potassium Oxide, K2O	1.71
Titanium Dioxide, TiO2	0.98
Manganese Dioxide, MnO2	0.09
Phosphorus Pentoxide, P2O5	0.34
Strontium Oxide, SrO	0.35
Barium Oxide, BaO	0.62
Sulfur Trioxide, SO3	0.99
Loss on Ignition (750°C)	0.42
Total	100.00
Moisture (105°C), as Received	0.09

Analysis per ASTM C 311

Charles R. Wilson
Division Manager

MEMBER ACIL

Figure 9-3: Chemical analysis of fly ash

COARSE AGGREGATE SIEVE ANALYSIS

Table 9-1: Coarse aggregate sieve analysis

Sieve	*Sieve Wt. (kg)*	*Sample Wt. (kg)*	*Sieve*	*Opening (mm)*	*Percent Retained*	*Sample Weight*	*Percent Passing*	*Cumulative Percent Retained*
1.5"	8.748	8.748	1.5."	38.10	0.00	0.00	100.00	0.00
3/4"	7.468	8.096	3/4"	19.05	5.45	0.63	94.55	5.45
1/2"	7.324	12.556	1/2"	12.70	45.37	5.23	49.18	50.82
1/4"	8.608	13.712	1/4"	6.35	44.26	5.10	4.93	95.07
No. 4	6.954	7.330	No. 4	4.75	3.26	0.38	1.66	98.34
No.8	6.526	6.696	No.8	2.36	1.47	0.17	0.19	99.81
Pan	6.252	6.274	Pan	0.00	0.19	0.02	0.00	100.00
Total	51.880	63.412	11.53		100.0	11.53	250.52	

FINE AGGREGATE SIEVE ANALYSIS

Table 9-2: Fine aggregate sieve analysis (batch 1)

Sieve Opening (mm)	*Percent Retained*	*Sample Weight*	*Percent Passing*	*Cumulative Percent Retained*
9.525	0.00	0.0	100.00	0.00
4.75	4.55	59.5	95.45	4.55
2.36	18.71	244.5	76.74	23.26
1.18	13.74	179.5	63.00	37.00
0.6	12.53	163.7	50.47	49.53
0.3	34.51	451.0	15.96	84.04
0.15	14.10	184.2	1.86	98.14
Pan	1.86	24.3		100.00
	100.00	1306.7	403.47	
		Fineness Modulus	2.97	

Table 9-3: Fine aggregate sieve analysis (batch 2).

Sieve Opening (mm)	*Percent Retained*	*Sample Weight*	*Percent Passing*	*Cumulative Percent Retained*
9.525	0.00	0.0	100.00	0.00
4.75	5.29	68.0	94.71	5.29
2.36	20.63	265.2	74.08	25.92
1.18	13.95	179.3	60.13	39.87
0.6	12.42	159.7	47.70	52.30
0.3	33.70	433.2	14.00	86.00
0.15	12.35	158.8	1.65	98.35
Pan	1.65	21.2		100.00
	100.00	1285.4	392.27	
		Fineness Modulus	3.08	

MISCELLANEOUS

Figure 9-4: Slabs in ponding cycle at the OSU outdoor exposure site. Deicer containers can be seen at the far end.

Figure 9-5: Installed weather station at the OSU outdoor exposure site.

Figure 9-6: Reinforced concrete slabs in the F-T chamber.